LOUIE, DOOWAH

EXPERIMENTAL INVESTIGATION OF MODULATIONAL EFFECTS IN A MAGNETIZED PLASMA

City University of New York PH.D. 1980

PLEASE NOTE:

In all cases this material has been filmed in the best possible way from the available copy. Problems encountered with this document have been identified here with a check mark ✓.

1. Glossy photographs _____
2. Colored illustrations _____
3. Photographs with dark background ✓
4. Illustrations are poor copy _____
5. Print shows through as there is text on both sides of page _____
6. Indistinct, broken or small print on several pages ✓ throughout ✓
7. Tightly bound copy with print lost in spine _____
8. Computer printout pages with indistinct print _____
9. Page(s) _____ lacking when material received, and not available from school or author _____
10. Page(s) _____ seem to be missing in numbering only as text follows _____
11. Poor carbon copy _____
12. Not original copy, several pages with blurred type _____
13. Appendix pages are poor copy _____
14. Original copy with light type _____
15. Curling and wrinkled pages _____
16. Other _____

EXPERIMENTAL INVESTIGATION OF MODULATIONAL EFFECTS IN A MAGNETIZED PLASMA

by

Doowah Louie

A dissertation submitted to the Graduate Faculty in Physics in partial fulfillment of the requirement for the degree of Doctor of Philosophy, The City University of New York

1980

This manuscript has been read and accepted for the Graduate Faculty in Physics in satisfaction of the dissertation requirement for the degree of Doctor of Philosophy.

5/29/80
date

Leo Piserchuck
Co-Chairman of Examining Committee

Michael E. Baron
Co-Chairman of Examining Committee

6/18/80
date

Executive Officer

Supervisory Committee

The City University of New York

Abstract

EXPERIMENTAL INVESTIGATION OF MODULATIONAL EFFECTS IN A MAGNETIZED PLASMA

by

Doowah Louie

Advisers: Professor Michael E. Bacon

Professor Leo Diesendruck

Pulsed microwaves of frequency 2.43 GHz with 6 ms in pulse width are launched parallel to the external magnetic field into a magnetized plasma in a mirror machine with mirror ratio of 1.27. The plasma is produced by the same microwave pulse by the method of Electron Cyclotron Resonance using hydrogen gas. When the hydrogen neutral pressure is about $2\text{-}3\times10^{-5}$ torr and the incident microwave power is about 150 watts, large modulations on all signals were observed and have been investigated. We attribute the modulation to a relaxation type oscillation in the plasma.

ACKNOWLEDGEMENTS

I would like to thank Dr. Michael E. Bacon and Dr. Leo Diesendruck for their help to make this thesis possible, Walter B. Koch, Charles Fries, Paul A. Schaedler, and Edward C. Kuhner for their help in purchasing, fabricating and trouble shooting the experimental apparatus. Also, I would like to thank all the people I met during the course of this work for their help and encouragement.

TABLE OF CONTENTS

I LIST OF FIGURES

II INTRODUCTION

There has been a great deal of interest in using electromagnetic waves for the purpose of plasma heating for fusion. High power laser and high power microwaves are currently used. Recently, there has been renewed interest in Electron Cyclotron Resonance heating[1-8]. Electron Cyclotron Resonance (ECR) is a well established technique for both production and heating of plasma[9,10]. Anomalous absorption was reported[11,12] in an ECR produced plasma. It is interesting that in these studies there is evidence of modulation effects before anomalous absorption occurs. This thesis involves an investigation of these modulations.

In our experiment, pulsed microwaves of frequency 2.43 GHz with a 6 ms pulse width are launched parallel to the external magnetic field into a magnetized plasma in a mirror machine with mirror ratio of 1.27. The plasma is produced in hydrogen by this microwave pulse by the method of Electron Cyclotron Resonance. When the hydrogen neutral pressure is about 2.0×10^{-5} torr and the incoming microwave power is about 150 watts, we observed a large amplitude modulation of $\sim$70 KHz on all observed signals. These signals include optical signals, diamagnetic loop signals, reflected and transmitted microwave signals, and K-band microwave interferometer signals. Langmuir probe signals also show very pro-

nounced modulations.

Both the integrated and the unintegrated diamagnetic signals indicate 70 KHz oscillations. From the unintegrated signals, we find that the oscillations are all in phase at all points. The amplitude of the oscillation approaches a minimum at magnetic field maxima. This indicates that the perpendicular plasma pressure varied periodically and in phase throughout the plasma and had nodes at the magnetic field maxima. Also, from the optical signals emitted from plasma taken from the end and from the sides of the plasma chamber, we found that all the optical signals are in phase. All these facts indicates that we have a standing wave.

From the spectrum analyzer signals, we found that the incident microwaves have one peak at 2.43 GHz but both the reflected and the transmitted signals have a center peak and symmetrically spaced upper and lower side bands. There seems to be at least two possible candidates to explain these observations : a four wave parametric process[15] or a relaxation oscillation[20].

The parametric excitation of low frequency oscillations in plasma by an incident microwave signal were observed in a number of experimental studies. Several of these observations have been explained as parametric coupling from the electron plasma resonances to low-frequency oscillation corresponding to a radial eigenfrequency of an ion acoustic wave excited in the

cylinder[13-19].

In an attempt to explain some of these experiments (eg reference 13), DuBois and Goldman developed the theory of a four wave parametric process to account for the incident, Stokes, anti-Stokes, and the ion acoustic wave. However, there was some doubt as to whether the observed spectrum was due to the four wave parametric process or due to a combination of ion acoustic mode enhancement and ordinary mixing.

In Mendel and Stern's relaxation experiment, microwaves of 4.4 GHz and 3.5 watts were sent in a C-band waveguide to a low pressure mercury d.c. discharge. The pump wave is perpendicular to the axis of the non-magnetized plasma. They found a low frequency oscillation f_1 of approximately 100 KHz in the reflected and the transmitted microwaves from the plasma. They found $f_1 \approx \frac{V_a}{2R}$ where R is the discharge tube radius, and V_a is the ion acoustic phase velocity given by $V_a = \sqrt{\frac{kT_e}{m_i}}$. T_e is the electron temperature, m_i is the mass of the mercury ion. They also found the emission of 10 GHz microwaves. Mendel and Stern explained this low frequency oscillation as relaxation. Their simplified model is the following. First, the plasma density rises due to higher ionization rate and the plasma continues to be heated due to microwave absorption at the broad thermal resonances, until the density reaches the point where the pump power is almost completely reflected due to

the strong coupling to the microwave system. The electrons then cool rapidly, thereby restoring the original well-defined Tonks-Dattner resonances. The density falls. The transmission of microwaves increases and the cycle is renewed. This type of relaxation oscillation is very similar to our experimental observations.

In section III, we give a general description of the experimental apparatus and techniques. In section IV, we give the experimental results. Section V discusses the phenomenology of the oscillations in an attempt to explain the experimental results. Section VI contains a discussion and conclusion.

REFERENCES

1. S. M. Wolfe, D. R. Cohen, R. J. Temkin, and K. Kreischer, Nuclear Fusion, 19, 389 (1979) and the references therein.

2. F. DeLuca, C. Maroli, V. Petrillo, Plasma Physics, 21, 1067 (1979).

3. I. Fidone, G. Granata, G. Ramponi, R. L. Meyer, Phys. Fluids, 21, 645 (1978).

4. R. M. Gilgenbach et al, Phys. Rev. Lett. 44, 647 (1980).

5. K. L. Wong, Phys. Fluids, 21, 2108 (1978).

6. P. C. Efthimion, V. Arunasalam, and J. C. Hosea, Phys. Rev. Lett. 44, 396 (1980).

7. A. A. Skovoroda and B. N. Shvilkin, Radio Engineering and Electronic Physics, 22, 148 (1977).

8. A. I. Anisimov, N. I. Vinogradov, and B. P. Poloskin, Sov. Phys. Tech. Phys. 20, 629, 1976.

9. R. A. Dandl et al, Nuclear Fusion, 4, 344 (1964).

10. W. B. Ard et al, Phys. Rev. Lett. 10, 87 (1963).

11. R. J. LaHaye et al, Phys. Fluids, 19, 457 (1976).

12. R. J. LaHaye et al, Phys. Fluids, 17, 1785 (1974).

13. R. A. Stern and N. Tzoar, Phys. Rev. Lett. 17, 903 (1966).

14. O. Demokan, H. C. S. Hsuan, K. E. Lonngren, and R. A. Stern, J. Appl. Phys, 41, 2122 (1970).

15. D. F. DuBois and M. V. Goldman, Phys. Rev. Lett. 19, 1105 (1967).

16. A. M. Messiaen and P. E. Vandenplas, Phys. Fluids, 12, 2406 (1969).

17. J. Asmussen, and Q. H. Lee, Appl. Phys. Lett. 15, 183 (1969).

18. R. M. Fredericks, J. Asmussen, Phys. Fluids, 15, 944 (1972).

19. L. A. Klein, and B. Chaeo, J. Appl. Phys. 42, 5218 (1974).

20. C. W. Mendel and R. A. Stern, J. Appl. Phys. 41, 734 (1970).

III EXPERIMENTAL APPARATUS

Basic experimental apparatus for this experiment is described below and is shown in figure 3.1.1 and figure 3.1.2.

3.1 Experimental Setup

3.1.1 Plasma Chamber

The vacuum chamber is made of a stainless steel tube of 12.7 cm inside diameter and 1 meter in length. Inside the stainless steel tube, there is another stainless steel tube with inside diameter of 8.79 cm and a wall thickness of 0.5 mm. This inner tube is used as a cylindrical waveguide to confine microwave fields and plasma. At one end of the tube, there is a vacuum seal between the rectangular waveguide and the chamber. Two piece of aluminum in semi-circular shape were placed between rectangular and cylindrical waveguides. The other end of the plasma chamber is sealed by a stainless steel flange. At the center of the end flange, a 1/4 inch hole was made to insert the axial Langmuir probe, the rf loop probe, or to hold a piece of clear plastic to transmit the optical signals. A Viton O ring is used around the probes as a vacuum seal. At the center of the plasma chamber (70 cm from the end flange), there are three access ports. One is on the top and the other two are on opposite sides of the chamber. All three ports are sealed with flanges

and copper gaskets. the top flange is used to hold the radial Langmuir probe. The other two ports are for the the purpose of holding the K band microwave horns for the K band interferometer, or with a change of flange to mount the terminals of nine 100 turn diamagnetic coils which are wound around the stainless steel liner as shown in figure 3.1.1. These coils are used to monitor the perpendicular plasma pressure.

3.1.2 DC Magnetic Field

Four big water cooled coils are used in this experiment to produce the DC magnetic field. The coils are equipped with a set of 4 flux return bars which concentrate the return flux so that the field strength inside the coils is approximately that of an infinite solenoid. The power supply used is a Bertan Associates model 1064 which is a low ripple high current DC power supply. The magnetic field profile when the DC current is at the working current of 28 amp is shown in figure 3.1.3. The DC magnetic coils are spaced so as to produce a magnetic well at the center of the chamber with a mirror ratio of 1.27. A 100 turn DC aiding magnetic coil is placed at about 55 cm from the end of the chamber. This coil is used to vary the separation of the magnetic field maxima.

3.1.3 Vacuum System

The pumping system used consists of a mechanical pump and a two-inch air cooled oil diffusion pump with liquid nitrogen cold trap. The pressure in the plasma chamber is monitored by an ionization guage. With liquid nitrogen in the cold trap, the plasma chamber can be pumped down to a base presure of 2.0×10^{-7} torr. Hydrogen gas is leaked into the plasma chamber through an variable leak control (Vactronic Model 25XL), and monitored by a thermocouple gauge. Since a relatively large pressure change at the thermocouple gauge is required to change the plasma chamber pressure, the plasma chamber pressure can be easily controlled to $\pm 1 \times 10^{-6}$ torr.

3.1.4 Microwave System

The microwave source is an Amperex DX-20G magnetron operated at the power level of $\lesssim 1$ kilowatt. The magnetron output frequency is about 2.43 GHz. The magnetron is operated in the pulsed mode with a pulse width of 6 ms. The magnetron can be set to pulse every 20 seconds or fired manually. The microwaves are sent to the plasma chamber through the S band waveguides shown schematically in figure 3.1.2. The circulator and the isolator are used to keep the reflected microwaves from coming back into the magnetron. In order to detect the incident

forward signal, a directional coupler is used. The reflected signal can be detected from the cross guide coupler.

3.1.5 Signal Recording

The plasma is produced by the electron cyclotron resonance absorption of the right circularly polarized component of the incident microwaves. Since the microwaves are pulsed with a pulse width of only 6 ms, the various diagnostic signals (described in next section) are displayed on a Tektronix model 555 scope. Permanent records of signals were recorded on Polaroid type 107 land films.

FIGURE CAPTIONS

Figure 3.1.1 Plasma chamber and external DC magnetic coils and the locations of diagnostic tools. From the end flange to the S band waveguide end is 90 cm long. ID of the inner stainless steel tube is 8.79 cm.

Figure 3.1.2 Schematic diagram of the microwave system.

Figure 3.1.3 Profile of the external DC magnetic field.

FIG 3.1.1

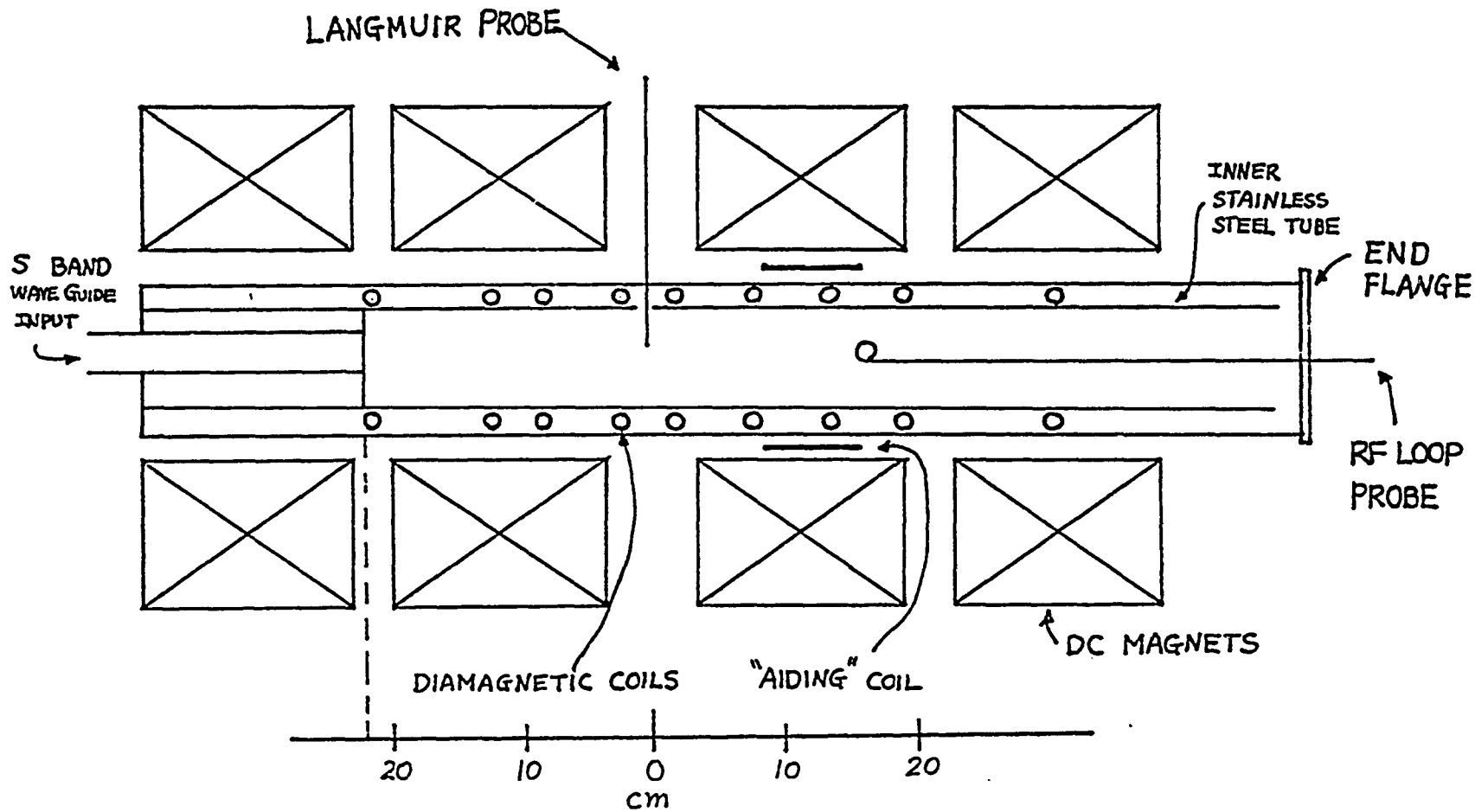
LANGMUIR PROBE
INNER STAINLESS STEEL TUBE
END FLANGE
S BAND WAVE GUIDE INPUT
RF LOOP PROBE
DC MAGNETS
DIAMAGNETIC COILS
"AIDING" COIL
20
10
0
10
20
cm

FIG 3.1.2

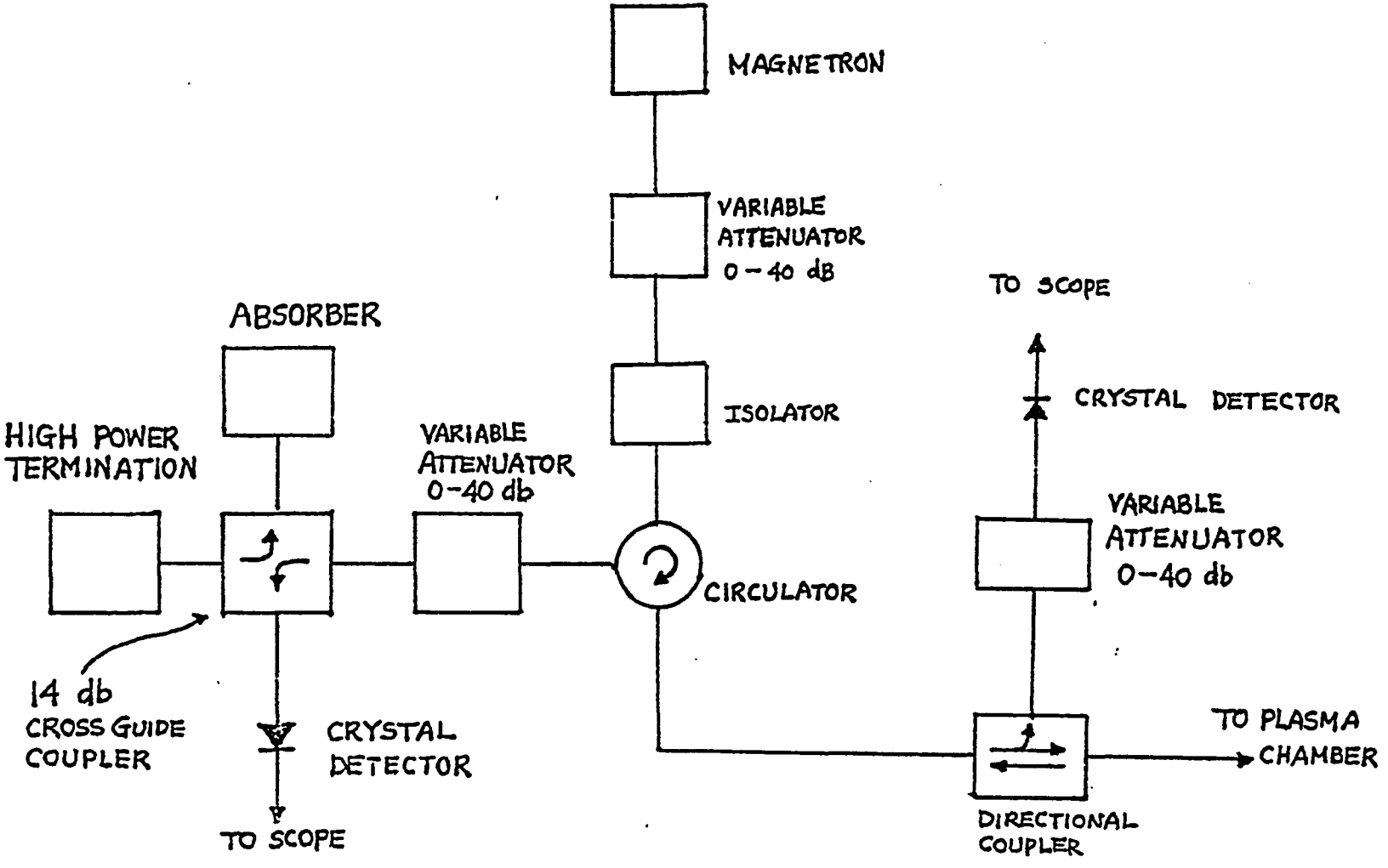
MAGNETRON
VARIABLE ATTENUATOR 0 – 40 dB
ABSORBER
TO SCOPE
CRYSTAL DETECTOR
ISOLATOR
HIGH POWER TERMINATION
VARIABLE ATTENUATOR 0-40 db
VARIABLE ATTENUATOR 0-40 db
CIRCULATOR
14 db CROSS GUIDE COUPLER
CRYSTAL DETECTOR
TO PLASMA CHAMBER
TO SCOPE
DIRECTIONAL COUPLER

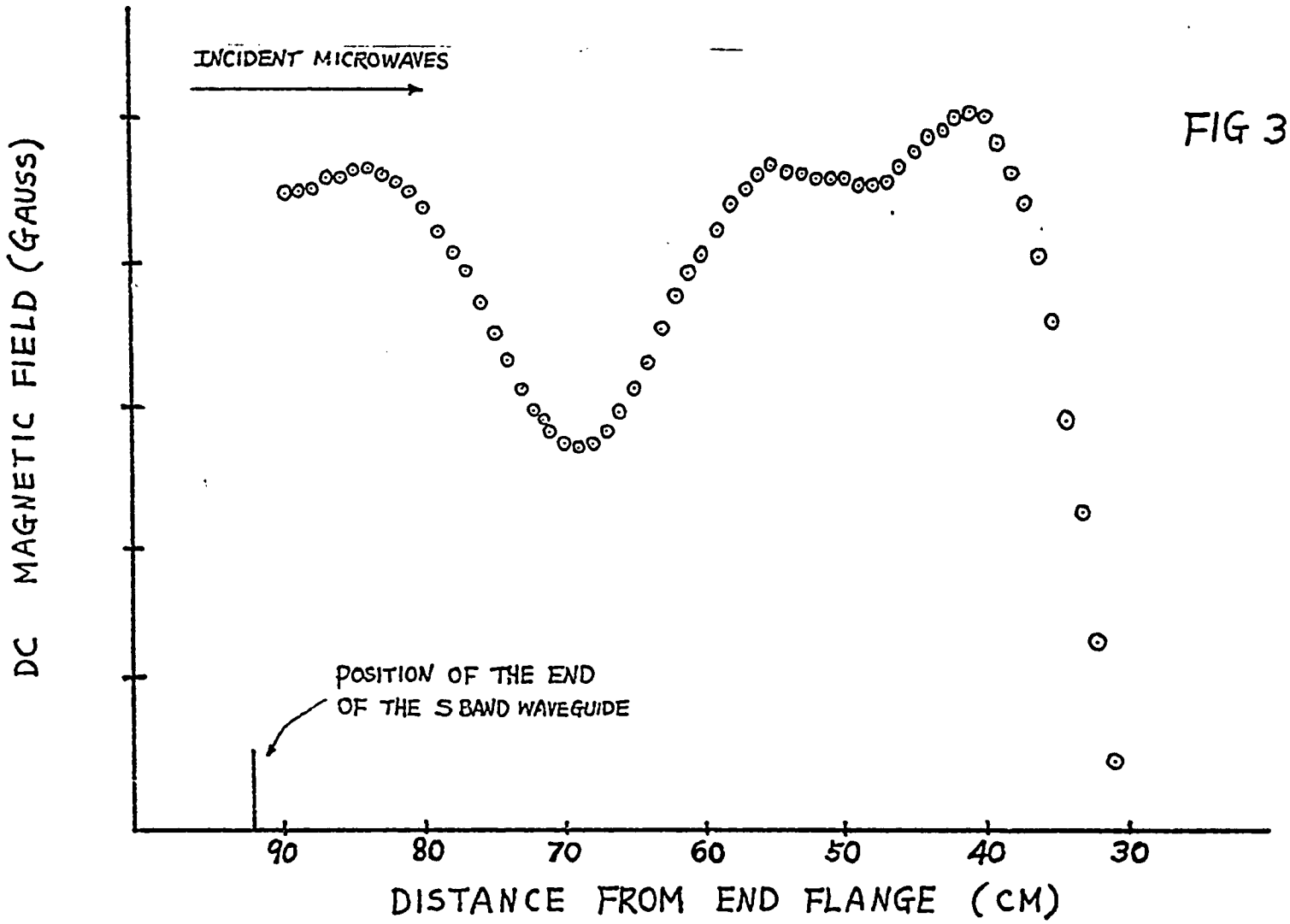
INCIDENT MICROWAVES
DC MAGNETIC FIELD (GAUSS)
POSITION OF THE END
OF THE S BAND WAVEGUIDE
90
80
70
60
50
40
30
DISTANCE FROM END FLANGE (CM)

FIG 3.1.3

3.2 Diagnostic Techniques

In our experiment, various techniques were used to diagnose the plasma such as diamagnetic coils, Langmuir probes, K-band microwave interferometer, RF loop probe, optical method, spectral analysis etc. Although the Langmuir probe is a very useful tool to diagnose plasma, it may not give correct result for plasma density when the probe is in a RF field[1]. However, it should still give the correct order of magnitude for the electron temperature[1]. We use the diamagnetic loop together with the electron temperature obtained from the Langmuir probe to determine the plasma density. Due to the multiple internal reflection of the microwaves in the plasma chamber, it may be difficult to obtain an accurate result for density using the microwave interferometer. Nonetheless we use the interferometer to check the order of magnitude of the electron density. In the following we give a general description of the diagnostic techniques.

3.2.1 Diamagnetic Coil

Diamagnetic coils are used to measure the perpendicular plasma pressure $P_\perp$ by detecting the diamagnetic effect due to the plasma. As the plasma is created, the diamagnetic current increases, the magnetic fields decreases inside the plasma and the magnetic flux enclosed by the diamagnetic coil decreases. As a result, an induced emf $\mathcal{E}$ will appear on the coil[2]:

$$\mathcal{E} = \frac{\mu_0 N A}{B_0} \frac{dP_\perp}{dt} \qquad 3.2.1.1$$

where N is the number of turns of the diamagnetic coil, A is the area of the coil, B_0 is the external DC magnetic field. The induced signals are integrated using a Tektronix Type O plug-in unit. The induced voltage is

$$V = \frac{\mu_0 N A}{RC B_0} P_\perp \qquad 3.2.1.2$$

where R is the resistance and C is the capacitance of of the integrating circuit. The diamagnetic coils used in this experiment consisted of 100 turns of wire wrapped around the inner stainless steel tube positioned as shown in figure 3.1.1.

From expression 3.2.1.2, one can estimate $P_\perp$ if A, V, R, C, and B_0 are known. Assuming we have ideal gas

$P_\perp = n_e K_B T_{e\perp}$ and using the T_e from Langmuir probe data assuming $T_e = T_{e\perp}$, one can estimate the density of plasma. Since the thickness of the inner stainless steel tube is about 0.5 mm, the presence of the inner stainless steel tube has very little effect on the diamagnetic coil signals at frequencies around 70 KHz.

As we shall see in next section all of our diagnostic signals including the diamagnetic loop signals (both integrated and unintegrated) are modulated at $\omega_0 \approx 2\pi \times 70$ KHz. The only variable in equations 3.2.1.1, and 3.2.1.2 is $P_\perp \propto n_e T_{e\perp}$. For our situation, then $P_\perp$ can be written as

$$P_\perp \propto P_{\perp 0}\left(1 + \frac{\Delta P_\perp}{2P_{\perp 0}} \cos(\omega_0 t + \alpha)\right)$$

This variation in $P_\perp$ can be due to either a variation in n_e or $T_{e\perp}$ alone or in general to a variation in both (with the same frequency ω_0). It is found that the modulation of the integrated signal is sometimes very small because of the RC factor in equation 3.2.1.1, and that it is more convenient, especially when comparing the modulations induced in different coils, to observe the unintegrated signal. This signal shows substantial modulation as one might expect because of the absence of the RC factor and the DC term. We note that the integrated and unintegrated signals should be $\frac{\pi}{2}$ out of phase.

3.2.2 Langmuir Probe

Langmuir probes are used to measure the electron temperature and to obtain an order of magnitude estimate of the plasma density. The two Langmuir probes used in this experiment are cylindrical probes which are made of a very fine wire of 0.08 mm in radius. A length of 2 mm is exposed to plasma and the rest of the wire is insulated by alumina as shown in figure 3.2.2.1. One of the Langmuir probes is inserted axially into the chamber from the stainless steel end flange. The other one is inserted into the chamber radially. Both Langmuir probes were oriented perpendicular to the external DC magnetic field.

A schematic diagram of the Langmuir probe is shown in figure 3.2.2.2. Dependent on the sign of the bias voltage to the probe, one can collect electron current or ion current. We assume that we have Maxwellian distribution and the presence of the probe does not disturb the local plasma density too much. We also assume that the probe dimensions are small compared to the electron and the ion mean free path. Due to the fact that the mass of ion M_i is much larger than the mass of electron m_e, electrons arrive at the probe much faster than ions. In order to collect ions, the probe should be biased at a negative potential with respect to the wall of the cylindrical chamber so that all the electrons are repelled. The random ion current I_i collected by the

the probe of area A is[3] :

$$I_i = \frac{A N_i e}{4}\sqrt{\frac{2K_B T_i}{m_i}} \qquad 3.2.2.1$$

where N_i is the ion density. The existence of sheath increases the effective collecting area of the probe. For $T_e >> T_i$, the current collected can be corrected as[4] :

$$I_i = 0.4\, A N_i e\sqrt{\frac{2K_B T_e}{m_i}} \qquad 3.2.2.2$$

The presence of the static magnetic field does not change the thermodynamics of the plasma very much. The electron current is given by

$$I_e = I_o e^{-\frac{eV}{K_B T_e}} \qquad 3.2.2.3$$

Experimentally, it is found that the $ln|I_e|$ vs applied biased voltage curve is linear from which T_e can be found.

In case of thick sheath, one can use conservation of energy and momentum to get the following expersion[4] :

$$I^2 = 4A^2 J_r^2 \left(1 - \frac{eV}{K_B T_i}\right) \qquad 3.2.2.4$$

where K_B is the Boltzmann constant, T_e is the electron temperature, T_i is the ion temperature, I is the collected probe current, A is the physical probe area, and J_r is the random current:

$$J_r = \frac{1}{2} ne \sqrt{\frac{2K_B T_i}{\pi m_i}} \qquad 3.2.2.5$$

Plotting the I_i^2 vs applied voltage curve, the slope S in the linear region is given by[5] :

$$S = \frac{2}{\pi} A^2 \frac{e^3}{m_i} n_i^2 \qquad 3.2.2.6$$

will give the density of the plasma. One can see that the slope S does not dependent on T_e or T_i.

FIGURE CAPTIONS

Figure 3.2.2.1 Axial and radial Langmuir probe.

Figure 3.2.2.2 Circuit diagram for Langmuir probe.

FIG 3.2.2.1

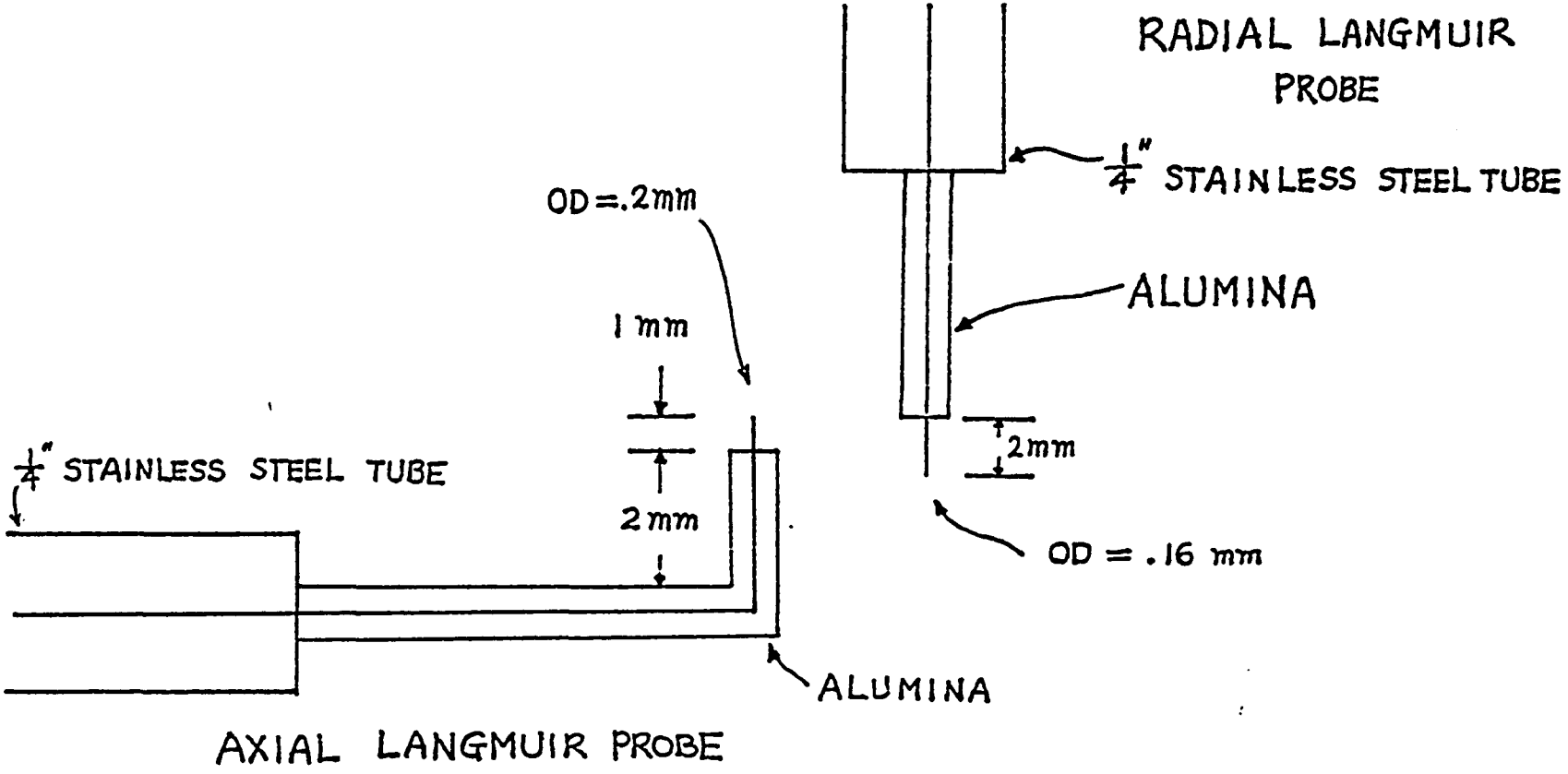
RADIAL LANGMUIR PROBE
1/4" STAINLESS STEEL TUBE
ALUMINA
2mm
OD = .16 mm
OD=.2mm
1 mm
2mm
1/4" STAINLESS STEEL TUBE
ALUMINA
AXIAL LANGMUIR PROBE

FIG 3.2.2.2

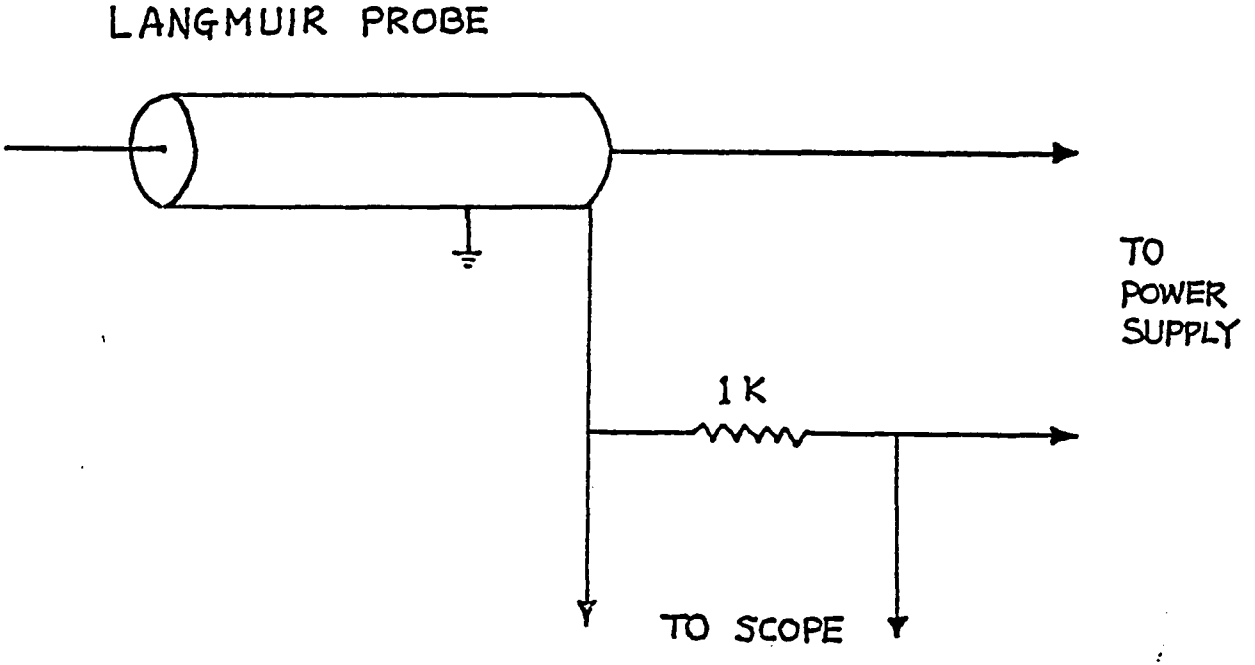

3.2.3 Microwave Interferometer

The microwave interferometer is used to confirm the average plasma density at the midplane of the magnetic mirror center. The details of the microwave interferometer setup is shown in figure 3.2.3.1. Microwave signal from a sweep oscillator is transmitted along the K band waveguide and then split into two components. One component is sent through the plasma using two K band microwave horns sitting on opposite sides of the chamber. The horns are situated at the midplane of the magnetic mirror and perpendicular to the external DC magnetic field. The other component of the microwave is sent along the waveguide outside the plasma and through the phase shifter. Both paths of the microwave are combined in a magic tee. We adjust the microwave signal amplitudes in both paths to be the same when there is no plasma in the plasma chamber, and adjust the phase shifter so that the two microwave signals are in phase. We observe the output signal of the added arm of the magic tee. Since the relation between the time average of the square of the output signal amplitude of the added arm of the magic tee $\langle S^2 \rangle$ and the signal amplitude A of the two paths of the microwave is:

$$\langle S^2 \rangle = \frac{A^2}{2}(1+\cos\phi) \qquad 3.2.3.1$$

where ϕ is the phase angle between the two paths of microwave signals. The existence of plasma will decrease the index of refraction for microwave. There will be phase shift between the two paths of microwave when there is plasma inside the plasma chamber. Therefore, by comparing the signal amplitudes from the output of the added arm of the magic tee at the time when there is plasma and at the time when there is no plasma, one can find the phase shift due to the presence of the plasma.

In this experiment, we use the K band microwave interferometer in such a way that it will have the minimum effect on the existing plasma. An ordinary wave ($\vec{E} /\!/ \vec{B}_0$) is launched from the K band microwave horn across the plasma chamber. The dispersion relation of the ordinary mode[6] :

$$\frac{K^2C^2}{\omega^2} = 1 - \frac{\omega_p^2}{\omega^2} \qquad 3.2.3.2$$

where K is the wave number, ω is the angular frequency of the K band microwave, ω_p is the angular plasma frequency. For our case, using $\omega_p^2 << \omega^2$, we have the following experssion:

$$\frac{KC}{\omega} \sim 1 - \frac{1}{2}\frac{\omega_p^2}{\omega^2} \qquad 3.2.3.3$$

Substituting for ω_p^2 , the average plasma density across the path length 2a (a = the radius of the plasma chamber) is given by[7] :

$$n\,(1/cm^3) = \frac{118.4\ f_{(Hz)}}{2a_{(cm)}}\ \Delta\phi_{(rad)} \qquad 3.2.3.4$$

FIGURE CAPTION

Figure 3.2.3.1 Schematic diagram of the K band microwave interferometer.

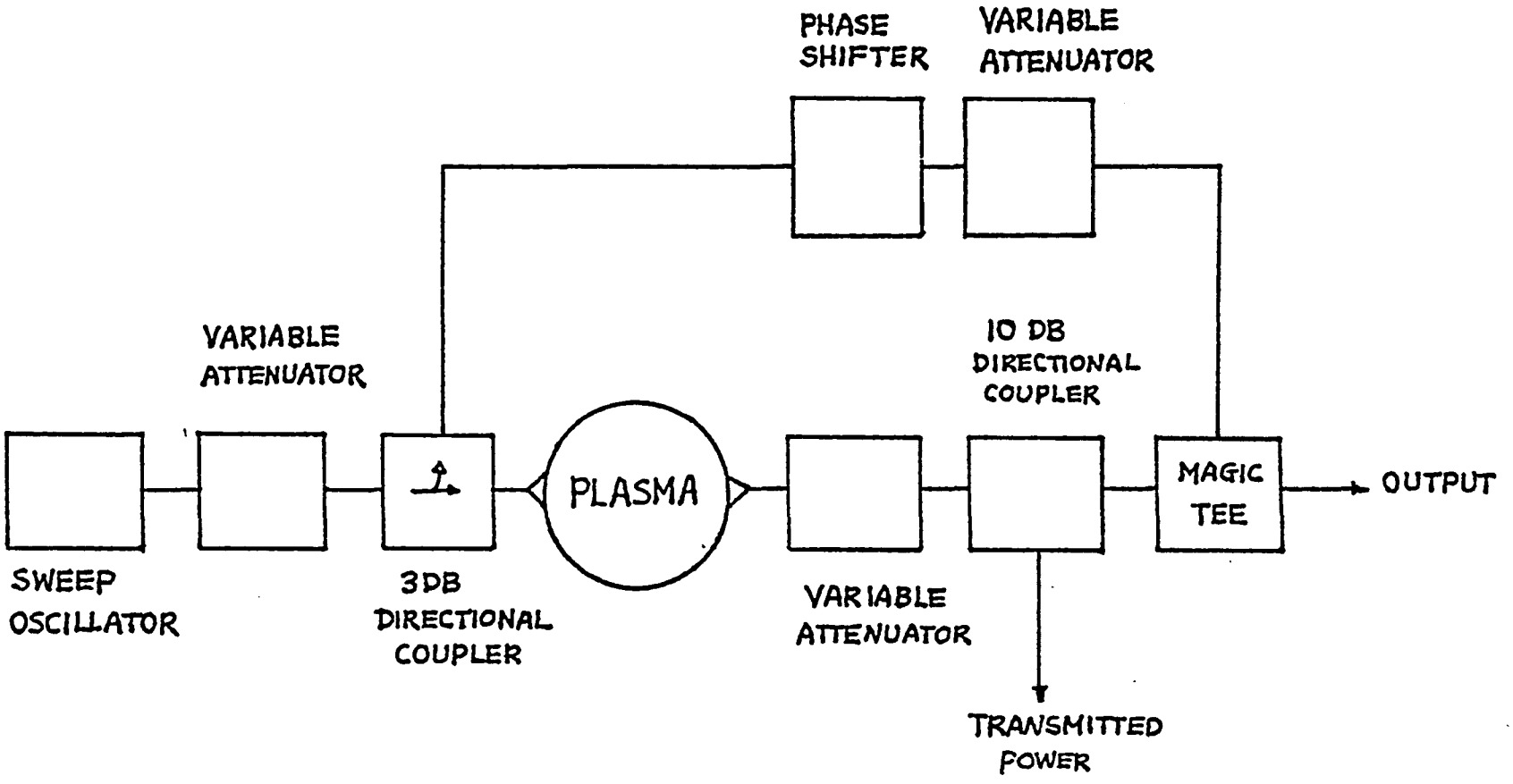
PHASE SHIFTER
VARIABLE ATTENUATOR
VARIABLE ATTENUATOR
10 DB DIRECTIONAL COUPLER
PLASMA
MAGIC TEE
OUTPUT
SWEEP OSCILLATOR
3DB DIRECTIONAL COUPLER
VARIABLE ATTENUATOR
TRANSMITTED POWER

FIG 3.2.3.1

3.2.4 RF Probe

The rf probe used is a loop probe as shown in figure 3.2.4.1. The loop probe is made of a coaxial cable bended in a form of a circle of 1 cm in diameter. The inner wire of the coaxial cable is then spot welded to the outer copper conductor. The whole loop probe was coated with low vapor pressure resin to minimize the disturbance of the plasma.

In order to make sure that the loop probe couples only to the wave magnetic field and not to the wave electric field, a TM_{010} microwave cavity was used. In this TM_{010} cavity, microwave was sent in so that only TM_{010} mode exists in the cavity[8]:

$$E_z \propto J_0\left(2.405\frac{r}{a}\right) \qquad 3.2.4.1$$

$$H_\theta \propto J_1\left(2.405\frac{r}{a}\right) \qquad 3.2.4.2$$

where J_0 , J_1 are Bessel functions, a is the radius of cavity. The normalized field profiles of E_z and H_θ are plotted on figure 3.2.4.2. To see whether the loop probe coupled to E_z or H_θ field, the loop probe was first inserted radially into the cavity with the plane of the loop probe parallel to the axis of the cavity. This is

the case when the loop probe is supposed to couple only to the H_θ field. The result of this measurement is plotted on figure 3.2.4.3. When the loop probe is inserted radially into the cavity with the plane of the loop probe perpendicular to the axis of the cavity, the loop probe is supposed to couple the E_z field. It is found that when the probe is in this orientation, there is no signal picked up by the probe. From this fact and from figure 3.2.4.3, one can conclude that the loop probe only couples to the wave magnetic field.

FIGURE CAPTIONS

Figure 3.2.4.1 RF loop probe.

Figure 3.2.4.2. Theoretical TM_{010} field curves.

Figure 3.2.4.3 The response of the loop rf probe at different locations in the TM_{010} cavity with the probe oriented to couple the cavity wave magnetic field.

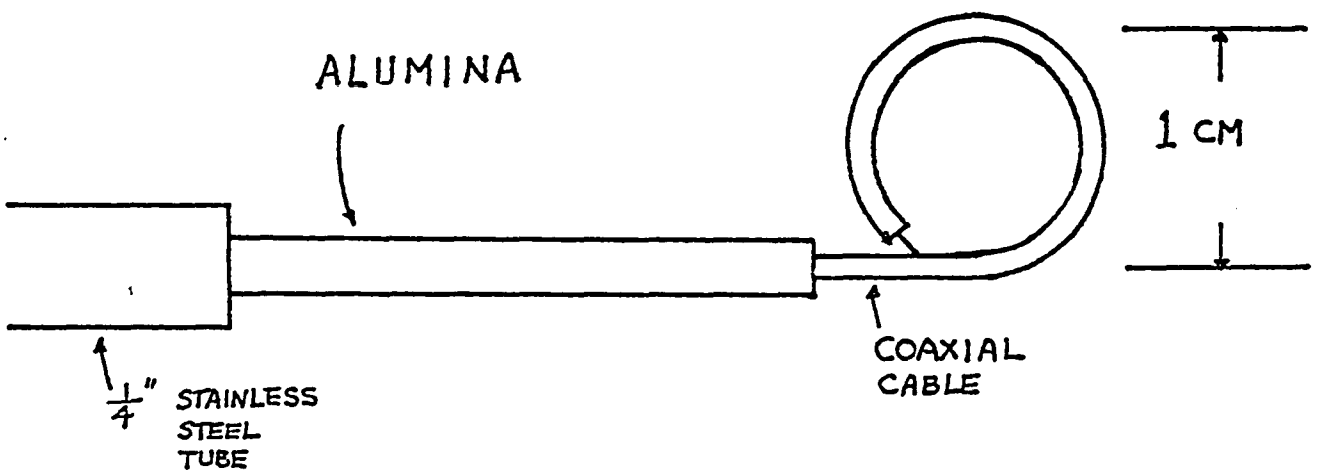

RF LOOP PROBE

FIG 3.2.4.1

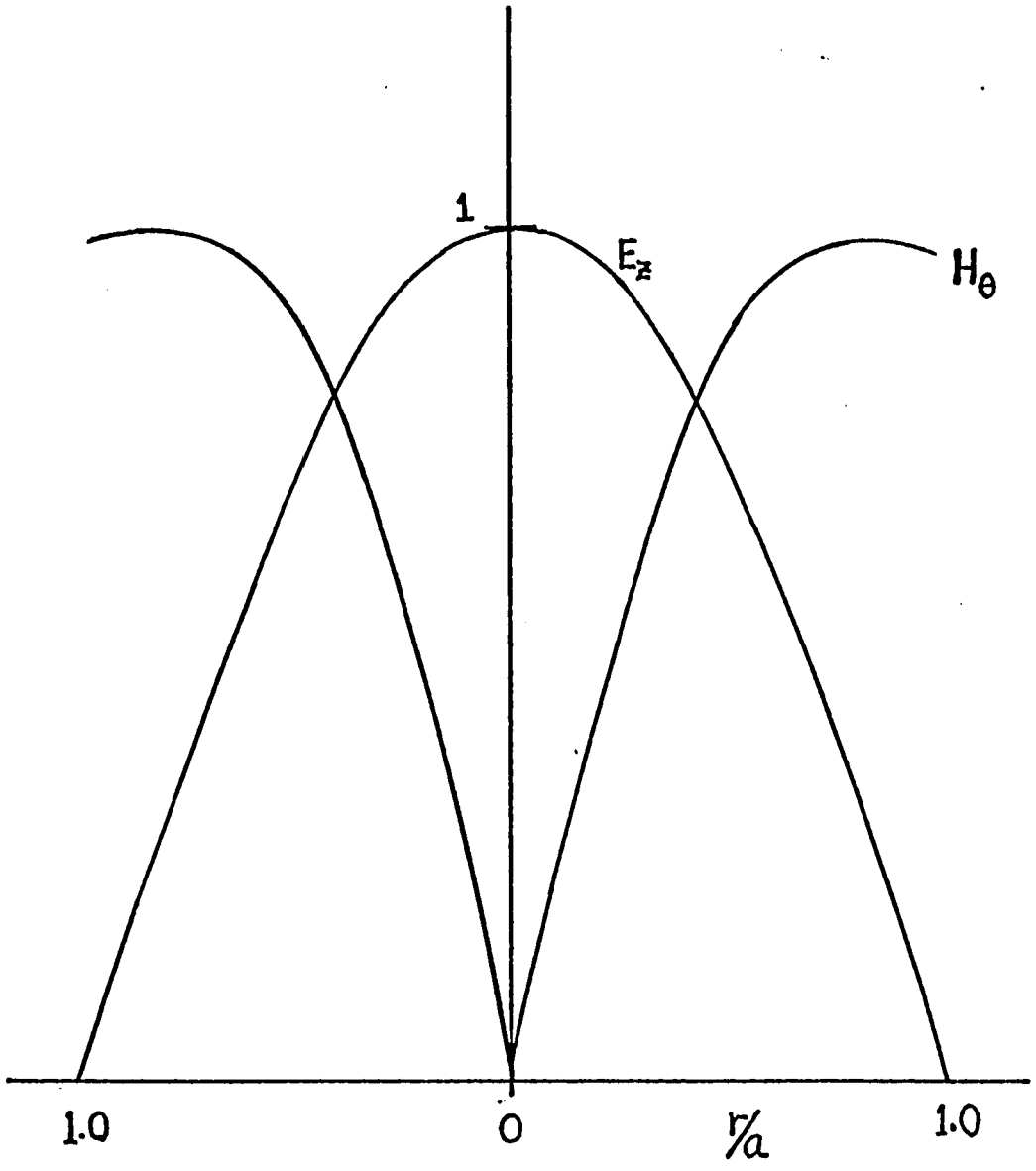

FIG 3.2.4.2

FIG 3.2.4.3

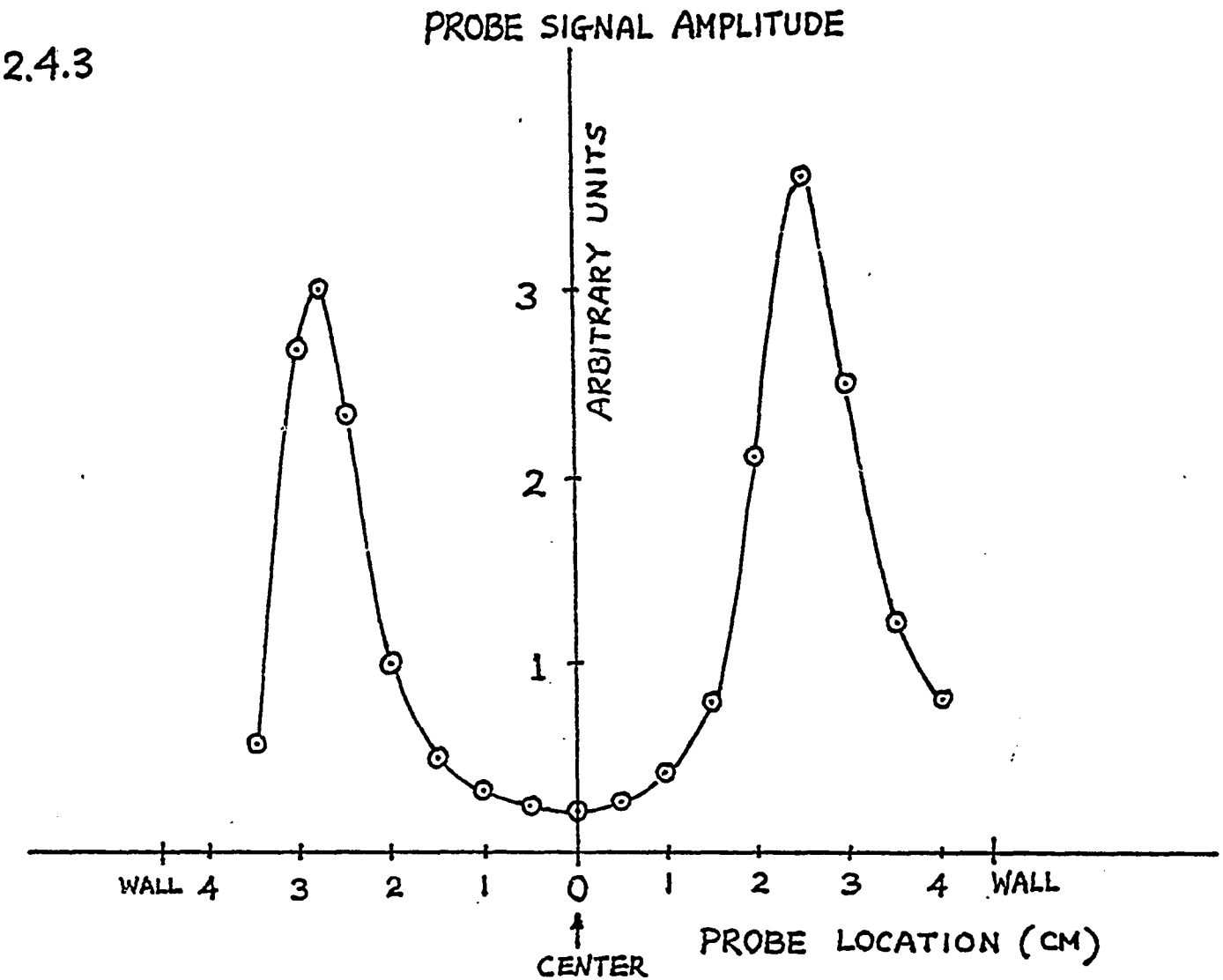
PROBE SIGNAL AMPLITUDE
ARBITRARY UNITS
3
2
1
WALL 4 3 2 1 0 1 2 3 4 WALL
CENTER
PROBE LOCATION (CM)

3.2.5 Optical Diagnostics

In our plasma, we observed light emission from the plasma. If we apply Steady-State Corona Model to our plasma, we assume the followings: the electrons of the plasma have a Maxwellian velocity distribution, ions are cool so that the ion-ion collision are negligible, the population densities of the excited level are determined by a balance between the rate of collisional excitation due to electrons from the ground level and the rate of spontaneous radiative decay of the level in question to all allowed levels below[9] :

$$n_e n_A(g) \chi(T_e, g \to p) = n_p \sum_{r<p} A(p \to r) \qquad 3.2.5.1$$

where n_e is the electron density, $n_A(g)$ is the ground state atom density, χ is the electron collisional excitation coefficient, n_p is the population in the level of interest, $A(p \to r)$ is the atomic transition probability. The intensity of a given spectral line (ignoring induced emission and absorption) is given by[9]

$$I_{p \to g} = \frac{1}{4\pi} \int n_e n_A(g) \chi(T_e, g \to p) \frac{A(p \to g)}{\sum_{r<p} A(p \to r)} h\nu \, ds \qquad 3.2.5.2$$

The integration is over the depth of the plasma viewed by the detector.

For the case of continuum radiation, the free-bound continuum emission coefficient can be written as[10]:

$$\mathcal{E}^{fb} = C_1 \frac{n_e n_i}{T^{3/2}} Z^4 e^{\frac{\chi_{z-1}-h\nu}{kT_e}} \sum_n \frac{G_n(\nu)}{n^3} e^{-\frac{E_n}{kT_e}} \qquad 3.2.5.3$$

where C_1 is 1.719×10^{-33} cgs unit, n_e is the electron density, n_i is the ion density, χ_{z-1} is the atom ionization energy, E_n is the excitation energy level of the principal quantum number n, $G_n(\nu)$ is the Graunt factor. The free-free continuum emission coefficient can be written as[11]:

$$\mathcal{E}^{ff} = C_2 \frac{Z^2}{T^{1/2}} n_e n_i e^{\frac{-h\nu}{kT_e}} \qquad 3.2.5.4$$

where C_2 is 5.443×10^{-39} cgs unit. The total continuum emission coefficient is

$$\mathcal{E}_T = \mathcal{E}^{fb} + \mathcal{E}^{ff}$$

$$= n_e n_i \left\{ \frac{C_1}{T^{3/2}} e^{\frac{\chi_{z-1}-h\nu}{kT_e}} \sum_n G_n(\nu) e^{-\frac{E_n}{kT_e}} + \frac{C_2}{T^{1/2}} e^{\frac{-h\nu}{kT_e}} \right\} \qquad 3.2.5.5$$

Form equations 3.2.5.3, 3.2.5.5, we can see that if n_e, n_i, and/or T_e are modulated at $\omega/2\pi$, the observed light signals will also be modulated at the same frequency.

In order to see light signals of any particular wavelength region, we can use filters to pick out the desire region. The experimental setup to detect visible

light signals emitted by the plasma is shown in figure 3.2.5.1. Light emitted from the plasma is collected by the optical cable through a small clear plastic window either at one of the side ports or at the end port and then connected to the photomultiplier tube (RCA 6342A). The photomultiplier is sensitive from 3000 Å to 6600 Å. The output of the photomultiplier is displayed on the scope. The power supply used is a Hewlett Packard DC power supply model 6515A.

FIGURE CAPTION

Figure 3.2.5.1 Experimental setup of optical method.

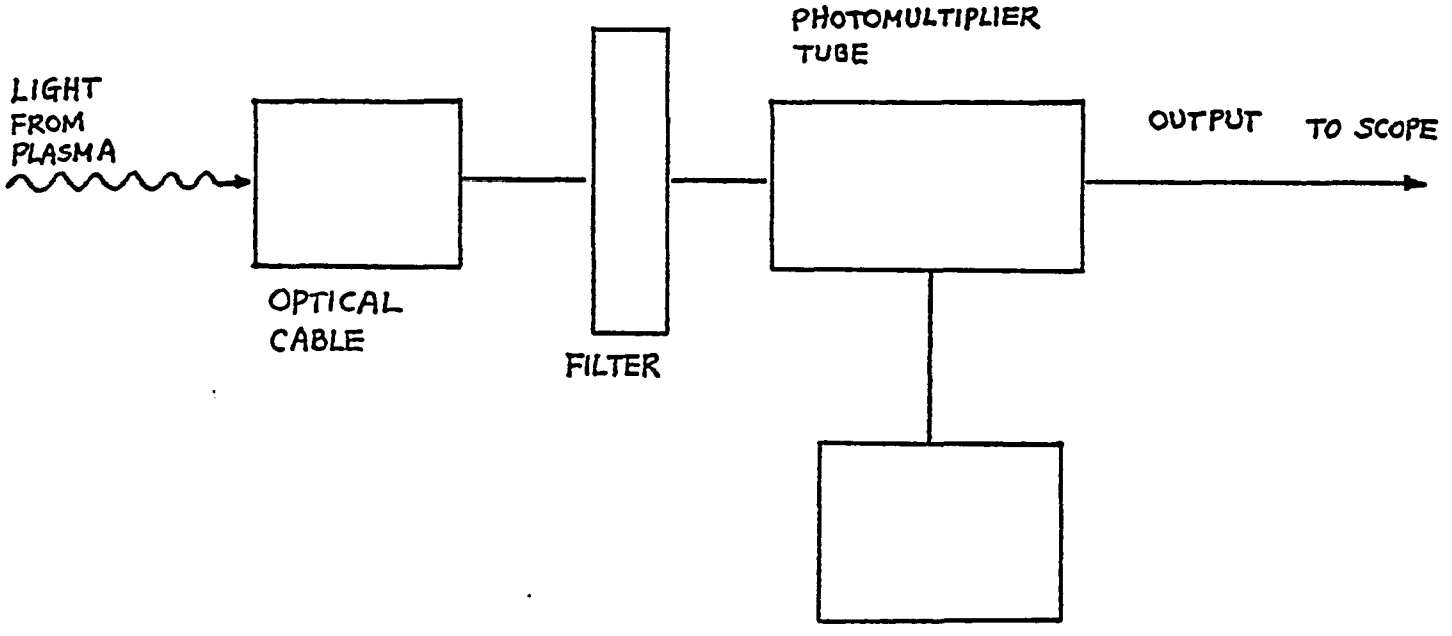
LIGHT
FROM
PLASMA
OPTICAL
CABLE
FILTER
PHOTOMULTIPLIER
TUBE
OUTPUT
TO SCOPE
DC POWER
SUPPLY

FIG 3.2.5.1

3.2.6 Spectral Analysis

In order to measure the frequency components of the microwave signals, both microwave receiver and spectrum analyzer were used. The microwave receiver used is a Polarad Model R microwave receiver with two plug-in units : Model RS from 2 GHz to 4.2 GHz, Model RM-T from 4.2 GHz to 7.7 GHz. The spectrum analyzer used is a Tektronix Spectrum Analyzer plug-in unit Type IL40. It can be used to scan frequencies from 1.5 GHz to 40 GHz with dispersion down to 1 KHz.

3.2.7 Phase Shift Correction

In order to check the correct phase relationships between all observed signals, we checked the phase shift of our signal detecting methods as followings:

Figure 3.2.7.1 is the schematic diagram of the setup to detect the phase shift of the optical signals. The wide range oscillator used was a Hewlett Packard model 200CD. The DC power supply used was a Hewlett Packard Power Supply model 6515A. The photomultiplier used was a RCA Photomultiplier Tube model 6342A. Light emitted from the LED was transmitted through the optical cable, then collected by the photomultiplier. The phase of the output of the photomultiplier was then compared to the phase of the voltage across the resistor. Using different frequency settings of the wide range oscillator from 55.5 KHz to 76.9 KHz, it was found that the optical signal from the photomultiplier circuit was about 1.5 μs behind the wide range oscillator applied voltage signal across the resistor as shown in figure 3.2.7.2. In figure 3.2.7.3, the upper trace is the wide range oscillator signal, the lower trace is the photomultiplier signal. The time scale is 5 μs/div. The phase shift is 1.5 μs. This correction must be applied to all photomultiplier signals.

In order to determine the possible delay of the reflected and the transmitted S-band microwave signals, the experimental setup as shown in figure 3.2.7.4 was

used. Continuous microwave source from a Raytheon microwave power generator model PGM01X1 at 2.45 GHz was amplitude modulated by a pin modulator (General Microwave model 1952) driven by a wide range oscillator with a period of 14 μs. The reflected and the transmitted microwave signals were detected as shown in figure 3.2.7.4. In figure 3.2.7.5, the upper signal is the reflected signal and the lower trace is the wide range oscillator signal. Since the pin modulator is an absorptive type, the minima of the reflected signal coincided with the maxima of the oscillator signals. This indicated that there is no circuit induced phase shift in the detection of the reflected signals. In figure 3.2.7.6, the top trace is the transmitted signal, the lower trace is the reflected signal. It is clear that the reflected and the transmitted signals are in phase. From these two pictures, one can conclude that there is no circuit induced phase shift of the reflected and the transmitted signals.

FIGURE CAPTIONS

Figure 3.2.7.1 Setup used to detect the phase shift of the optical method.

Figure 3.2.7.2 Phase shift of optical signals.

Figure 3.2.7.3 The upper signal is the wide range oscillator output. The lower signal is the photomultiplier signal. The time scale is 5 μs/div.

Figure 3.2.7.4 Setup used to detect the reflected and the transmitted signal phase shift.

Figure 3.2.7.5 The lower signal is the wide range oscillator signal. The upper signal is the reflected signal. The time scale is 5 μs/div.

Figure 3.2.7.6 The upper signal is the transmitted signal. The lower signal is the reflected signal. The time scale is 5 μs/div.

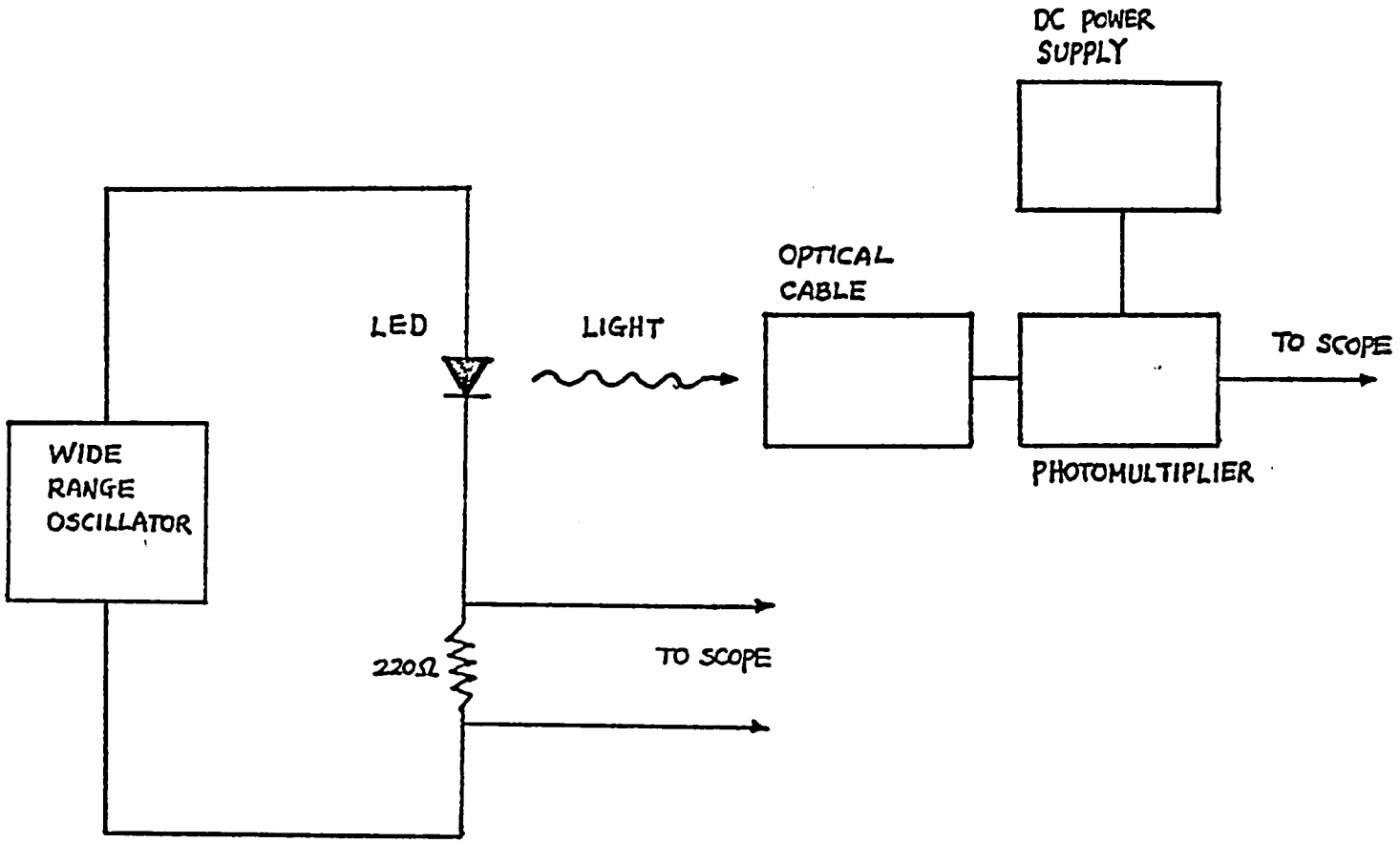
DC POWER
SUPPLY
OPTICAL
CABLE
LED
LIGHT
TO SCOPE
WIDE
RANGE
OSCILLATOR
PHOTOMULTIPLIER
220Ω
TO SCOPE

FIG 3.2.7.1

FIG 3.2.7.2

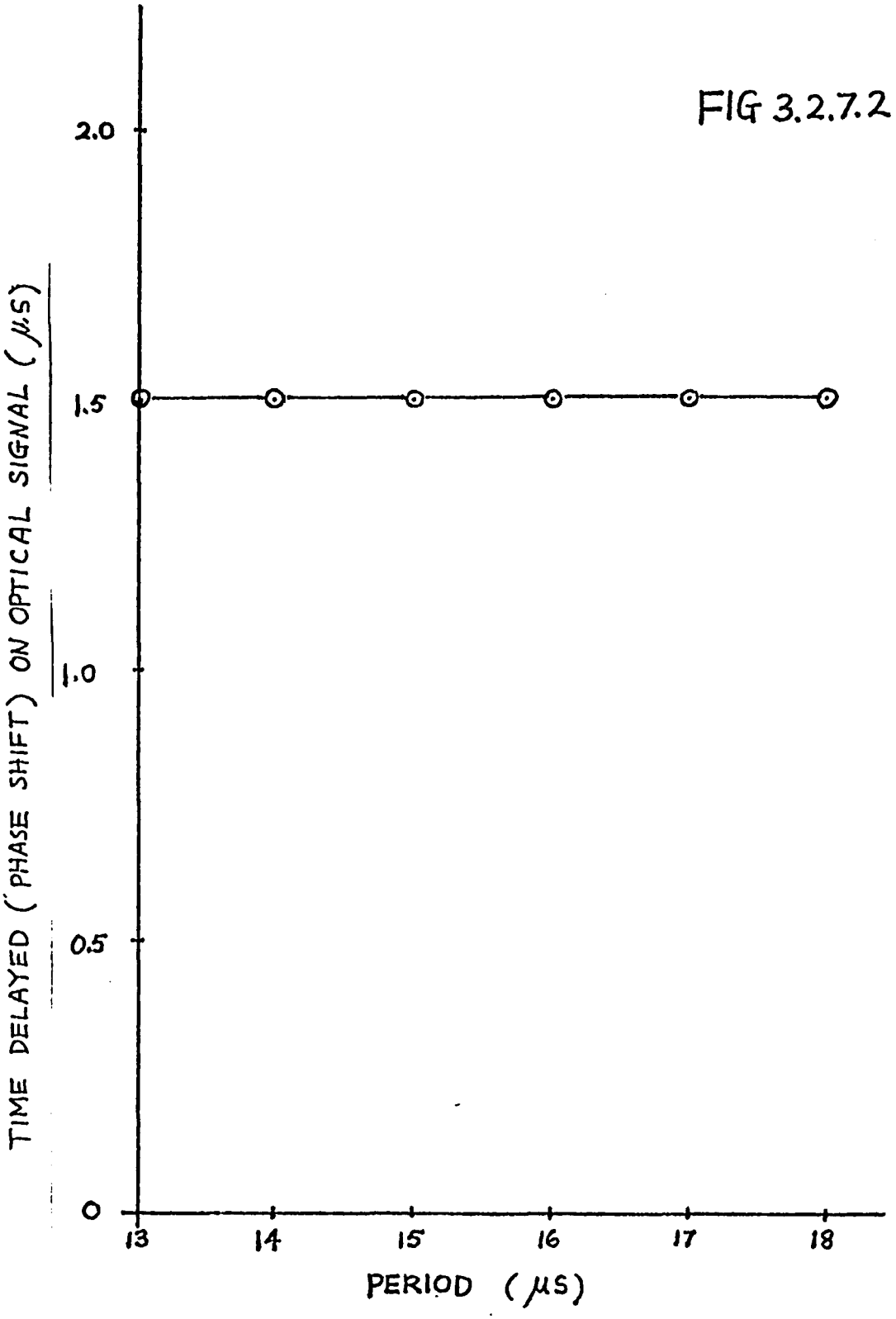
2.0
1.5
1.0
0.5
0
TIME DELAYED ('PHASE SHIFT) ON OPTICAL SIGNAL (μS)
13
14
15
16
17
18
PERIOD (μS)

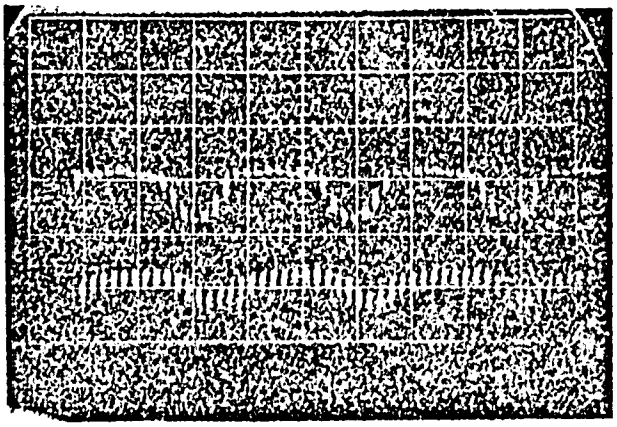

FIG 3.2.7.3

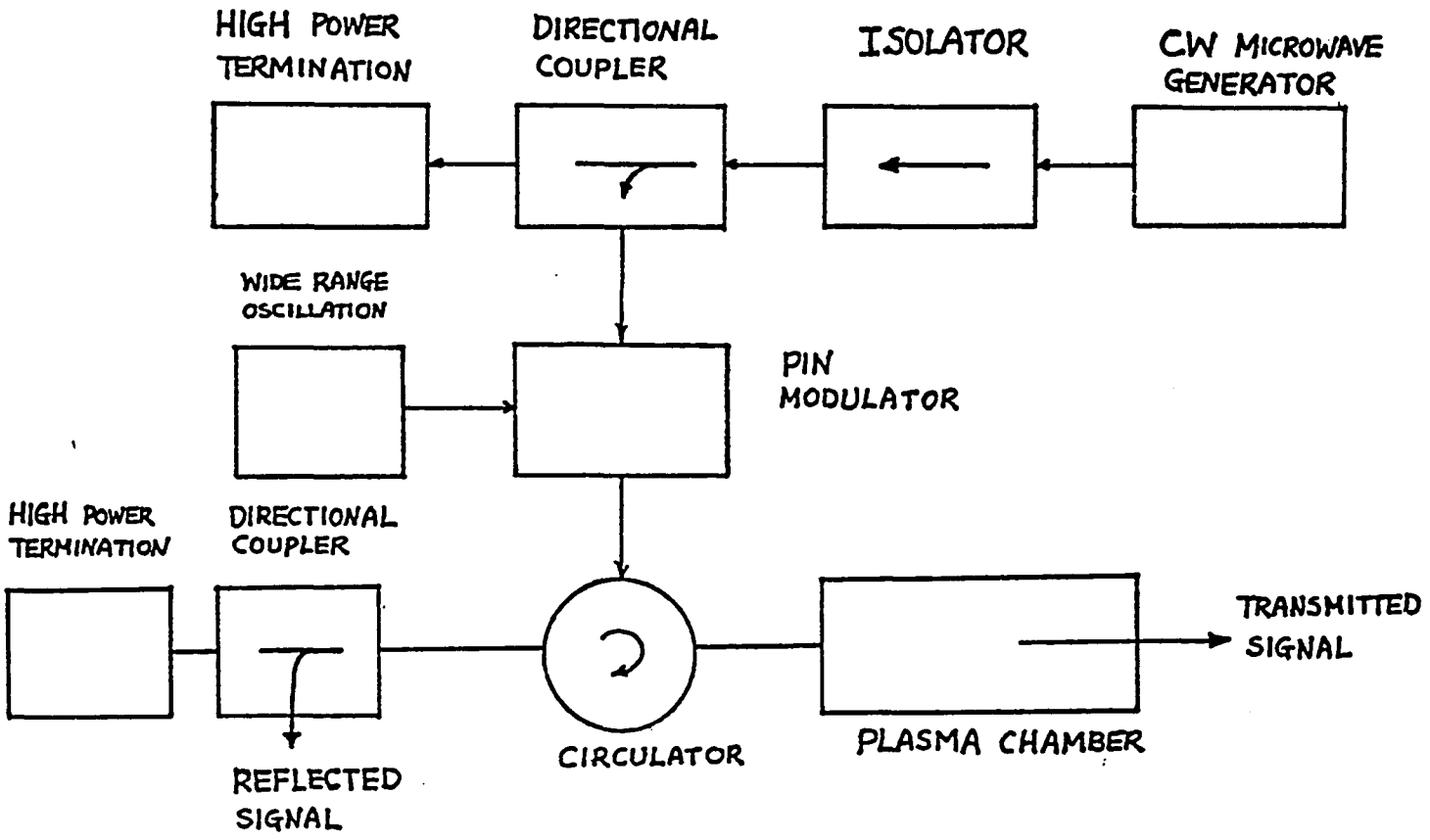
HIGH POWER TERMINATION
DIRECTIONAL COUPLER
ISOLATOR
CW MICROWAVE GENERATOR
WIDE RANGE OSCILLATION
PIN MODULATOR
HIGH POWER TERMINATION
DIRECTIONAL COUPLER
TRANSMITTED SIGNAL
CIRCULATOR
PLASMA CHAMBER
REFLECTED SIGNAL

FIG 3.2.7.4

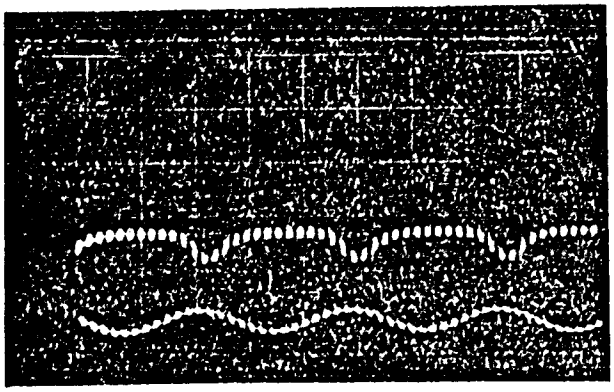

FIG 3.2.7.5

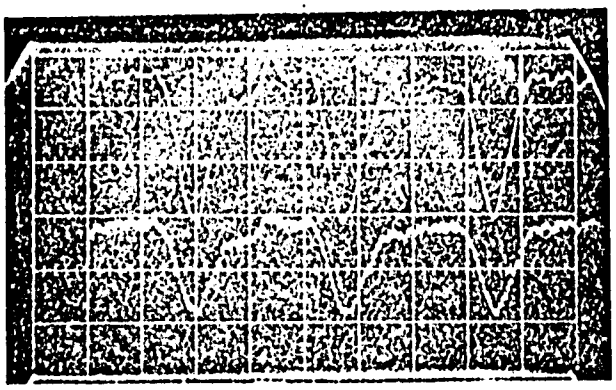

FIG 3.2.7.6

3.2.8 Aiding DC Coil

The Aiding DC coil is a 100 turns coil wound in a form of circular coil of 3 inches in width and 6 inches in inside diameter and 1/4 inch in thickness as shown in figure 3.2.8.1. The purpose of using the Aiding coil can be described as following. Since the cylindrical waveguide chamber is in an axial mirror DC magnetic field configuration, one can decrease the width of the magnetic well by placing the Aiding coil between the magnetic field maxima. Since the length of the plasma is determined by the width of the magnetic well, we can decrease the width of the magnetic well by increasing the Aiding coil current and thus we decrease the length of the plasma. Since the wavelength of the low frequency oscillation depends on the length of the plasma we should be able to vary the modulation frequency. So, in order to change the modulation frequency, the Aiding coil is used.

FIGURE CAPTIONS

Figure 3.2.8.1 Aiding DC coil.

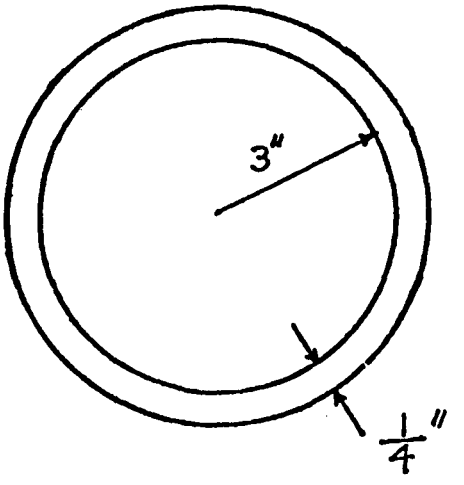

AXIAL VIEW

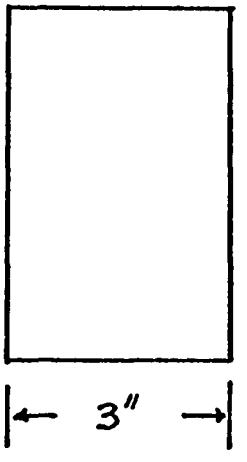

SIDE VIEW

FIG 3.2.8.1

REFERENCES

1. V. A. Godyak and O. A. Popov, Sov. Phy. Tech. Phys., 22, 461 (1977).

2. N. K. Krall and A. W. Trivelpiece, Principles of Plasma Physics, McGraw-Hill Book Co., (1973) pp 628-629.

3. M. A. Heald and C. B. Wharton, Plasma Diagnostics with Microwaves, John Wiley and Sons, Inc., (1965) pp 378-80.

4. D. Bohm et al, The Characteristics of Electrical Discharge in Magnetic Fields, McGraw-Hill Book Co., (1949) chapter 2.

5. R. H. Huddlestone and S. L. Leonard, Plasma Diagnostic Techniques, Academic Press (1965) pp 128-131.

6. T. J. M. Boyd and J. J. Sanderson, Plasma Dynamics, Thomas Nelson and Son Ltd, London, (1969) pp 173.

7. Same as 2, pp 120-123.

8. J. D. Jackson, Classical Electrodynamics, John Wiley and Sons Inc., (1962) pp 252-254.

9. R. H. Huddlestone and S. L. Leonard, Plasma Diagnostic Techniques, Academic Press (1965) pp 209.

10. W. Lochte-Holtgreven ed, Plasma Diagnostics, John Wiley & Sons, Inc., (1968) pp 34.

11. Same as 10, pp 40.

IV EXPERIMENTAL RESULTS

4.1 Basic Microwave Source Measurement

4.1.1 Pulse Form, Duration and Input Power

The typical pulse form of the incident microwave source signal is shown on figure 4.1.1.1. The duration of the pulse is about 6 ms. The input power shown in figure 4.1.1.1 is about 140 watts.

4.1.2 Incident Microwave Spectrum

The incident microwave spectrum was studied using two different approaches:

A Microwave Receiver

The incident microwave was scanned through the frequency range of 2 GHz to 7.7 GHz using Polarad Model R microwave receiver with two plug-in units : Model RS from 2 GHz to 4.2 GHz, Model RM-T from 4.2 GHz to 7.7 GHz. The output of the microwave receiver when the tunning frequency setting is at 2.43 GHz is shown in figure 4.1.2.1. The spectrum of the incident microwave source is shown on figure 4.1.2.2. The spectrum indicates the microwave peak is at 2.43 GHz. The funny shape is possibly due to the improper grounding of the microwave receiver circuitry.

B Spectrum Analyzer

The incident microwave signal was measured with Tektronix Spectrum Analyzer plug-in unit model IL40. The typical signals are shown in figure 4.1.2.3. The center frequency is set at 2.43 GHz with dispersion of 200 KHz and sweeping rate of 0.1 ms. The four different pictures were taken from the same incident microwave signal but for different shots. It is clear that the incident microwave frequency is different from shot to shot. Typically, it is found that it is about 500 KHz shot to shot, and 1 to 2 MHz variation during a pulse.

FIGURE CAPTIONS

Figure 4.1.1.1 Incident microwave source signal. The time scale is 1 ms/div.

Figure 4.1.2.1 Microwave receiver output signal for the incident microwave. The frequency setting is at 2.43 GHz. The time scale is 1 ms/div.

Figure 4.1.2.2 Spectrum of the incident microwave signal.

Figure 4.1.2.3 Spectrum analyzer output signal for the incident microwave. The center frequency is set at 2.43 GHz. Dispersion is set at 200 KHz/div.

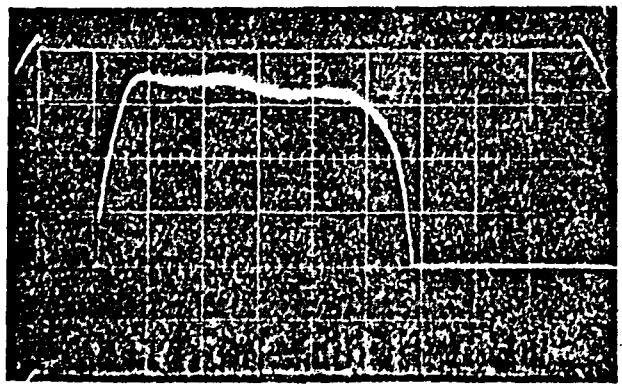

FIG 4.1.1.1

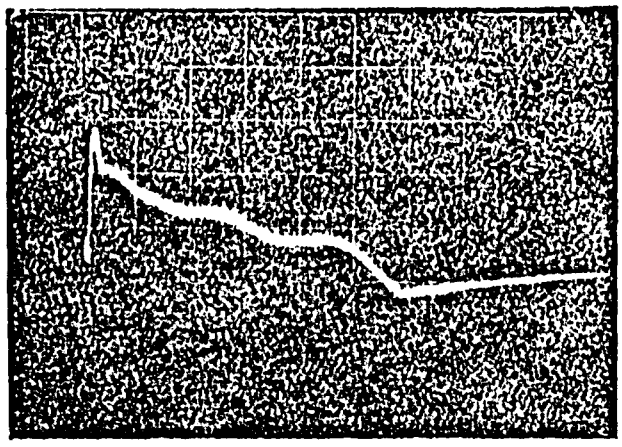

FIG 4.1.2.1

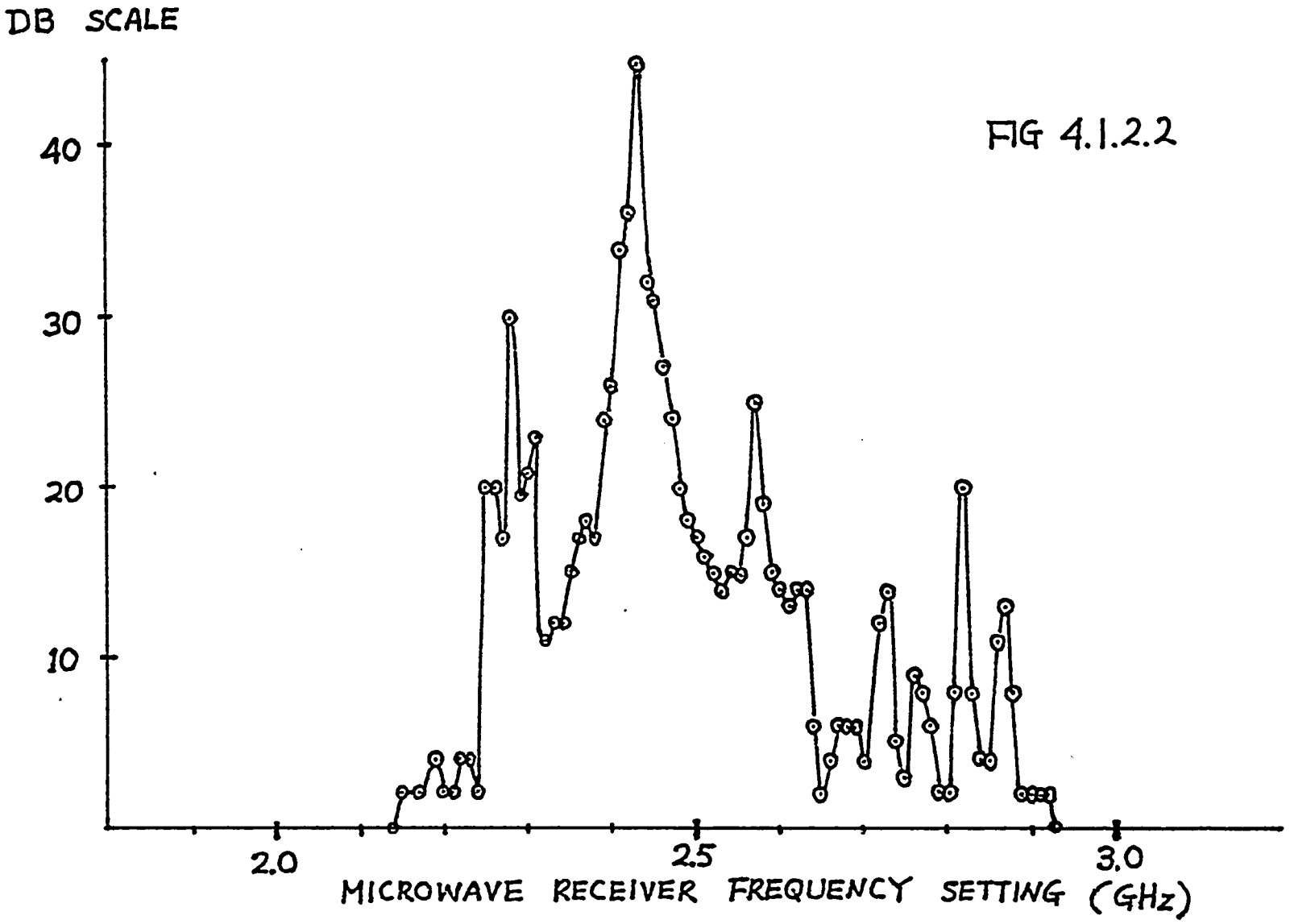
DB SCALE
40
30
20
10
2.0
2.5
3.0
MICROWAVE RECEIVER FREQUENCY SETTING (GHz)

FIG 4.1.2.2

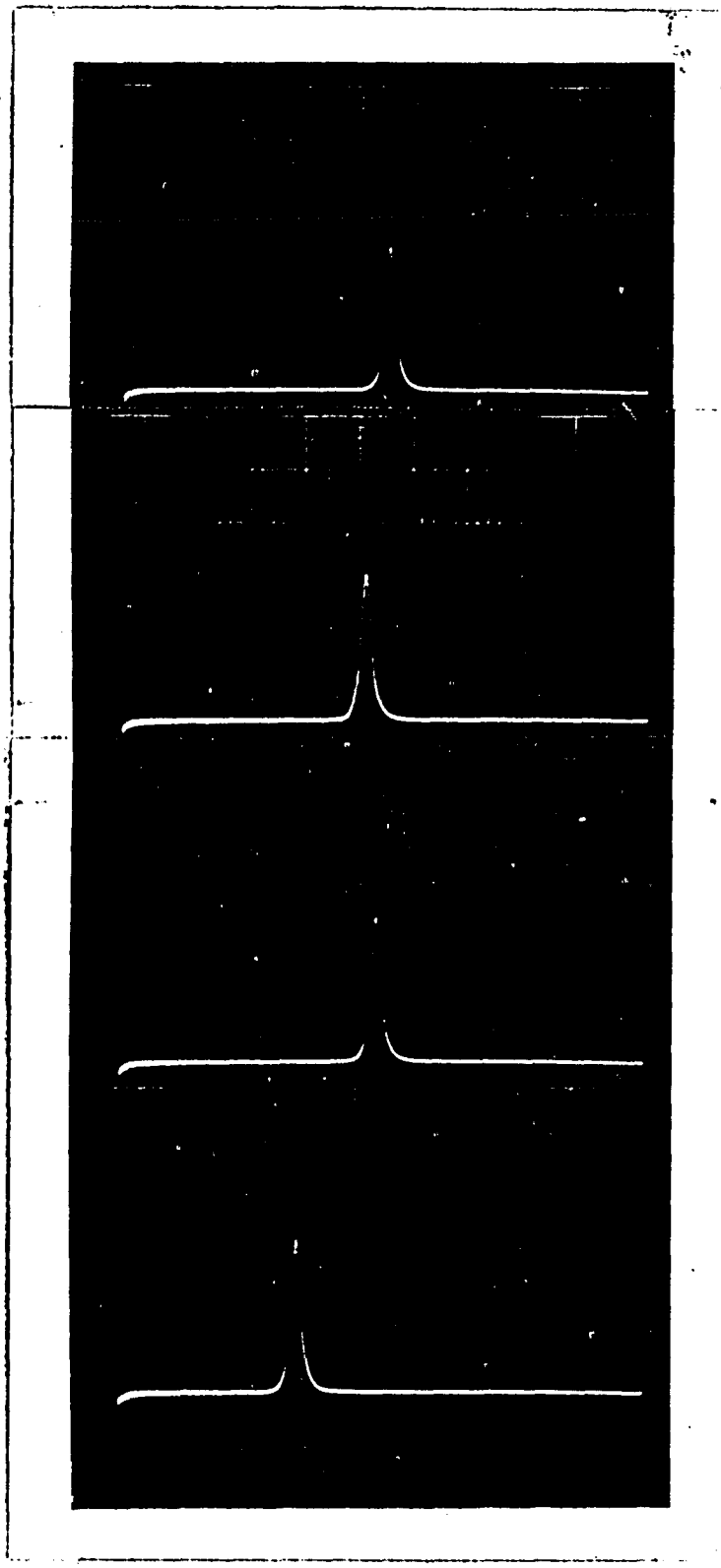

FIG 4.1.2.3

4.2 General Properties of Plasma

4.2.1 Duration of Plasma

In figure 4.2.1.1, the top trace is the optical signal, middle trace is the incident microwave signal, the lower signal is the reflected microwave signal. The time scale is 1 ms per division. The incident microwave pulse is about 6 ms. Taking the optical signal as being indicative of plasma existence, the duration of plasma is seen to be about 5.6 ms. Figure 4.2.1.2 shows the beginning part of the three signals of figure 4.2.1.1. The time scale is 0.2 ms per division. The plasma is formed about 0.3 ms after the start of incident microwave. Figure 4.2.1.3 shows the last part of the three signal of figure 4.2.1.1. The time scale is at 0.1 ms per division. The plasma is seen to end when the microwaves cease.

4.2.2 Diamagnetic Coil Signal

The typical diamagnetic coil signal is shown in figure 4.2.2.1. This signal also indicate that the plasma lasted for about 5.6 ms consistent with the optical signal. The order of magnitude of the perpendicular plasma pressure $n_e T_e$ is estimated to be about 1.7×10^{12} ev/cc. In figure 4.2.2.2, the locations of the diamagnetic coils are plotted against the perpen-

dicular plasma pressure. One can see that the perpendicular plasma pressure is relatively higher around the magnetic field minimum, and symmetrical about the center of the plasma chamber.

4.2.3 Langmuir Probe

The typical Langmuir probe signals are shown in figure 4.2.3.1. Using different applied probe bias voltages, one can obtain the probe current vs bias voltage characteristic curve. A typical characteristic curve is shown in figure 4.2.3.2. In order to estimate the electron temperature, a semi-log graph of probe electron current vs applied bias probe voltage is plotted and shown in figure 4.2.3.3. The electron temperature is estimated to be 31 ± 3 ev from the linear portion of the curve. In order to estimate the plasma density, the saturated (probe ion current)^2 vs the bias voltage graph is plotted and shown in figure 4.2.3.4. The plasma density is estimated from the slope of the graph. The density of this set of data is about 4.68×10^{10}/cc. This gives an $n_e T_e$ of 1.45×10^{12} ev/cc in suprisingly fair agreement with the diamagnetic loop signal considering the positioning of the probe in the plasma and the uncertainty in interpretation of the Langmuir probe characteristic in strong rf fields.

FIGURE CAPTIONS

Figure 4.2.1.1 Top trace is the optical signal. The middle trace is the incident microwave signal. The lower trace is the reflected microwave signal. The time scale is 1 ms/div.

Figure 4.2.1.2 The beginning part of figure 4.2.1.1. The time scale is 0.2 ms/div.

Figure 4.2.1.3 The ending part of figure 4.2.1.1. The time scale is 0.1 ms/div.

Figure 4.2.2.1 The upper trace is the reflected signal. The lower trace is the diamagnetic coil signal. The time scale is 1 ms/div.

Figure 4.2.2.2 Perpendicular plasma pressure curve.

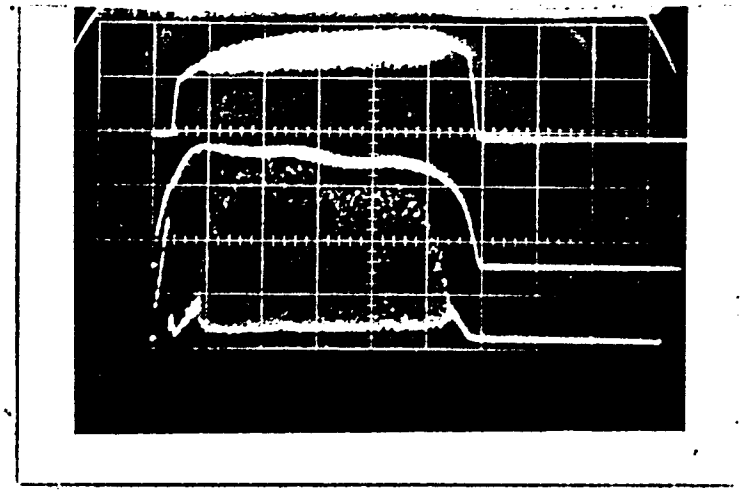

FIG 4.2.1.1

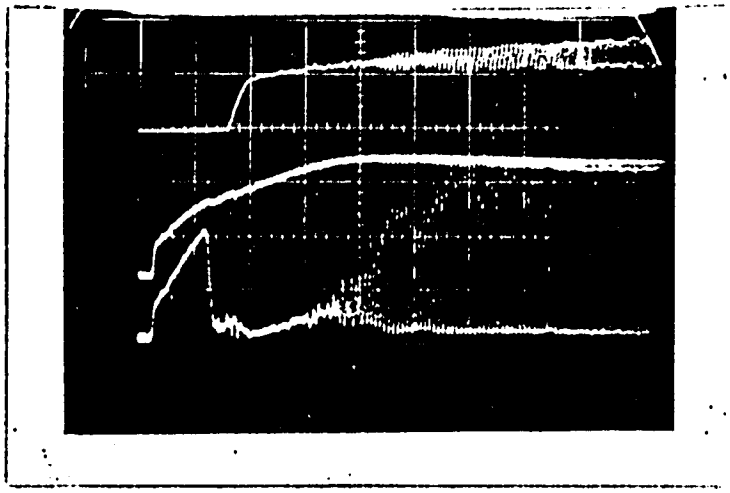

FIG 4.2.1.2

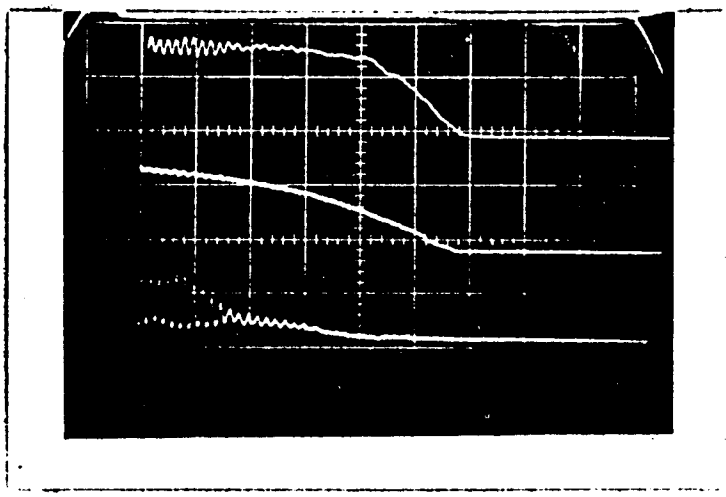

FIG 4.2.1.3

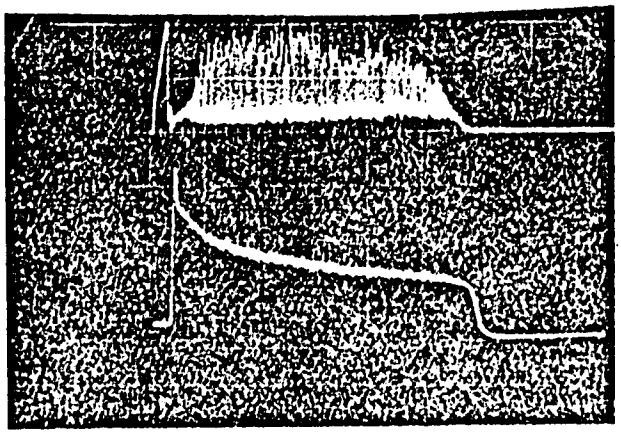

FIG 4.2.2.1

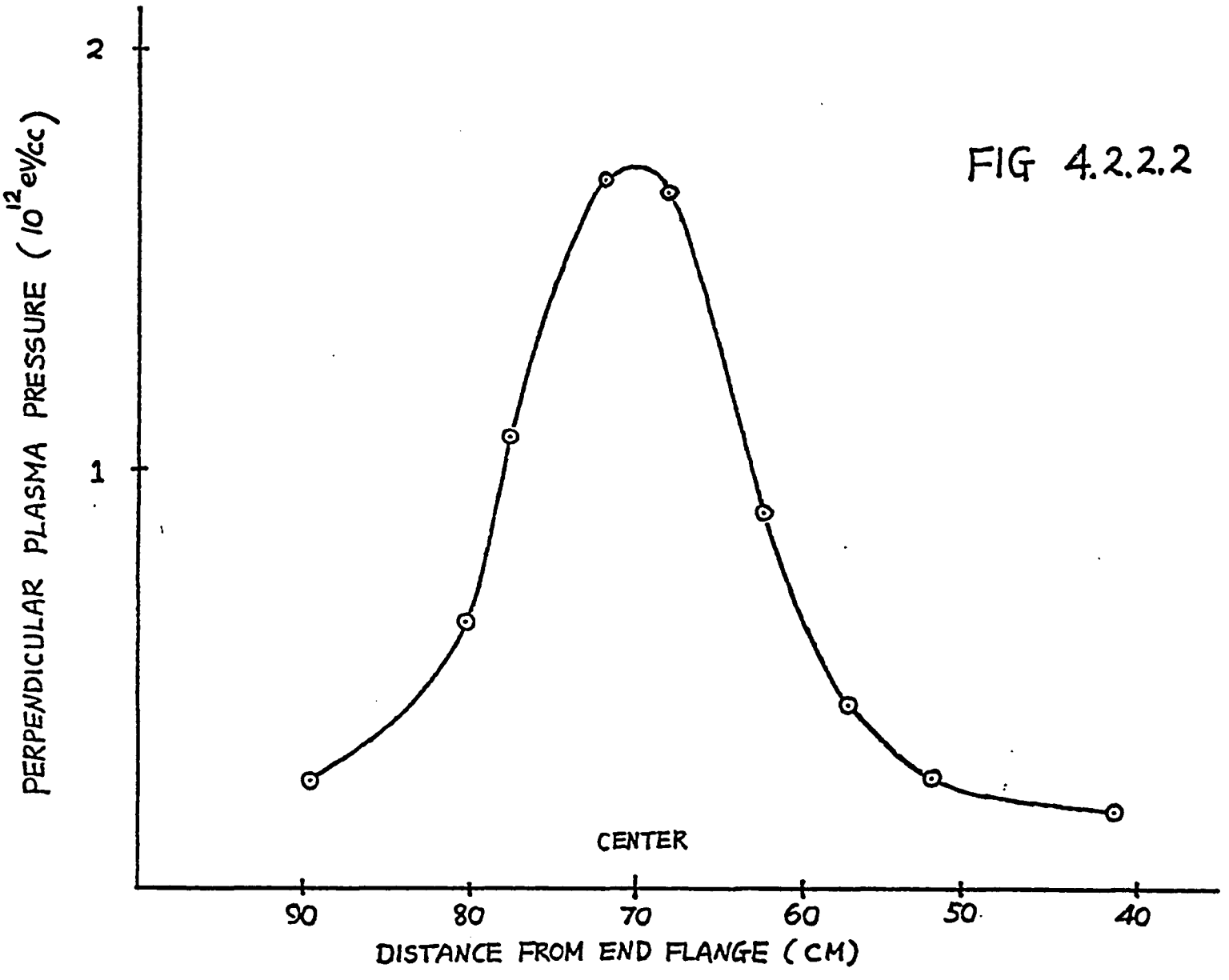
PERPENDICULAR PLASMA PRESSURE (10^{12} ev/cc)
2
1
CENTER
90
80
70
60
50
40
DISTANCE FROM END FLANGE (CM)

FIG 4.2.2.2

FIGURE CAPTIONS

Figure 4.2.3.1 Langmuir probe signals. In the upper half picture, the top trace is the Langmuir probe signal when the probe is biased at -20volts. The lower trace is the reflected microwave signal. The lower half picture is the same as the upper half, but the Langmuir probe is biased at -30 volts.

Figure 4.2.3.2 Langmuir probe characteristic curve.

Figure 4.2.3.3 Electron current vs applied voltage curve.

Figure 4.2.3.4 I_i^2 vs applied voltage curve.

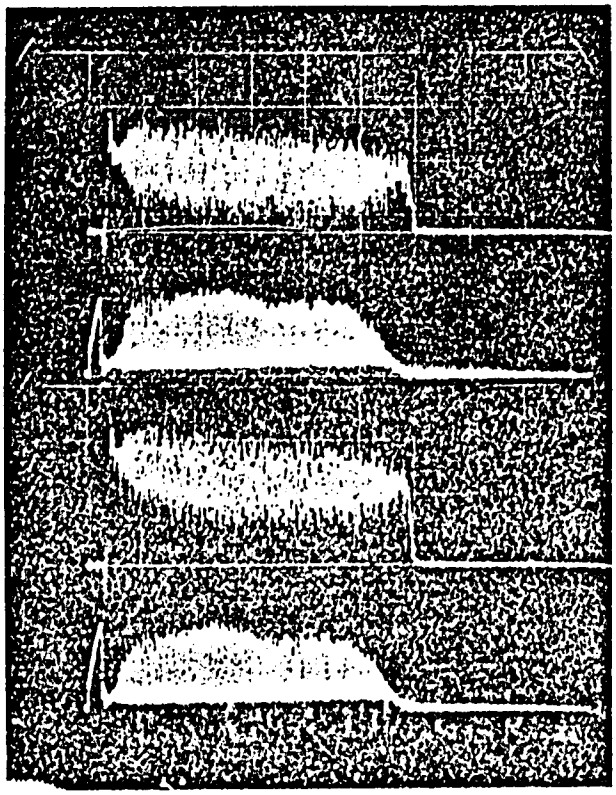

FIG 4.2.3.1

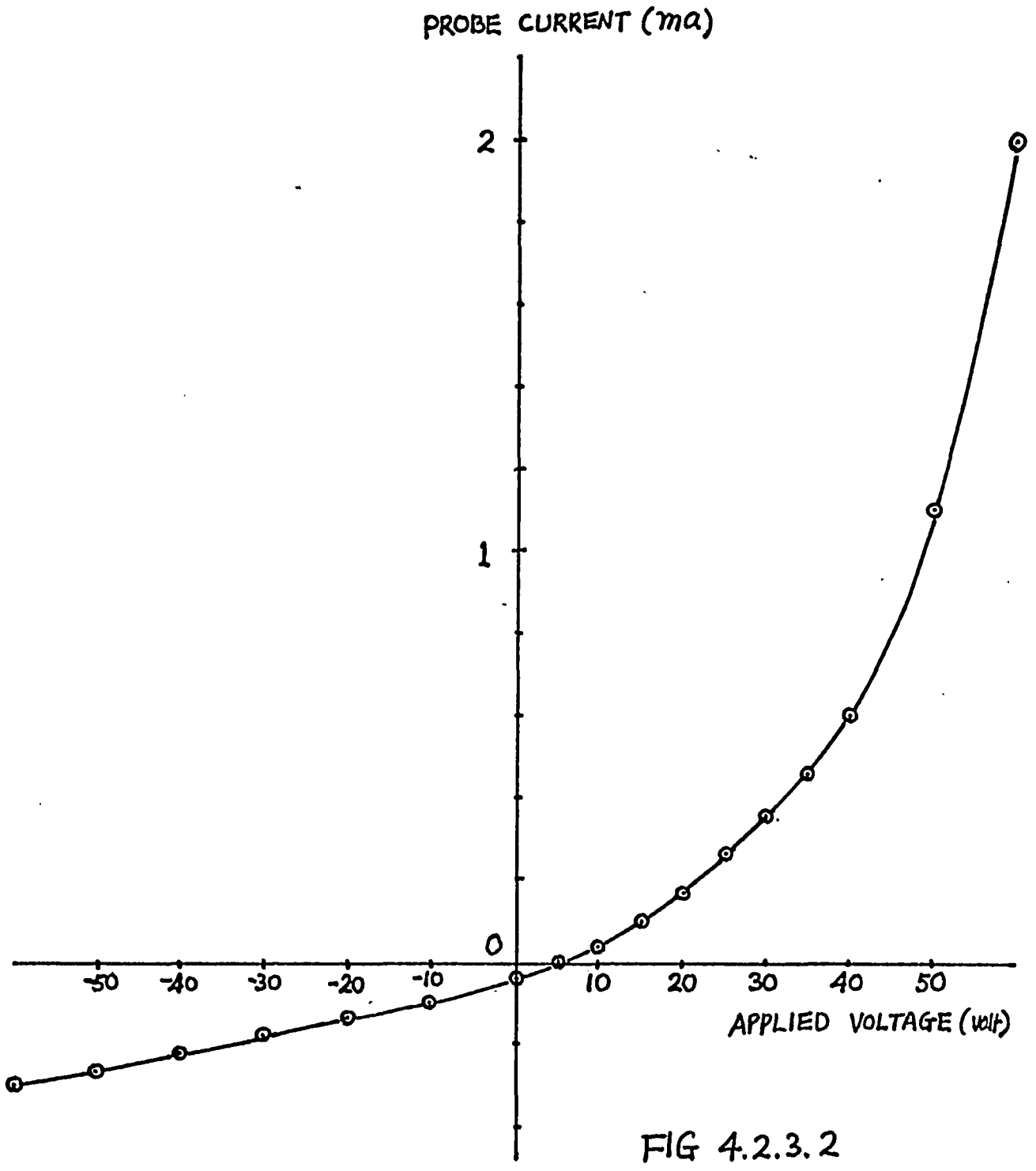
PROBE CURRENT (ma)
2
1
0
-50
-40
-30
-20
-10
10
20
30
40
50
APPLIED VOLTAGE (volt)

FIG 4.2.3.2

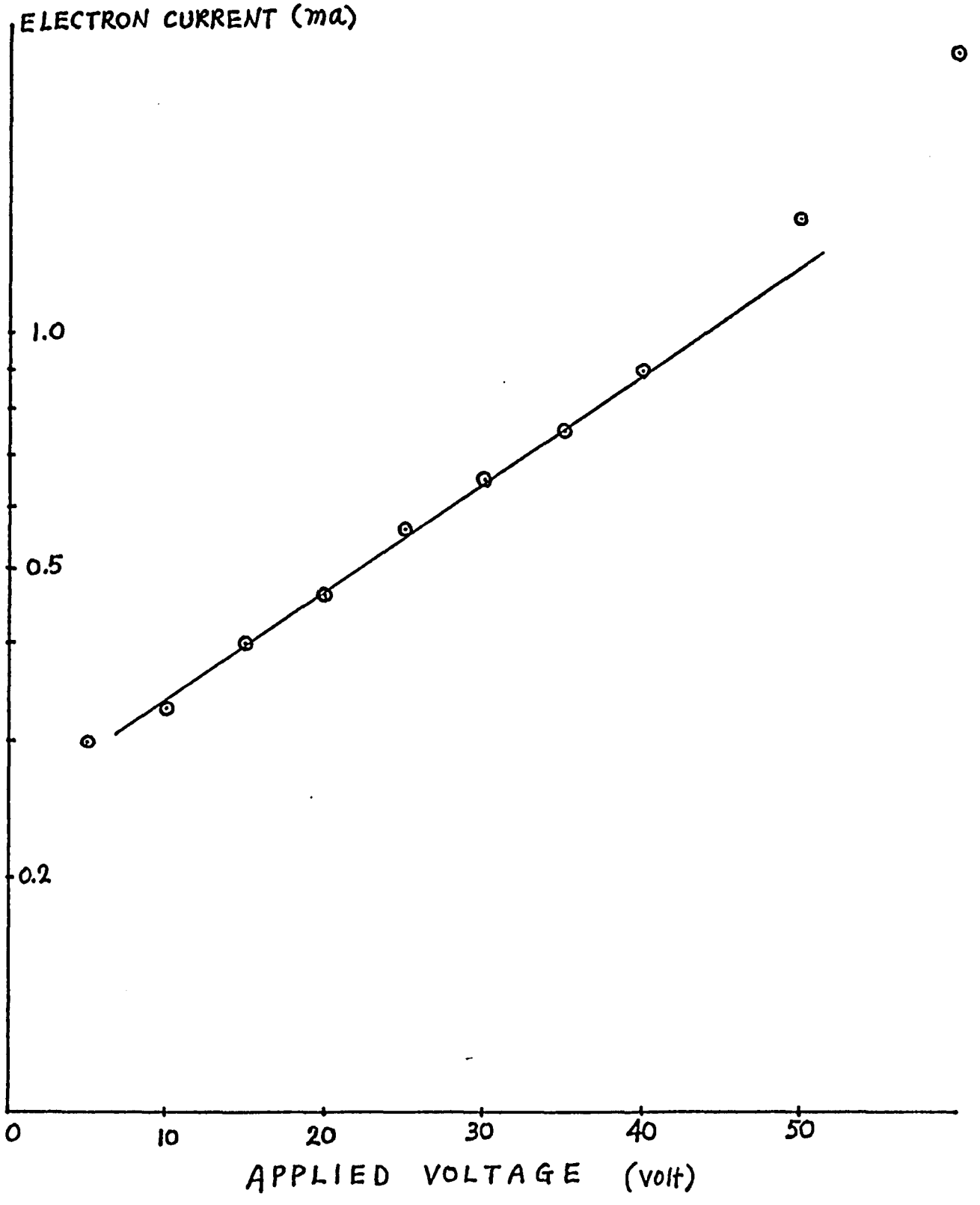
ELECTRON CURRENT (ma)
1.0
0.5
0.2
0
10
20
30
40
50
APPLIED VOLTAGE (volt)

FIG 4.2.3.3

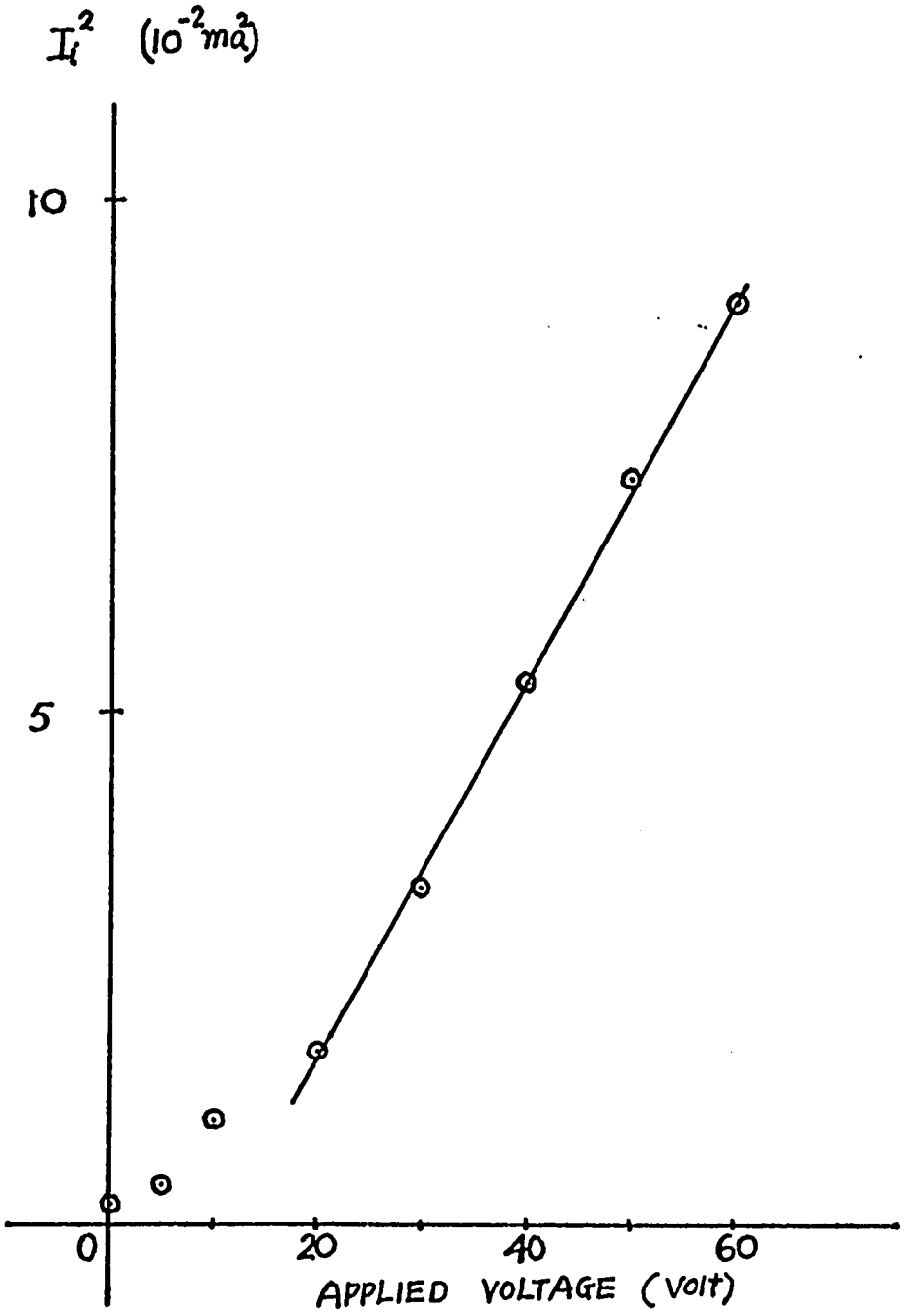

FIG 4.2.3.4

4.2.4 Microwave Interferometer

Experimentally, it is found that the K band transmitted microwave signal is changed due to multiple reflection. In order to estimate the density of plasma at midplane of plasma chamber, the following method was used. First, we measure the amplitude of the transmitted K band microwave signal when there is no plasma and the amplitude of the attenuated K band transmitted signal when there is plasma. The amplitude of the reference K band microwave signal is then set to that of the attenuated transmitted signal. Then adjust the phase shifter so that the signal amplitude from the adding arm of the magic T is equal to its half maximum. Reset the transmitted signal to its original amplitude. Then record the data when there is plasma. The upper half of figure 4.2.4.1 is the picture taken when there is plasma. The top trace is the transmitted K band microwave signal which remains unchanged while the lower trace signal from the adding arm of the magic tee is being recorded. The lower half of figure 4.2.4.1 was taken under the same condition as the upper half picture except that the phase shifter was adjusted so that the signal amplitude from the adding arm is at its maximum as indicated by the white arrow on figure 4.2.4.1. The density estimated from the upper picture is 4.4×10^{11}/cc. The density estimated from the lower picture is 3.5×10^{11}/cc. These numbers seem to be

high compare to the Langmuir probe data which is about 4.6×10^{10}/cc. It is possible that the density from the Langmuir probe data is lower because the probe is around the outer edge of the plasma, and we get a higher density around the center of the midplane of the plasma or due to the effects of multiple reflections.

FIGURE CAPTION

Figure 4.2.4.1 The top traces of both upper half and lower half picture are transmitted K band microwave signals. The lower trace of the upper picture is the interferometer output when the phase shifter is adjusted so that the signal from the adding arm of the magic tee is equal to its half maximum. The lower trace of the lower half picture is the interferometer output when the phase shifter is adjusted so that the signal from the adding arm of the magic tee is equal to its maximum.

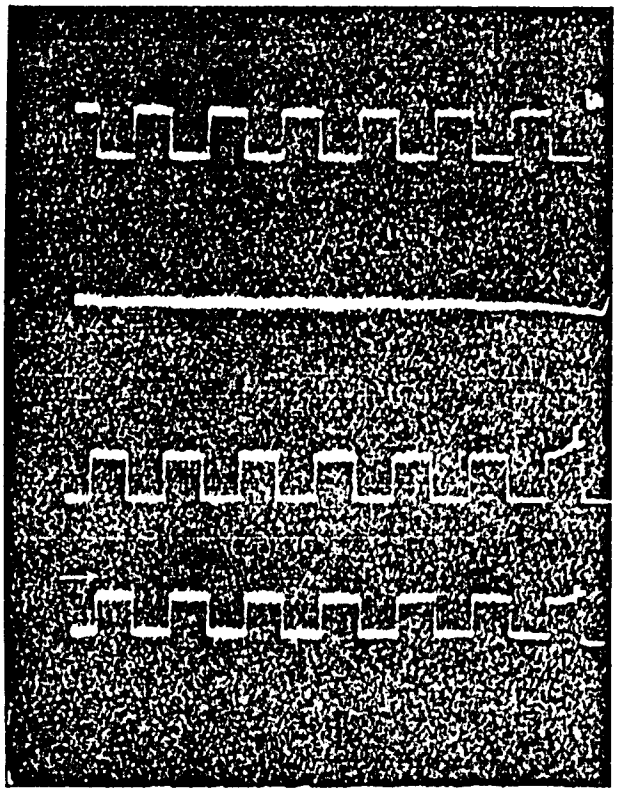

FIG 4.2.4.1

4.3 Detailed Study of The Modulations

As already mentioned we observed very strong modulation of all detected signals : reflected microwave signals, optical signals, loop probe signals, microwave interferometer signals. Experimentally, it is found that the modulation of signals, modulation frequency and the duration of the modulations all depend strongly on the neutral hydrogen pressure, incident microwave power and DC magnetic field. All These effects on the modulation will be presented in the following :

4.3.1 Reflected Signal

A General Appearance

The general appearance of the reflected microwave signal is shown in figure 4.3.1.1. The time scale is 1 ms/div. Figure 4.3.1.2 is taken at 2ms from the beginning of figure 4.3.1.1. The time scale is 5 μs/div. One can see that the modulation frequency is about 67 KHz. The modulation of the signal amplitude is about 86%.

B Growth Rate

The reflected signal is shown in figure 4.3.1.3. The sweep rate is 0.1 ms/div. One can see the rate of growth is about 1.4×10^4 /sec measured from 4.6 to 5.6 divisions of figure 4.3.1.3.

C Starting Power

When the neutral hydrogen pressure is about 2×10^{-5} torr, and the incident frequency is 2.43 GHz, the modulation of the reflected signals were observed when the incident power is above 90 watts. In figure 4.3.1.4, the top trace is the incident signal at about 90 watts, we see that the modulation of the reflected signal starts to appear.

D Variation of The Modulation Frequency

The modulation frequency depends strongly on neutral pressure, input power and magnetic field. The results are the following:

(1) Neutral Hydrogen Pressure

In figure 4.3.1.5, the modulation frequency is plotted against the neutral hydrogen pressure. It is clear that the modulation frequency increases with the neutral hydrogen pressure.

(2) Incident Power

In figure 4.3.1.6, the modulation frequency is plotted against the incident power. It seems clear that the modulation

frequency increases with the incident power when the incident power is between 110 and 120 watts but remains unchanged otherwise.

(3) Aiding Coil Current

In order to change the maximum fields separation, the Aiding coil was used. The variation of the modulation frequency with the Aiding coil current is shown in figure 4.3.1.7. The magnetic field profile is shown in figure 4.3.1.8. It seems clear that when we increased the Aiding coil current, we decreased the length of the plasma and we increased the modulation frequency.

(4) DC Magnetic Field Current

The effect of the DC magnetic field current setting on the modulation frequency is indicated in figure 4.3.1.9. It is seen that the modulation frequency remains unchanged when the DC magnetic field current is between 27.5 and 28.5 amp and disappeared when the DC magnetic field current is outside this range. The magnetic field profiles of different DC magnetic field current settings is shown in figure 4.3.1.10.

E Duration of The Modulation of Signals

The modulation duration of signals depends strongly on neutral hydrogen pressure, input power and magnetic field. The results are the following:

(1) Neutral Hydrogen Pressure

The duration of the modulation of signals is affected greatly by the neutral hydrogen pressure. The modulation of signals appears in a narrow region of 2.0×10^{-5} to 3.4×10^{-5} torr when the input microwave frequency is at 2.43 GHz. Outside this region, the modulation disappeared. In figure 4.3.1.11, the duration of the modulation vs the neutral hydrogen pressure is plotted. From this graph, one can see that the duration of the modulation decreased as the neutral hydrogen pressure increased.

(2) Input Microwave Power

The duration of the modulation depends on the input microwave power. In figure 4.3.1.12, the modulation duration vs the incident microwave power is plotted. There is a narrow incident microwave power range

of 60 watts over which one can see the modulation. Outside the range, the modulation disappeared.

(3) DC Magnetic Field Current

The duration of the modulation also depends on the DC magnetic current. The modulation duration vs DC magnetic field current is plotted in figure 4.3.1.13. One can see that the modulation is stable when the DC magnetic field current is about 28 amp. The modulation disappears when the DC magnetic field current is below 27.5 amp and above 28.5 amp.

F Spectral Analysis

When the reflected signal is connected to the microwave receiver, the spectrum determined as a shot by shot basis is shown on figure 4.3.1.14. Figure 4.3.1.15 shows the reflected signal when it is connected to the spectrum analyzer. The center frequency is 2.43 GHz. Sweeping rate is 0.1 ms. The dispersion is set at 100 KHz/div. One can see that is a small peak on each side of the central frequency. Figure 4.3.1.17 shows the setup of simulated

amplitude modulation of microwave signal. A microwave signal of 2.43 GHz is amplitude modulated at 70 KHz using a General Microwave model 1952 pin modulator. The amplitude modulated signal is displayed on figure 4.3.1.16 with spectrum analyzer center frequency at 2.43 GHz, sweeping rate .2ms and dispersion 100 KHz. We can see that the two figures are very similar.

FIGURE CAPTIONS

Figure 4.3.1.1 Microwave reflected signal. The time scale is 1 ms/div.

Figure 4.3.1.2 Reflected signal at 2 ms from the beginning of figure 4.3.1.1. The time scale is 5 μs/div.

Figure 4.3.1.3 Beginning part of the reflected signal. The time scale is 0.1 ms/div.

Figure 4.3.1.4 Incident microwave signal at 90 watts.

Figure 4.3.1.5 Modulation frequency vs neutral hydrogen pressure.

Figure 4.3.1.6 Modulation frequency vs incident power.

Figure 4.3.1.7 Modulation frequency vs Aiding coil current setting.

Figure 4.3.1.8 DC magnetic field profile (with Aiding coil magnetic field).

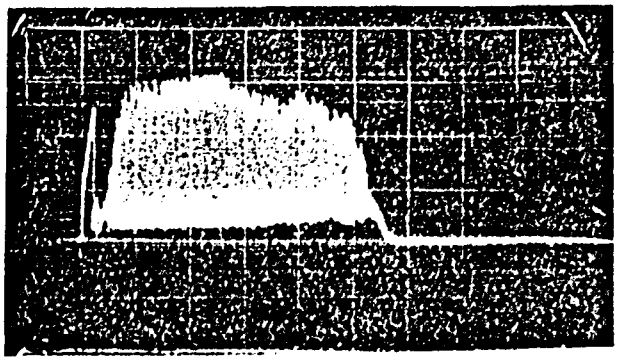

FIG 4.3.1.1

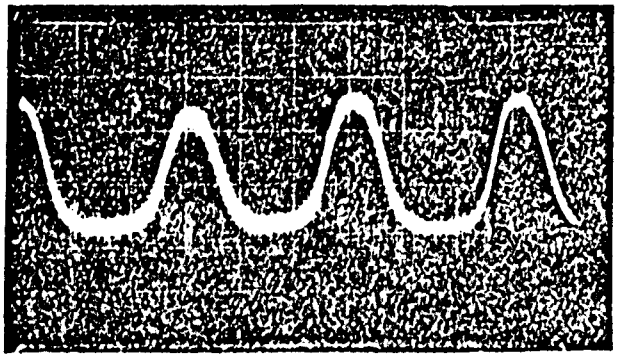

FIG 4.3.1.2

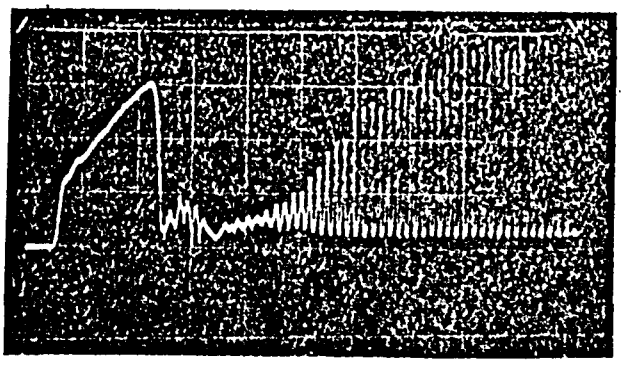

FIG 4.3.1.3

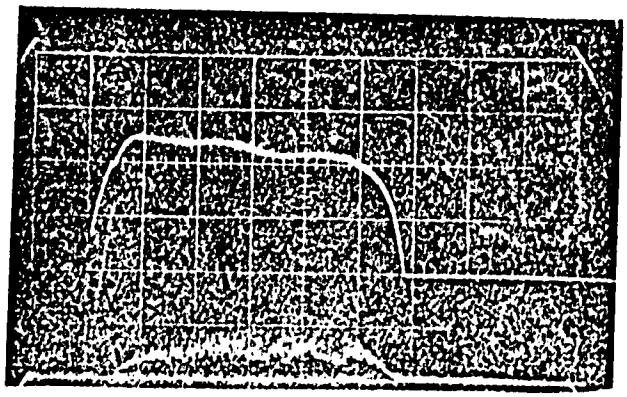

FIG 4.1.3.4

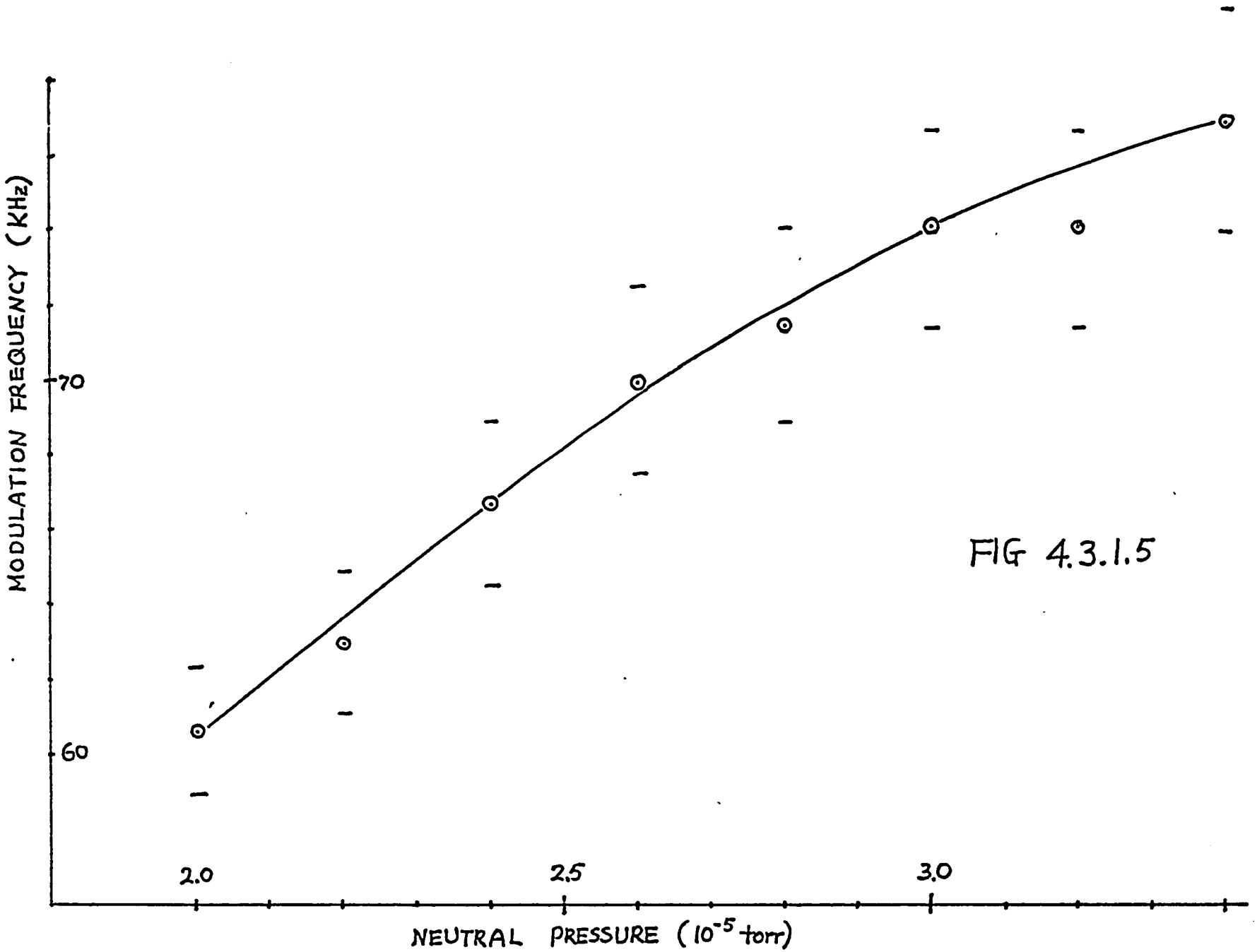
MODULATION FREQUENCY (KHz)
70
60
2.0
2.5
3.0
NEUTRAL PRESSURE (10^{-5} torr)

FIG 4.3.1.5

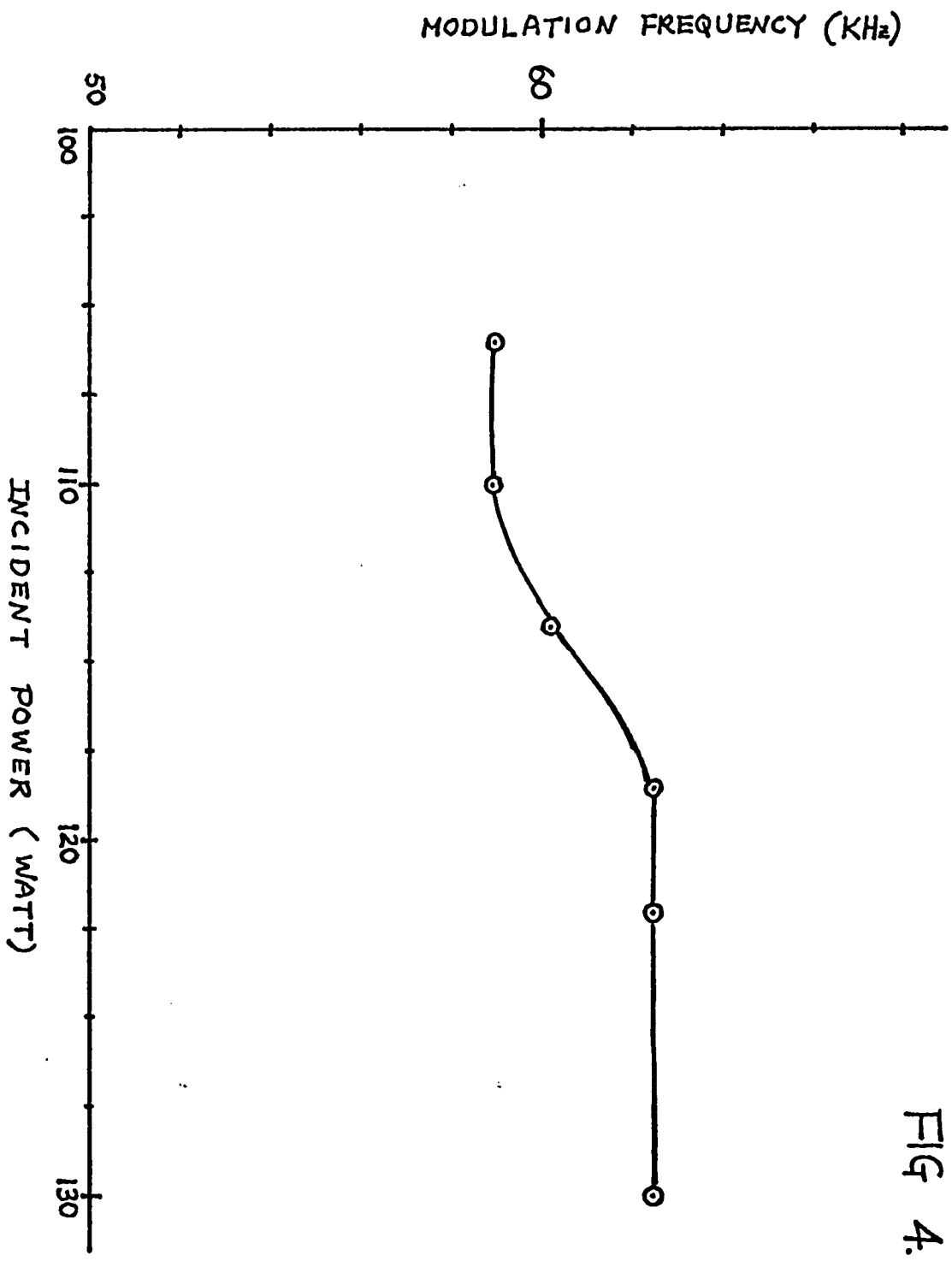
MODULATION FREQUENCY (KHz)
8
50
100
110
120
130
INCIDENT POWER (WATT)

FIG 4.3.1.6

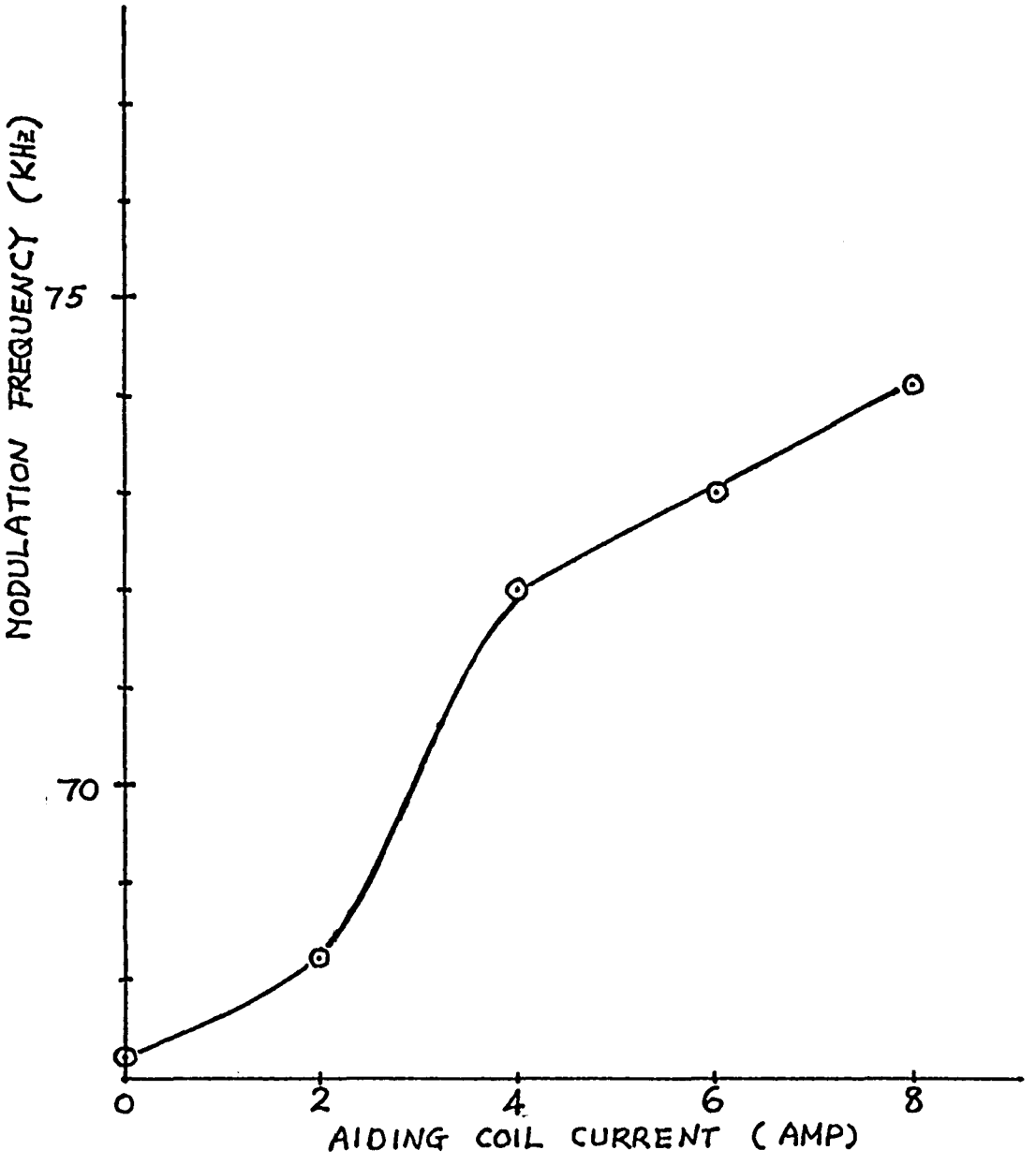
MODULATION FREQUENCY (KHz)
75
70
0
2
4
6
8
AIDING COIL CURRENT (AMP)

FIG 4.3.1.7

FIG 4.3.1.8

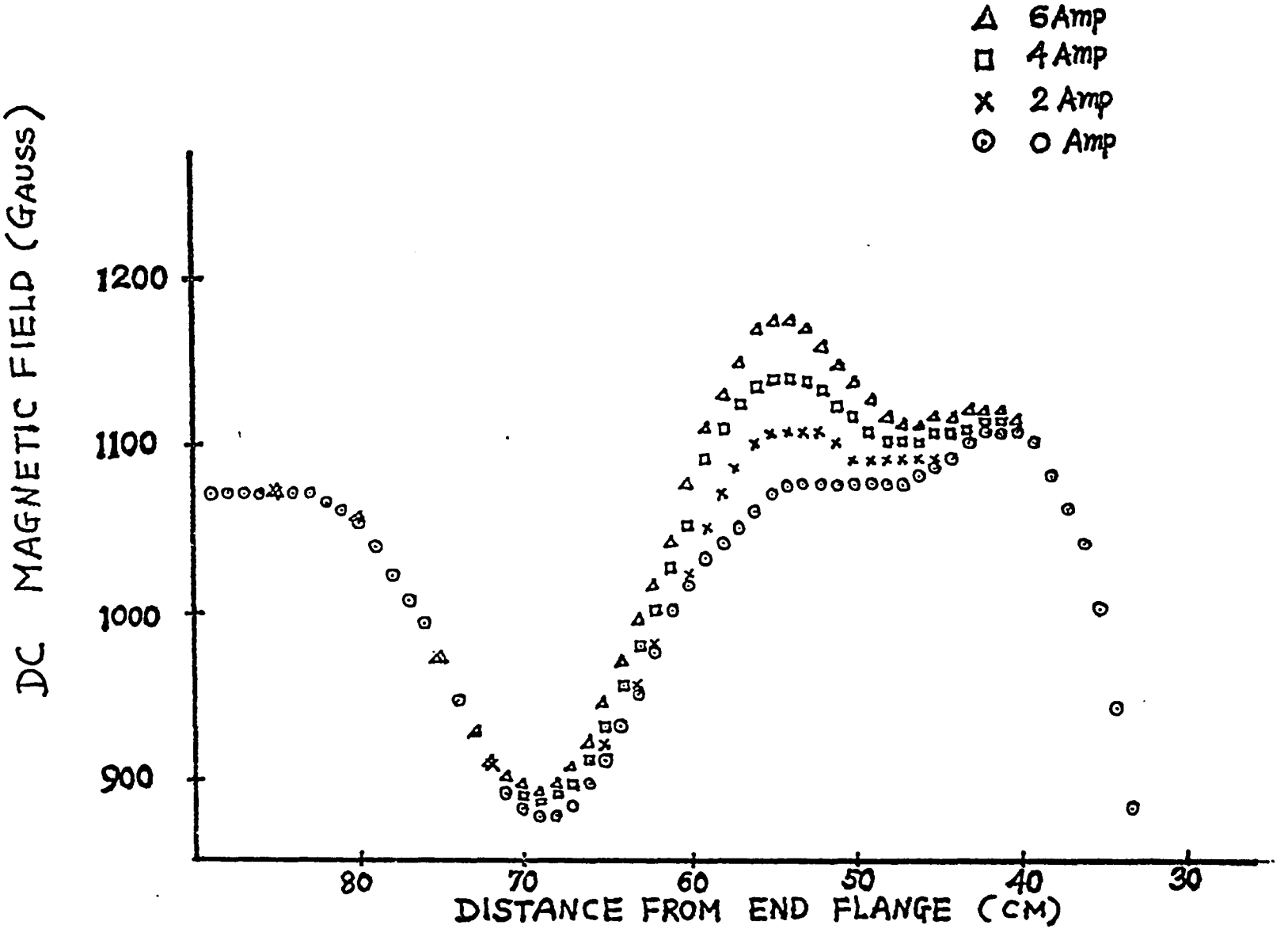
6 Amp
4 Amp
2 Amp
0 Amp
DC MAGNETIC FIELD (GAUSS)
1200
1100
1000
900
80
70
60
50
40
30
DISTANCE FROM END FLANGE (CM)

FIGURE CAPTIONS

Figure 4.3.1.9 Modulation frequency vs DC magnetic field current.

Figure 4.3.1.10 DC magnetic field profiles of different DC magnetic field current settings.

Figure 4.3.1.11 Modulation duration vs neutral hydrogen pressure.

Figure 4.3.1.12 Modulation duration vs incident power.

Figure 4.3.1.13 Modulation duration vs DC magnetic field current setting.

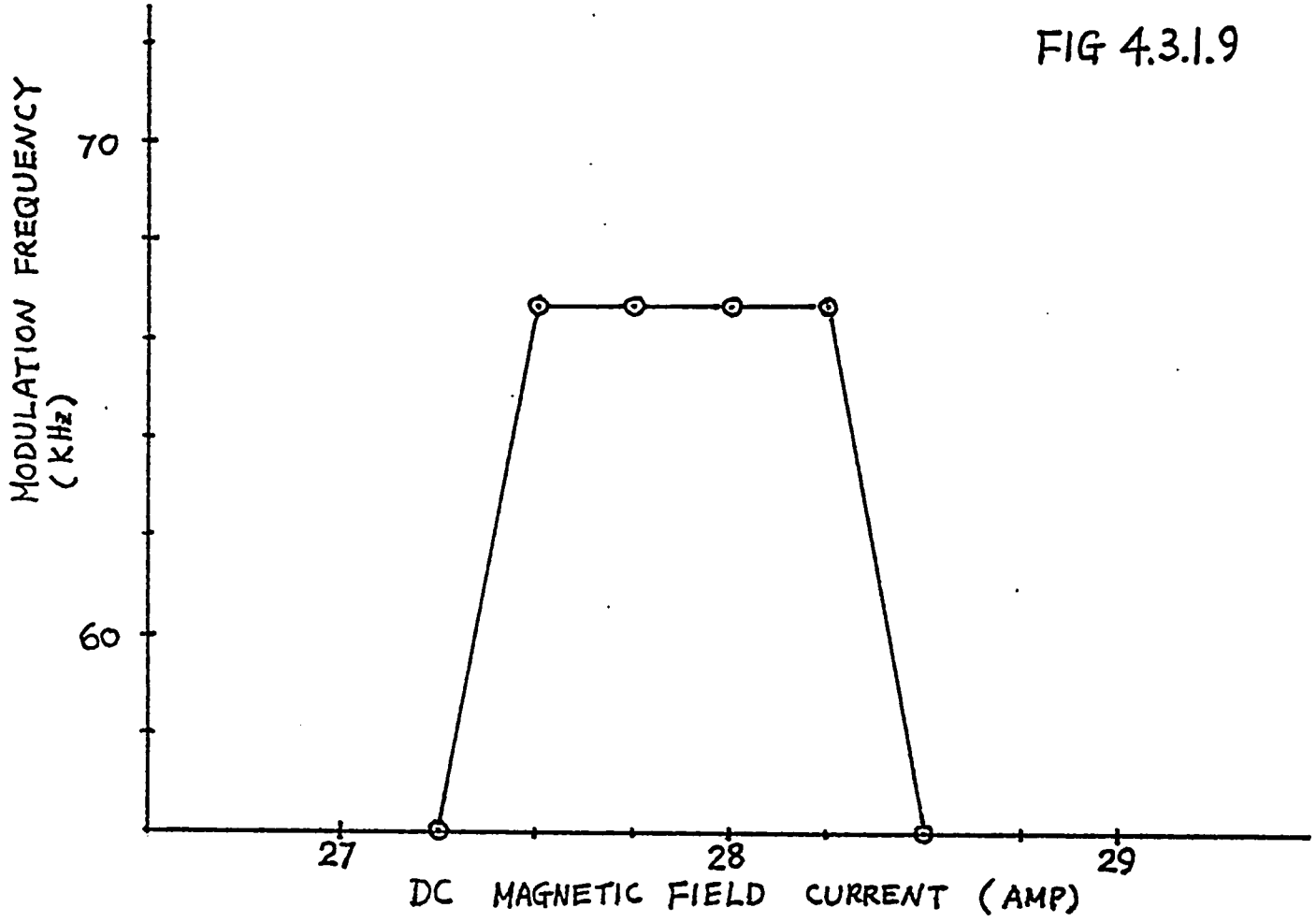
MODULATION FREQUENCY
(kHz)
70
60
27
28
29
DC MAGNETIC FIELD CURRENT (AMP)

FIG 4.3.1.9

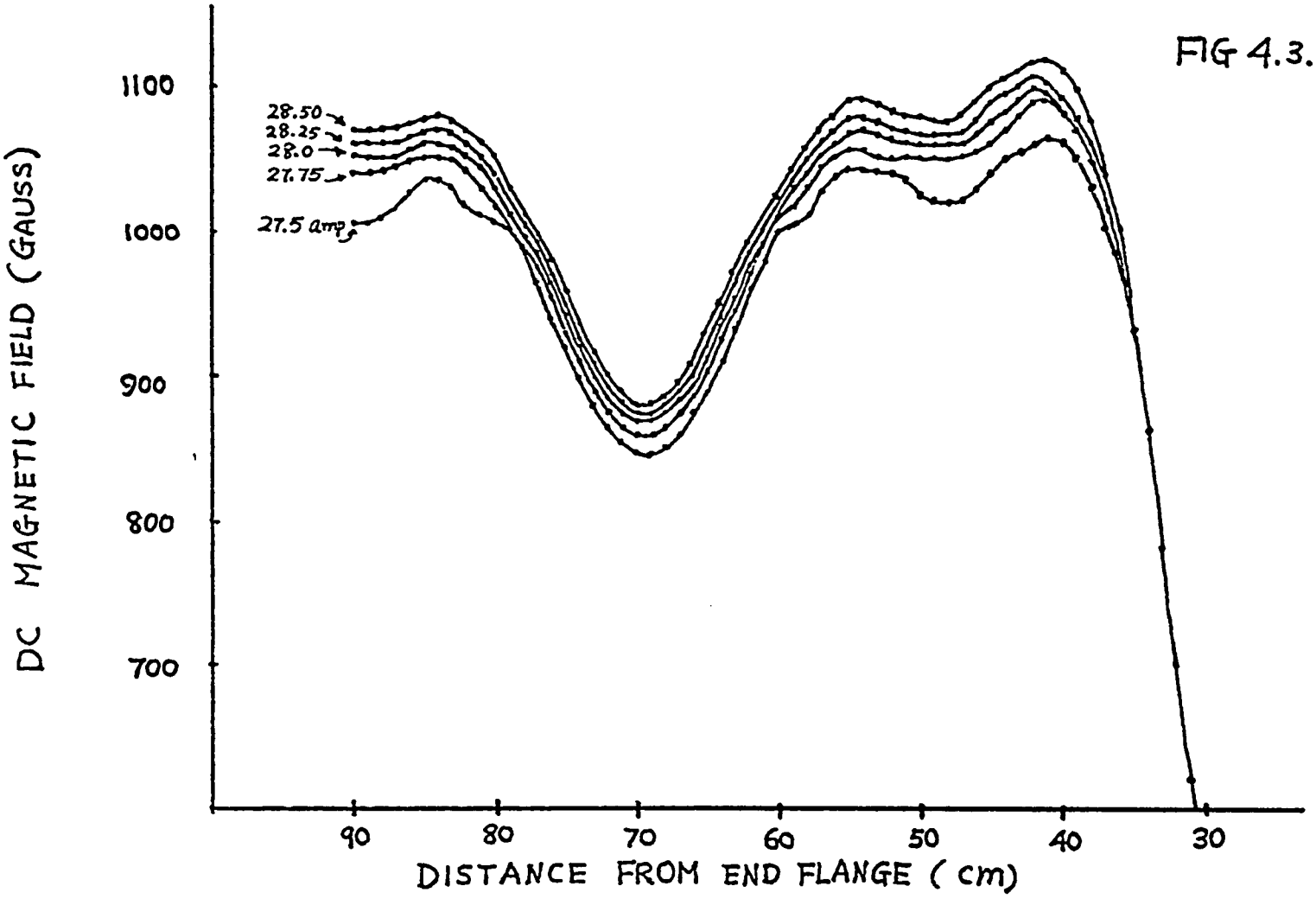
DC MAGNETIC FIELD (GAUSS)
1100
1000
900
800
700
28.50
28.25
28.0
27.75
27.5 amps
90
80
70
60
50
40
30
DISTANCE FROM END FLANGE (cm)

FIG 4.3.1.10

FIG 4.3.1.11

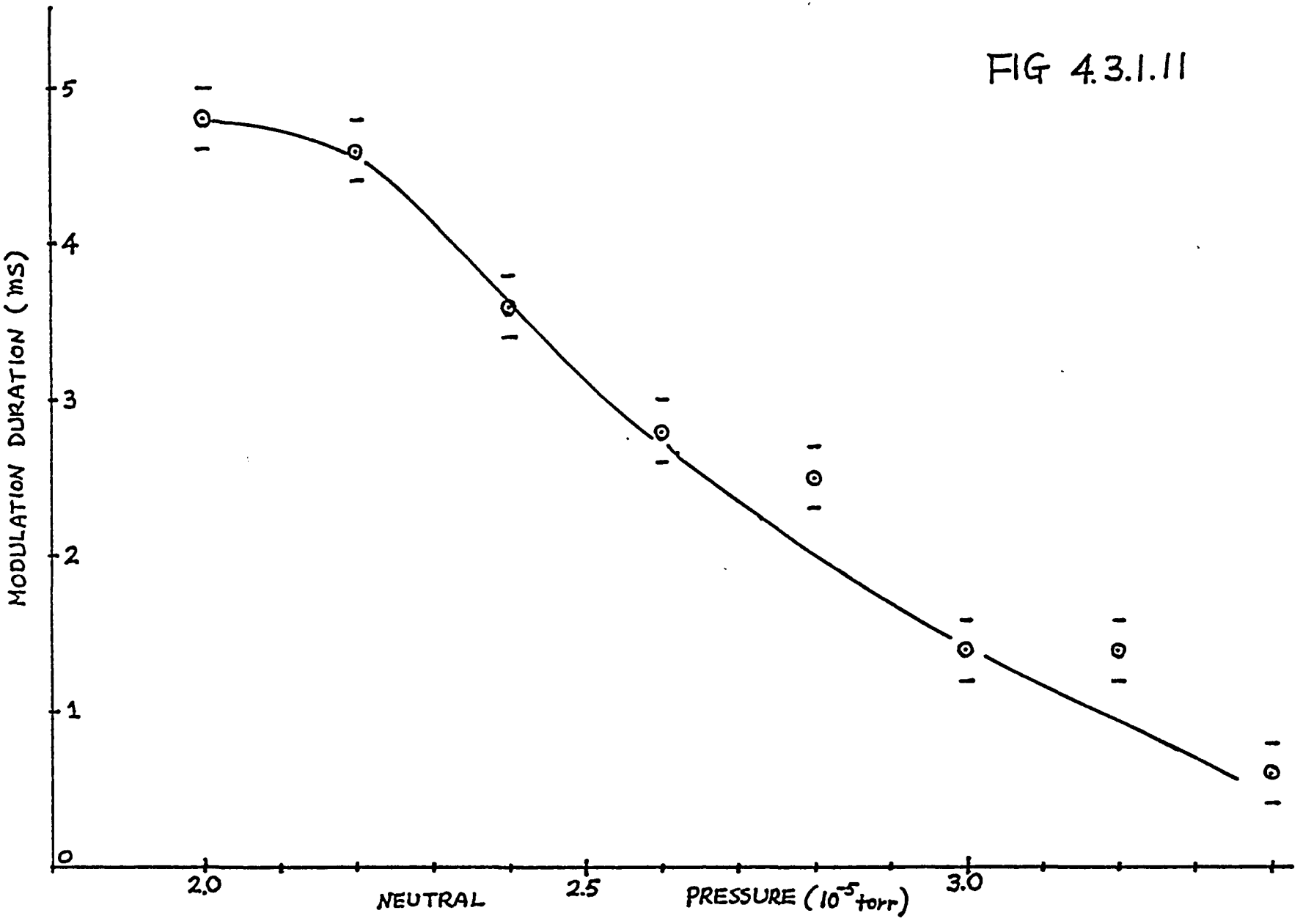
MODULATION DURATION (mS)
0
1
2
3
4
5
2.0
2.5
3.0
NEUTRAL PRESSURE (10^{-5} torr)

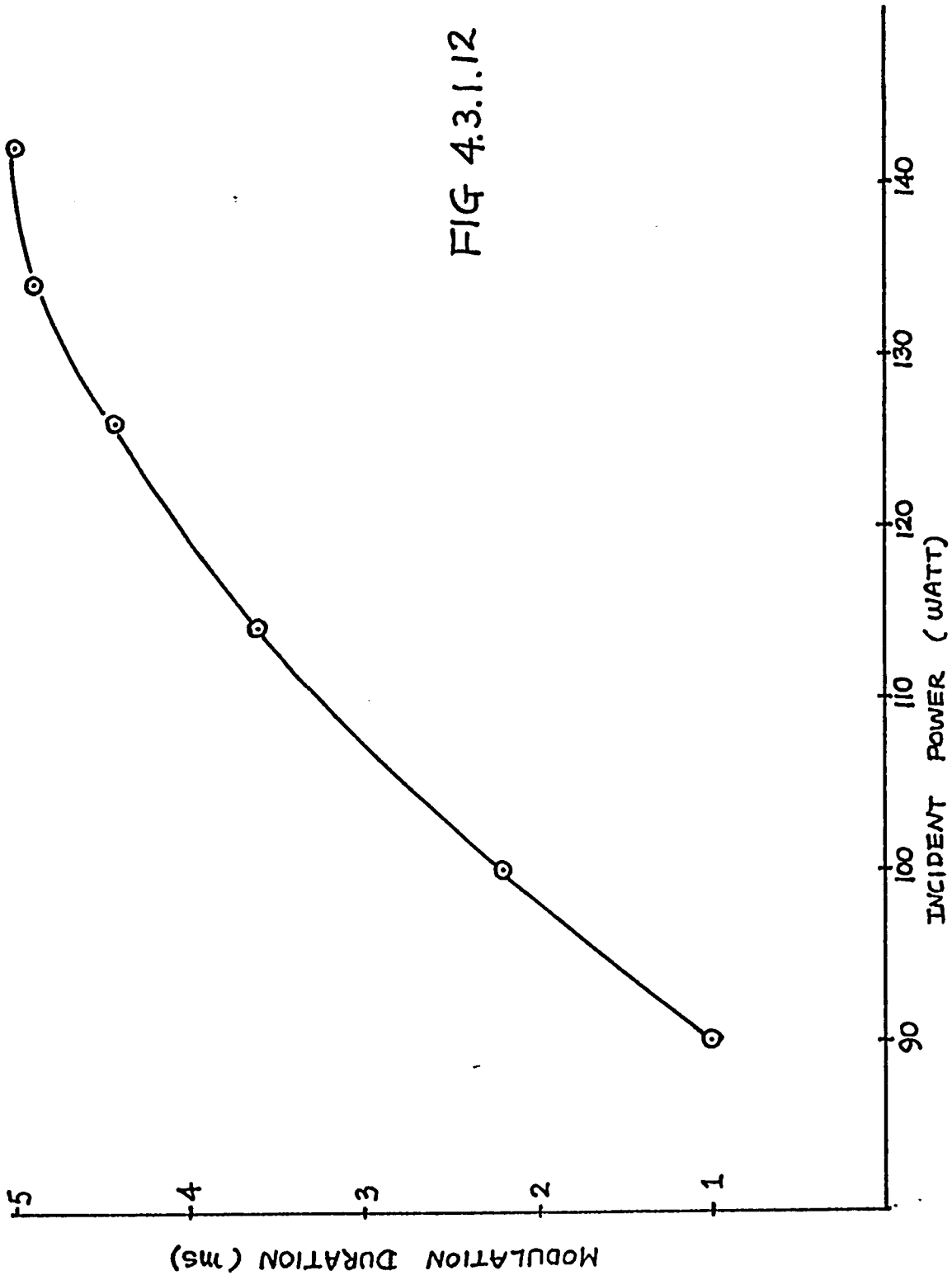
MODULATION DURATION (ms)
1
2
3
4
5
90
100
110
120
130
140
INCIDENT POWER (WATT)

FIG 4.3.1.12

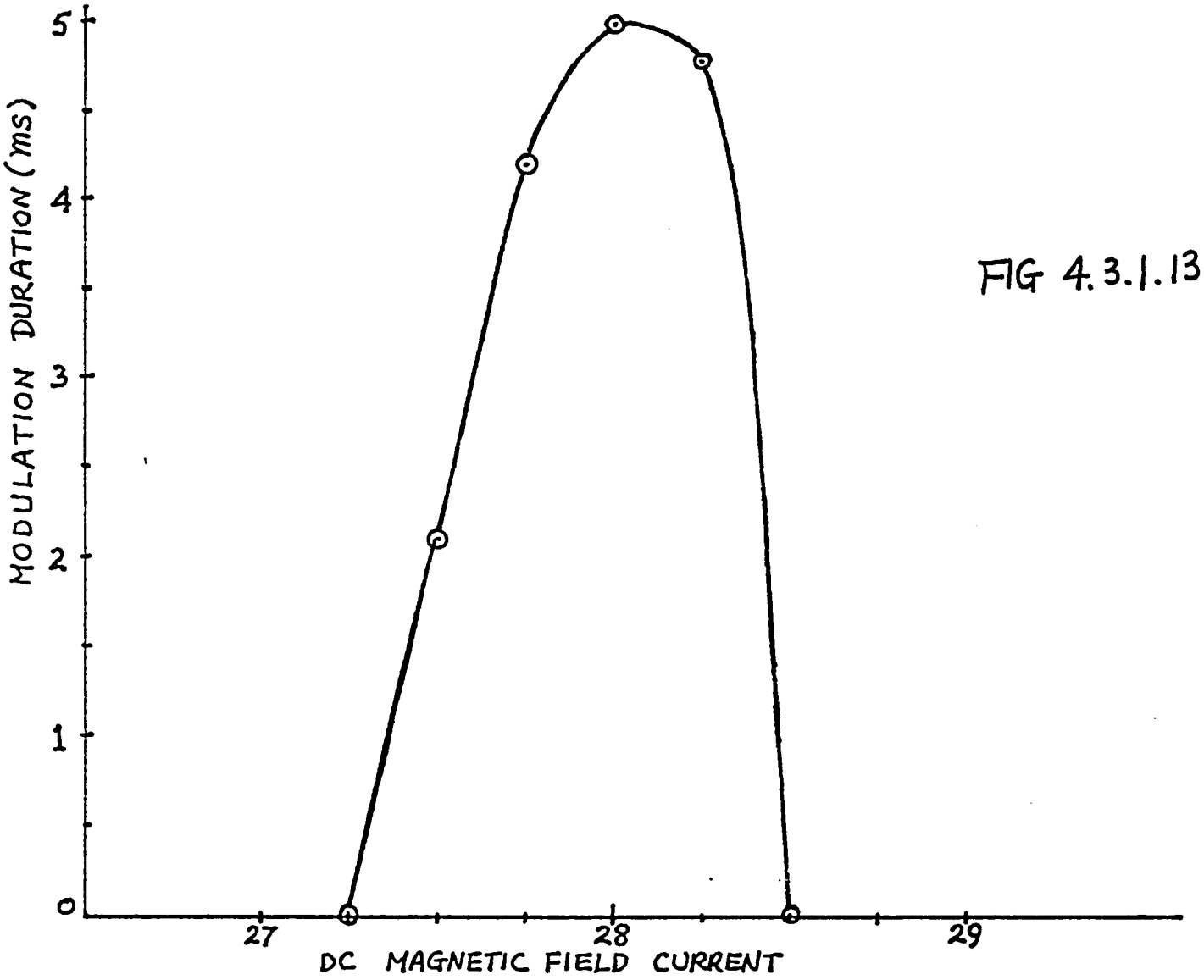
MODULATION DURATION (ms)
5
4
3
2
1
0
27
28
29
DC MAGNETIC FIELD CURRENT

FIG 4.3.1.13

FIGURE CAPTIONS

Figure 4.3.1.14 Microwave receiver frequency spectrum of reflected signal.

Figure 4.3.1.15 The upper trace is the reflected signal. The lower trace is the spectrum analyzer output signal. The sweeping rate is 0.1 ms. The dispersion is at 100 KHz. The central frequency is set at 2.43 GHz.

Figure 4.3.1.16 Spectrum analyzer output signal of a microwave signal amplitude modulated at 70 KHz. The center frequency of the spectrum analyzer is at 2.43 GHz. The dispersion is 100 KHz. The sweeping rate is 0.2 ms.

Figure 4.3.1.17 Setup for stimulated amplitude modulation of microwave signal.

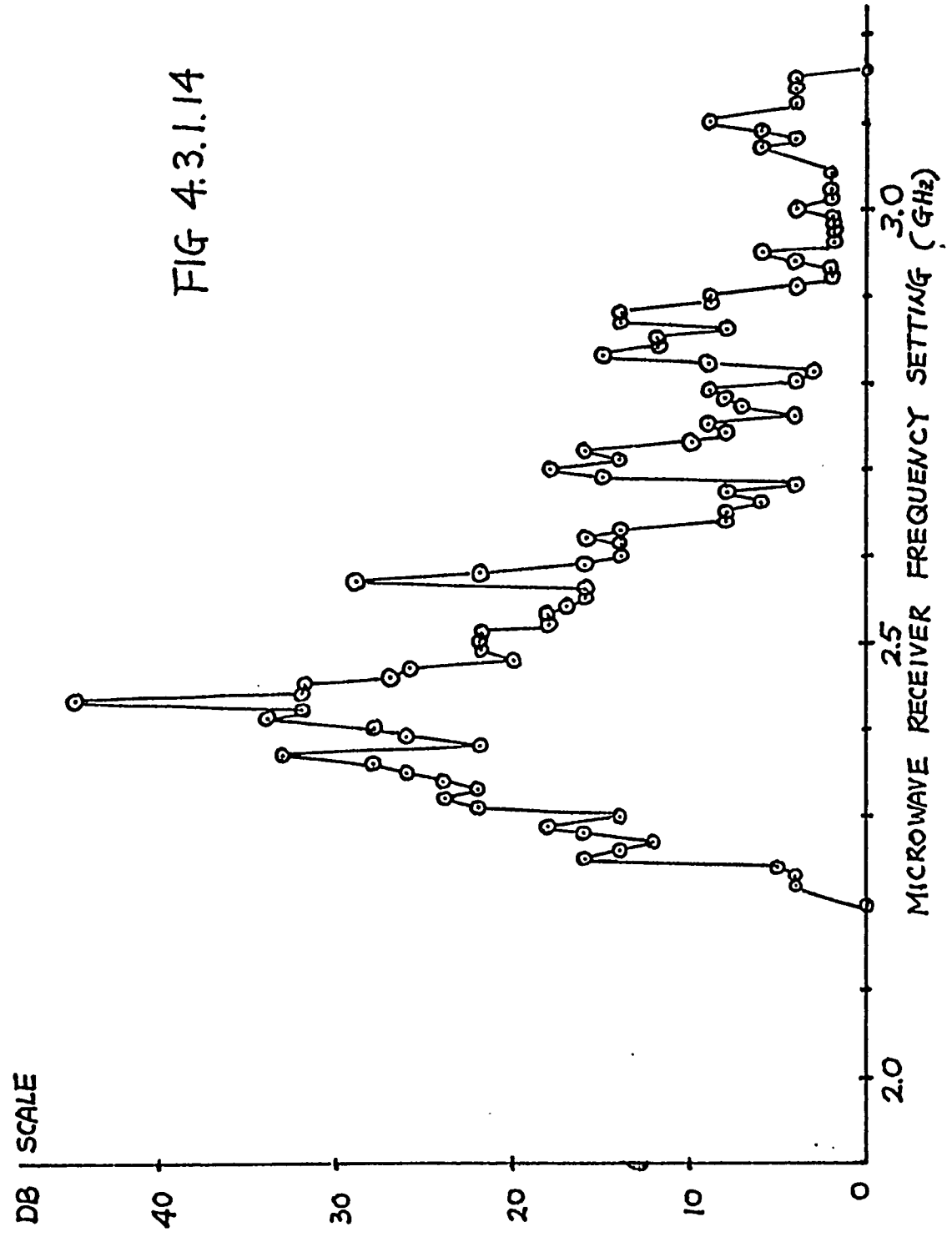
DB SCALE
40
30
20
10
0
2.0
2.5
3.0
MICROWAVE RECEIVER FREQUENCY SETTING (GHz)

FIG 4.3.1.14

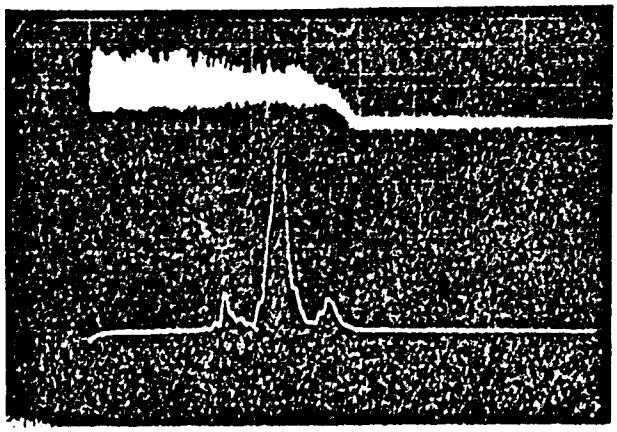

FIG 4.3.1.15

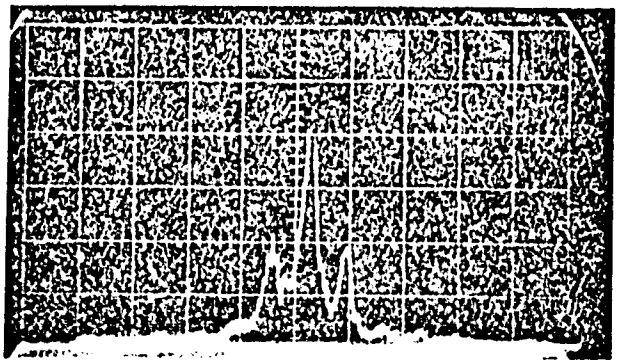

FIG 4.3.1.16

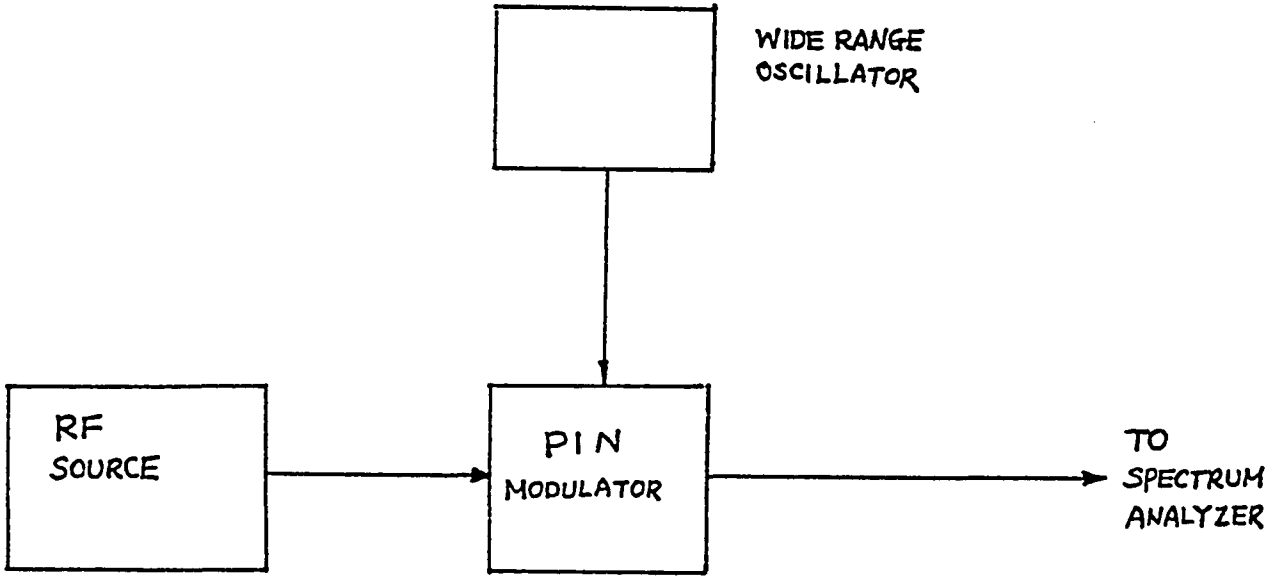
WIDE RANGE
OSCILLATOR
RF
SOURCE
PIN
MODULATOR
TO
SPECTRUM
ANALYZER

FIG 4.3.1.17

4.3.2 Detailed Look at Diamagnetic Loop Probe Signals

In figure 4.3.2.1, the top trace is the reflected signal, the lower trace is the integrated diamagnetic loop signal. The top picture is at 1 ms/div. The perpendicular plasma pressure is about 1.78×10^{12} ev/cc at the midpoint of the pulse. In the lower picture, the two traces are the same as the upper picture. The time scale is 10 μs/div. The peak to peak change in the perpendicular plasma pressure $\Delta(neTe)$ is about 1.78×10^{11} ev/cc. The ratio $\frac{\Delta(neTe)}{neTe}$ is about 0.1. One can see that the integrated diamagnetic signal peaks are about 3 μs ahead of the peaks of the reflected signal.

In figure 4.3.2.2, the reflected signal and the unintegrated diamagnetic coil signal are shown. The top picture is at 1 ms/div. The lower picture is at 5 μs/div. $\Delta(neTe)$ is about 1.64×10^{11} ev/cc which is about the same of that of the integrated signal. The zeroes of the unintegrated signal are about 3 μs ahead of the reflected signal peaks.

Experimentally, all the unintegrated signals are in phase as shown on figure 4.3.2.3. In figure 4.3.2.4, the top signal is the unintegrated signal, the lower signal is the integrated signal. We see that the unintegrated signal and the integrated signal are out of phase by $\frac{\pi}{2}$. The straight line on the unintegrated signal is the zero line. The maxima of the integrated signal correspond to the zeroes of the unintegrated

signals. In figure 4.3.2.5, the change in the perpendicular plasma $\Delta P_{\perp}$ is plotted. $\Delta P_{\perp}$ is lower than that of figure 4.3.2.1 and figure 4.3.2.2 because lower incident power was used.

FIGURE CAPTIONS

Figure 4.3.2.1 In both the upper and lower half picture, the top traces are the reflected signals and the lower traces are the integrated diamagnetic coil signals. In the upper half picture, the time scale is 1 ms/div. In the lower half picture, the time scale is 10 μs/div.

Figure 4.3.2.2 In both the upper and lower half picture, the top traces are the reflected signals and the lower traces are the unintegrated diamagnetic coil signals. In the upper half picture, the time scale is 1 ms/div. In the lower half picture, the time scale is 5 μs/div.

Figure 4.3.2.3 Unintegrated signals from 5 different diamagnetic coils. The time scale is 20 μs/div.

Figure 4.3.2.4 The upper trace is the unintegrated diamagnetic coil signal. The lower trace is the integrated diamagnetic coil signal. The time scale is 10 μs/div.

Figure 4.3.2.5 ΔR vs the diamagnetic coil location.

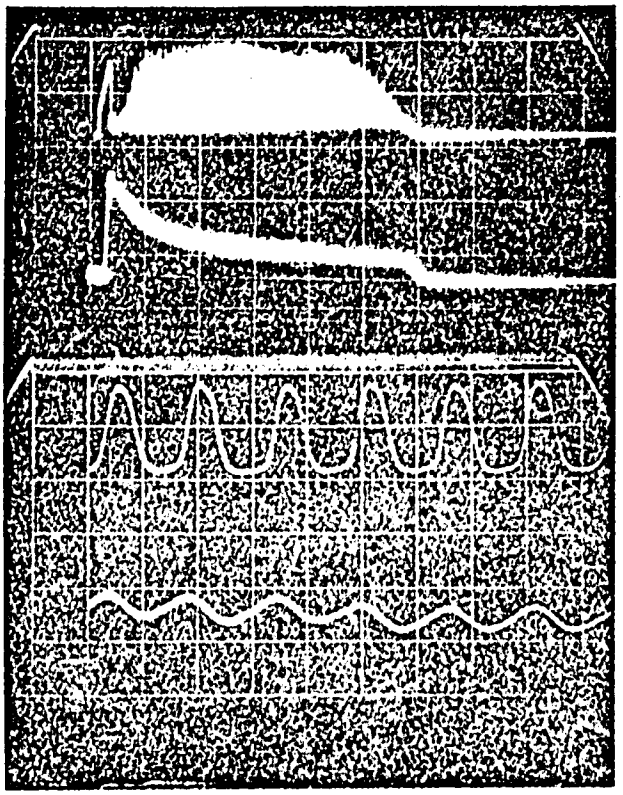

FIG 4.3.2.1

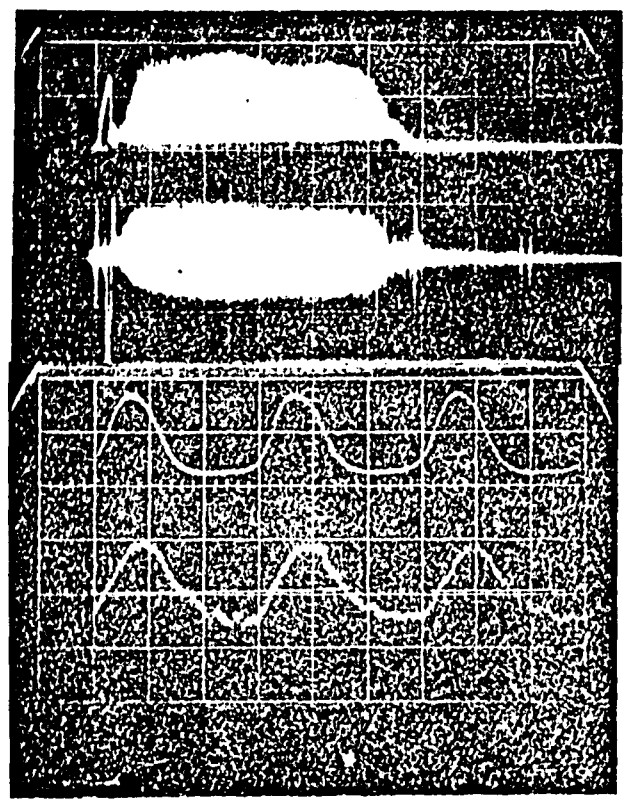

FIG 4.3.2.2

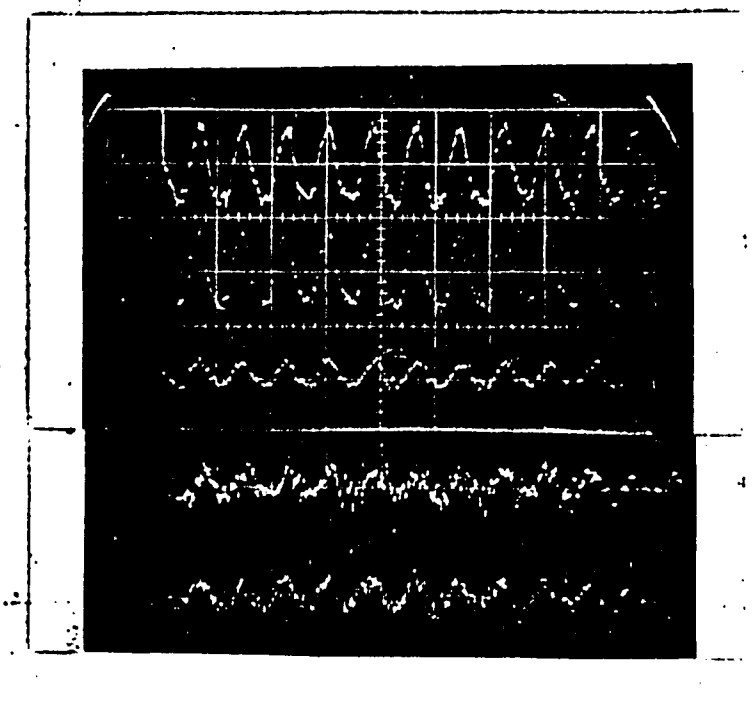

FIG 4.3.2.3

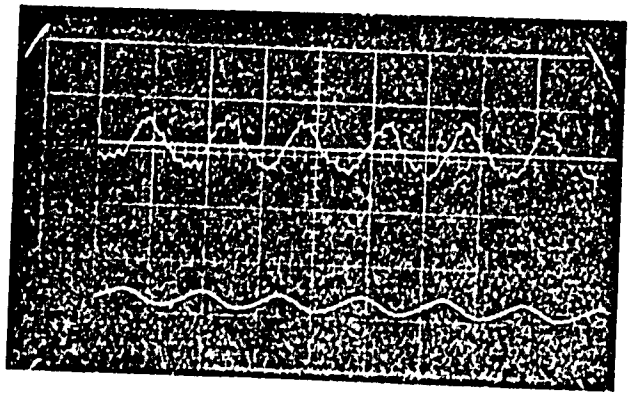

FIG 4.3.2.4

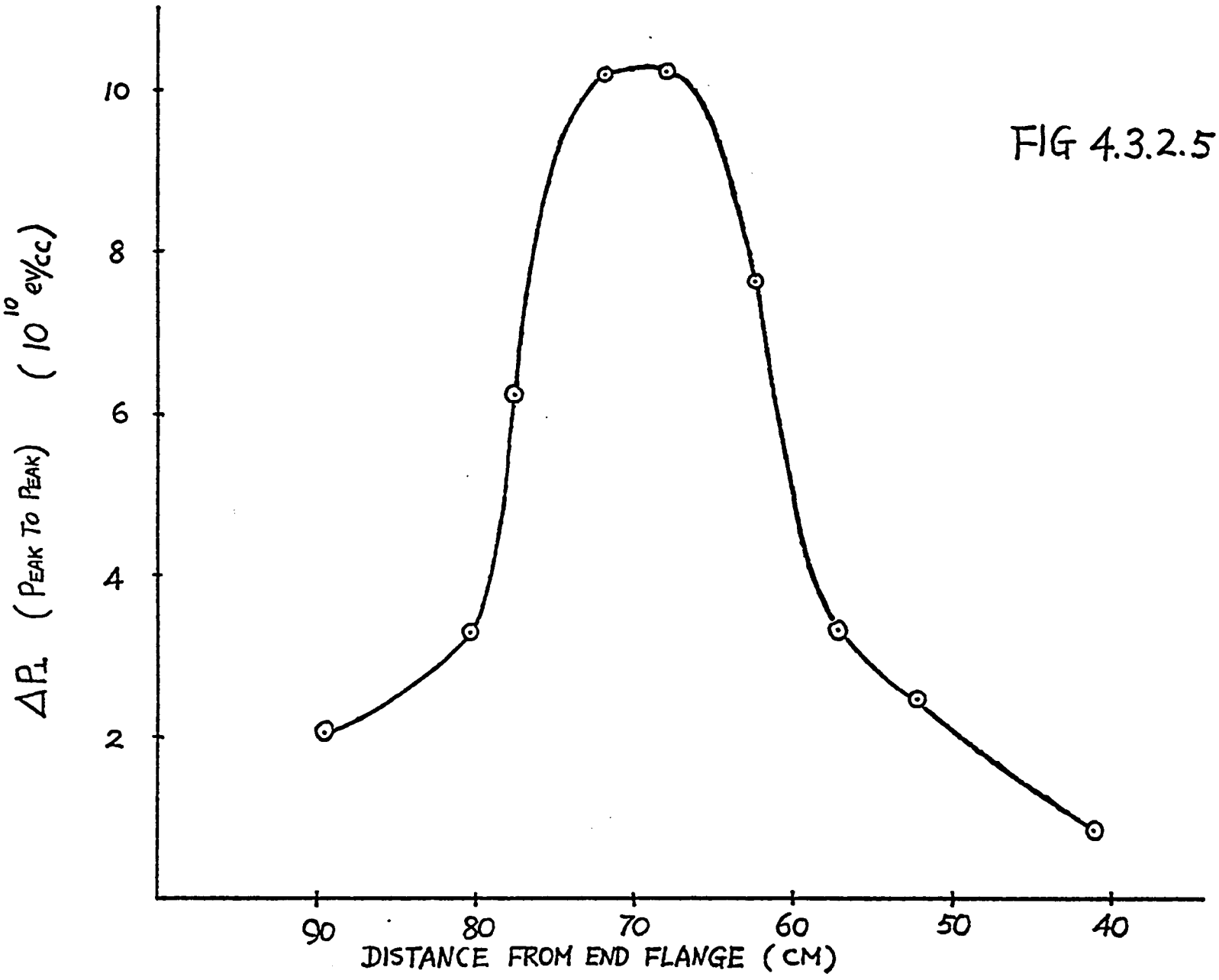
10
8
6
4
2
$\Delta P_\perp$ (PEAK TO PEAK) (10^{10} ev/cc)
90
80
70
60
50
40
DISTANCE FROM END FLANGE (CM)

FIG 4.3.2.5

4.3.3 Optical Signals

The upper trace of 4.3.3.1 shows a portion of the optical signal taken from the side at the center of the chamber. In figure 4.3.3.2, we show the optical signal taken from the end of the chamber. The lower trace in both case is the reflected signal. One can see that both optical signals are about 3.5 μs ahead of the reflected signal. In figure 4.3.3.3, 4.3.3.4, and 4.3.3.5, three different filters were used. In figure 4.3.3.3, a red filter CS2-58 was used to pass the H_α line. In figure 4.3.3.4, a blue filter CS5-59 was used to pass the H_β line. In figure 4.3.3.5, a Ditric Optic 570 3C yellow filter with half width of 92 Å (from 5670 to 5762 Å) was used to pass the continuum. One can see that all the optical signals were modulated at the same frequency as the reflected signal, and ahead of the reflected signal. The characteristic curves for the filters were shown in figure 4.3.3.6. Figure 4.3.3.7 is the same kind of picture as figure 4.3.3.3 to 4.3.3.5, but no filter was used. Figure 4.3.3.8 shows the same two signals of figure 4.3.3.7 with the time scale of 1 ms/div.

FIGURE CAPTIONS

Figure 4.3.3.1 The upper trace is the optical signal from the side of the chamber. The lower trace is the reflected signal. The time scale is 5 μs/div.

Figure 4.3.3.2 The upper trace is the optical signal from the end of the chamber. The lower trace is the reflected signal. The time scale is 5 μs/div.

Figure 4.3.3.3 The upper trace in both the upper and lower picture are the optical signal using a red filter CS2-58 to pass the H_α line. The lower traces in both half pictures are reflected signal. The time scale is 1 ms/div for the upper picture, 5 μs/div for the lower picture.

Figure 4.3.3.4 Same as figure 4.3.3.3, a blue filter CS5-59 was used to pass the H_β line.

Figure 4.3.3.5 Same as figure 4.3.3.3, a Ditric Optic 570 3C yellow filter was used to pass the continuum.

Figure 4.3.3.6 The characteristic curves of filters.

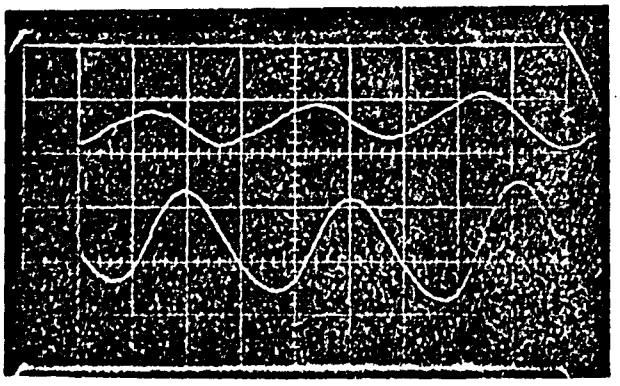

FIG 4.3.3.1

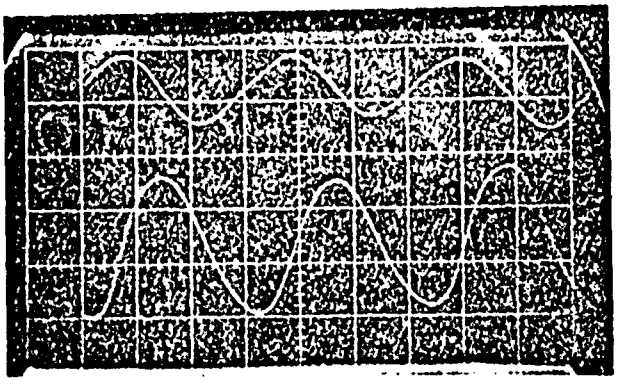

FIG 4.3.3.2

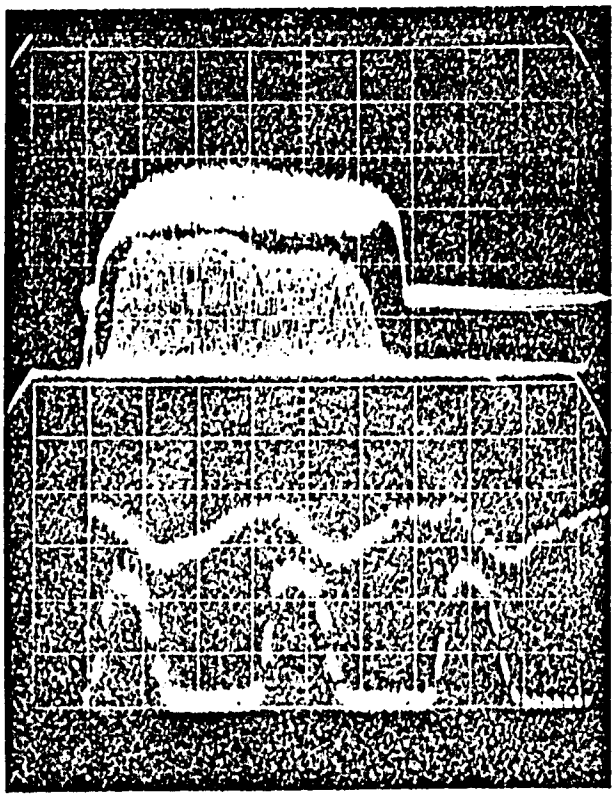

FIG 4.3.3.3

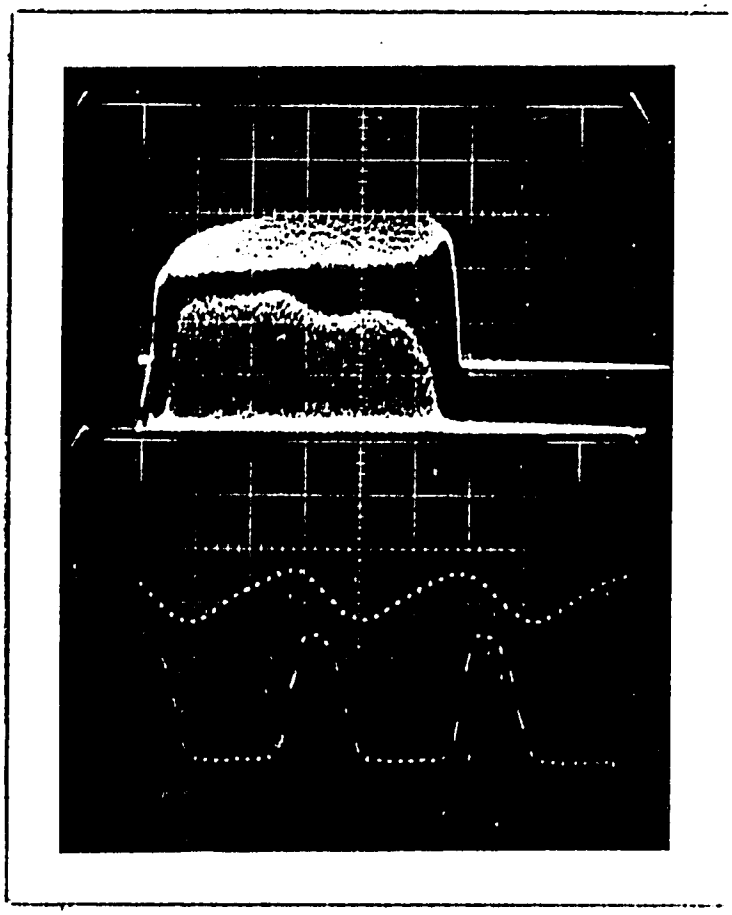

FIG 4.3.3.4

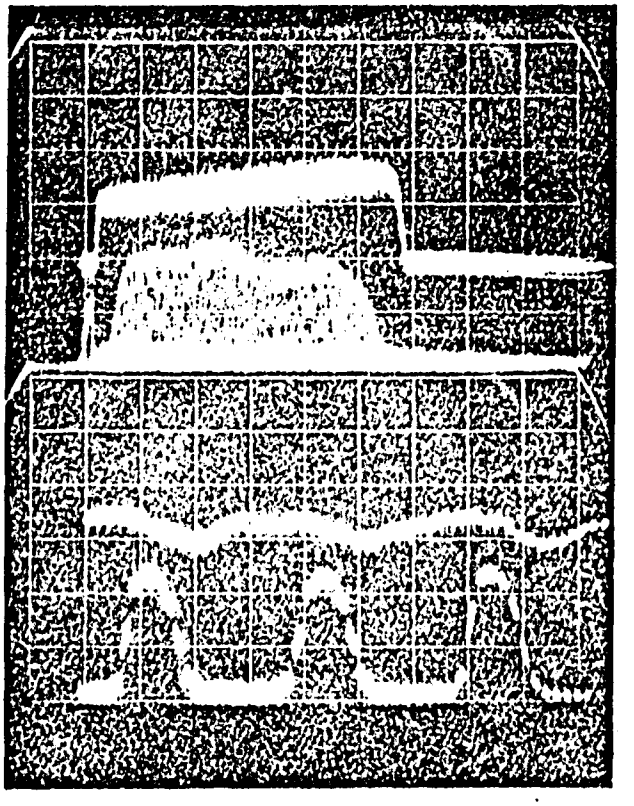

FIG 4.3.3.5

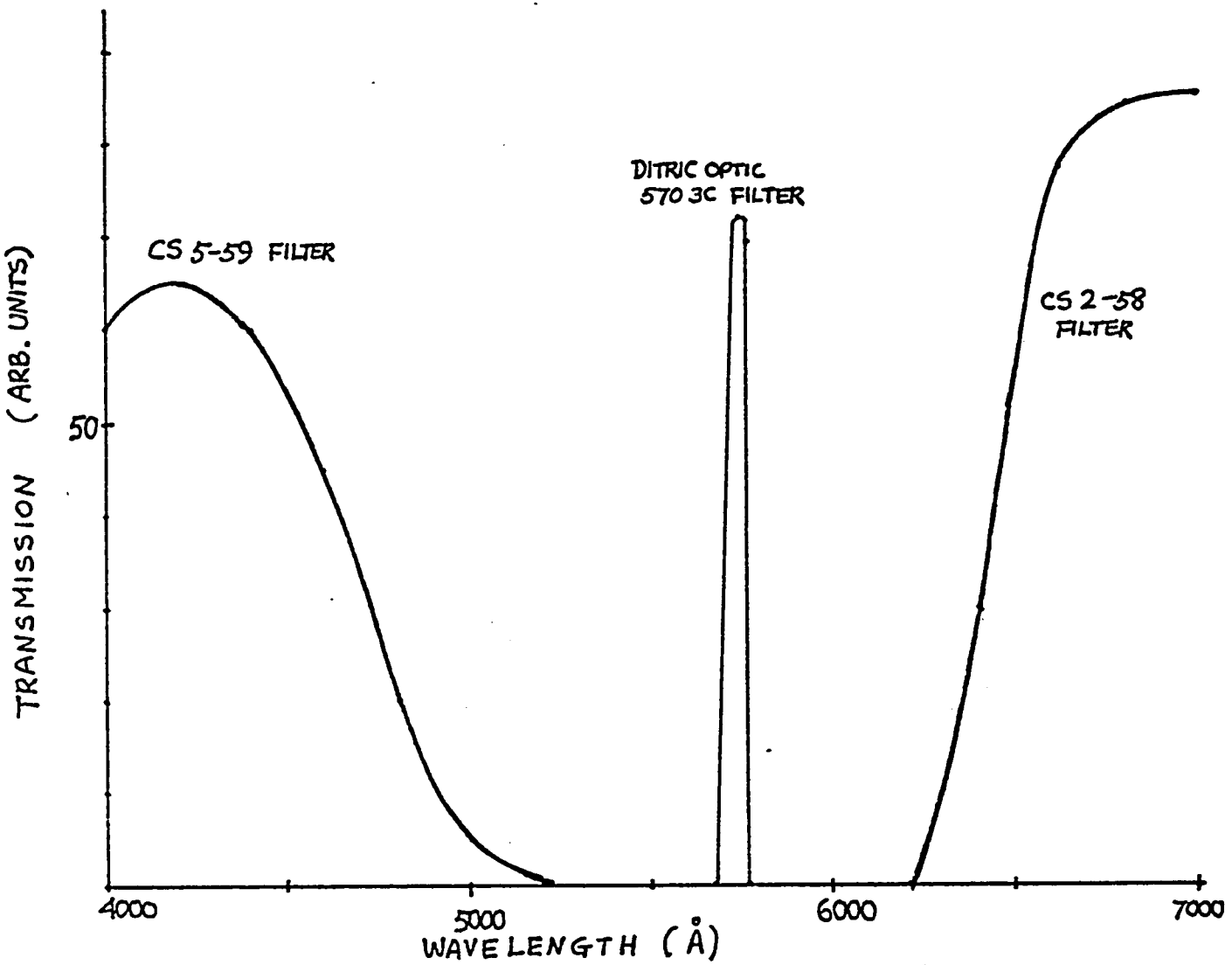
TRANSMISSION (ARB. UNITS)
50
CS 5-59 FILTER
DITRIC OPTIC
570 3C FILTER
CS 2-58
FILTER
4000
5000
6000
7000
WAVELENGTH (Å)

FIG 4.3.3.6

FIGURE CAPTIONS

Figure 4.3.3.7 The upper trace is the reflected signal. The lower trace is the optical signal. No filter was used. The time scale is 5 μs/div.

Figure 4.3.3.8 Same as 4.3.3.7. The time scale is 1 ms/div.

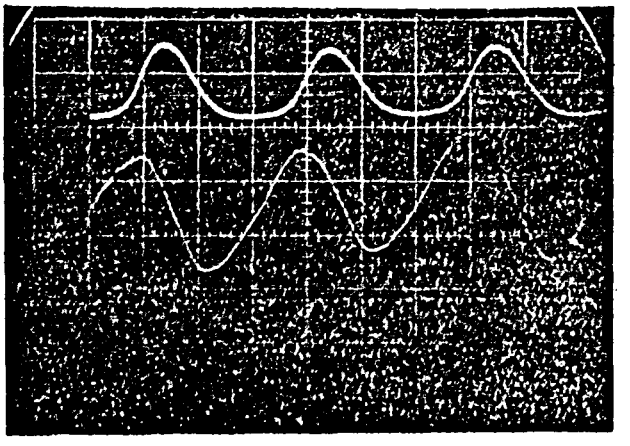

FIG 4.3.3.7

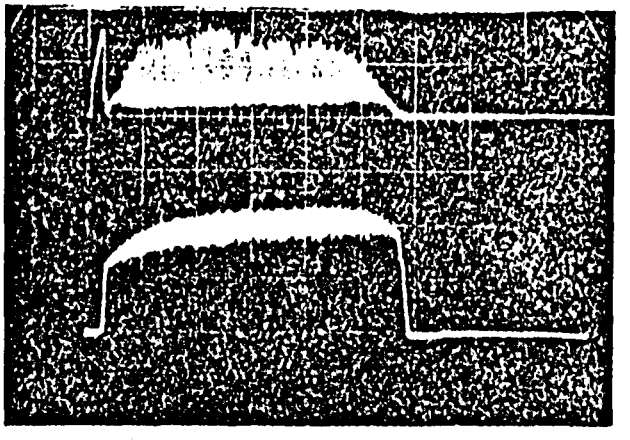

FIG 4.3.3.8

4.3.4 Loop Probe 'Transmitted Signal'

The loop probe was positioned between the plasma and the end flange and the signal was fed to a crystal detector (HP model 400B). The output of the crystal detector is shown in figure 4.3.4.1. When the transmitted signal is connected to the microwave reciver, the output of the microwave receiver is shown in figure 4.3.4.2 when the microwave receiver is set at 2.43 GHz, and in figure 4.3.4.3 when the microwave receiver is set at 4.89 GHz. When the transmitted signal is connected to microwave receiver, the spectrum of the loop probe transmitted signal is plotted in figure 4.3.4.4. When the transmitted signal is connected to the spectrum analyzer, the signal is similar to the reflected signal.

In order to find out whether the 4.89 GHz microwave is from the plasma or the magnetron microwave source, a Microlab/FXR model LA-30 low pass filter with cut off frequency at 3 GHz was used to filter out the higher frequency components of the incident signal before the signal was fed into the microwave receiver. It was found that when the microwave receiver set at 4.89 GHz, the signal was gone, but when the low pass filter is remove, the 4.89 GHz signal appears again. There, it is clear the 4.89 GHz microwave signal was from the magnetron source.

FIGURE CAPTIONS

Figure 4.3.4.1 In both the upper and lower half picture, the top traces are the reflected signal and the lower traces are the loop probe transmitted signal. The time scale for the upper picture is 1 ms/div. The time scale for the lower picture is 5 μs/div.

Figure 4.3.4.2 Microwave receiver output of the loop probe signal. In both the upper and lower picture, the top traces are the loop probe signal, and the lower traces are the reflected signal. The time scale is 1 ms/div for the top picture and 5 μs/div for the lower picture. The microwave receiver is set at 2.43 GHz.

Figure 4.3.4.3 Same as 4.3.4.2, but the microwave receiver is set at 4.89 GHz.

Figure 4.3.4.4 Spectrum of the loop probe transmitted signal using microwave receiver.

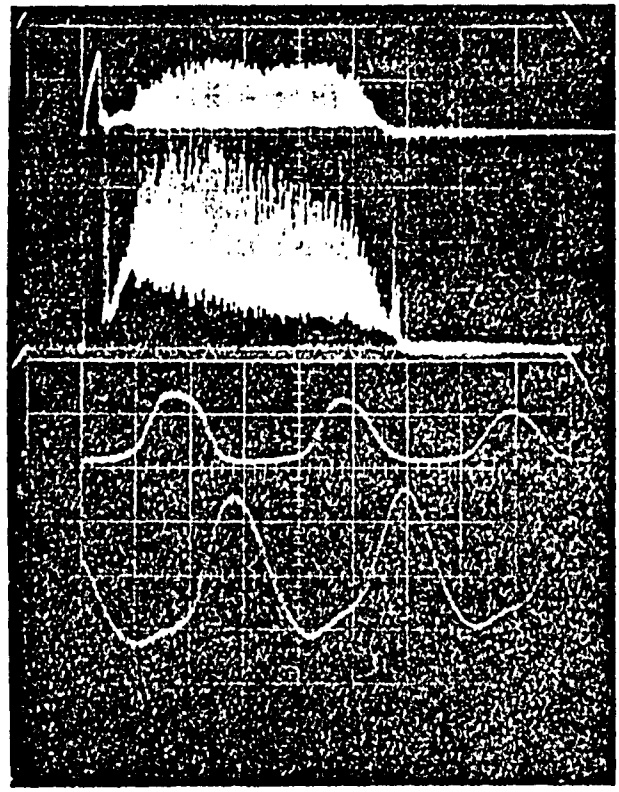

FIG 4.3.4.1

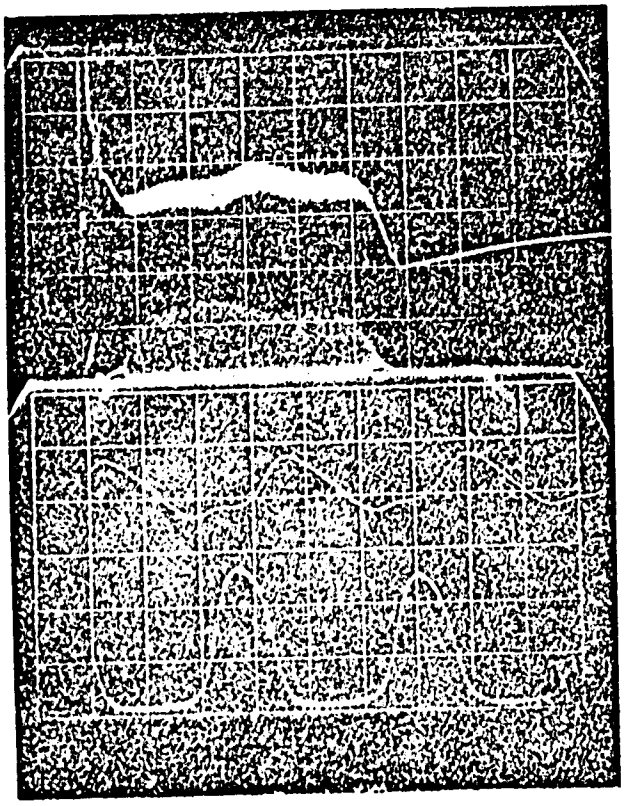

FIG 4.3.4.2

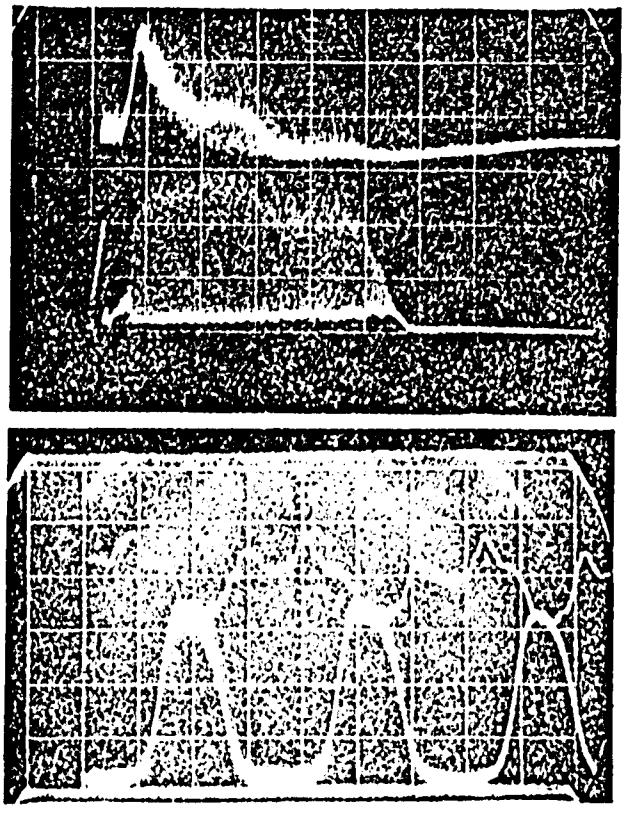

FIG 4.3.4.3

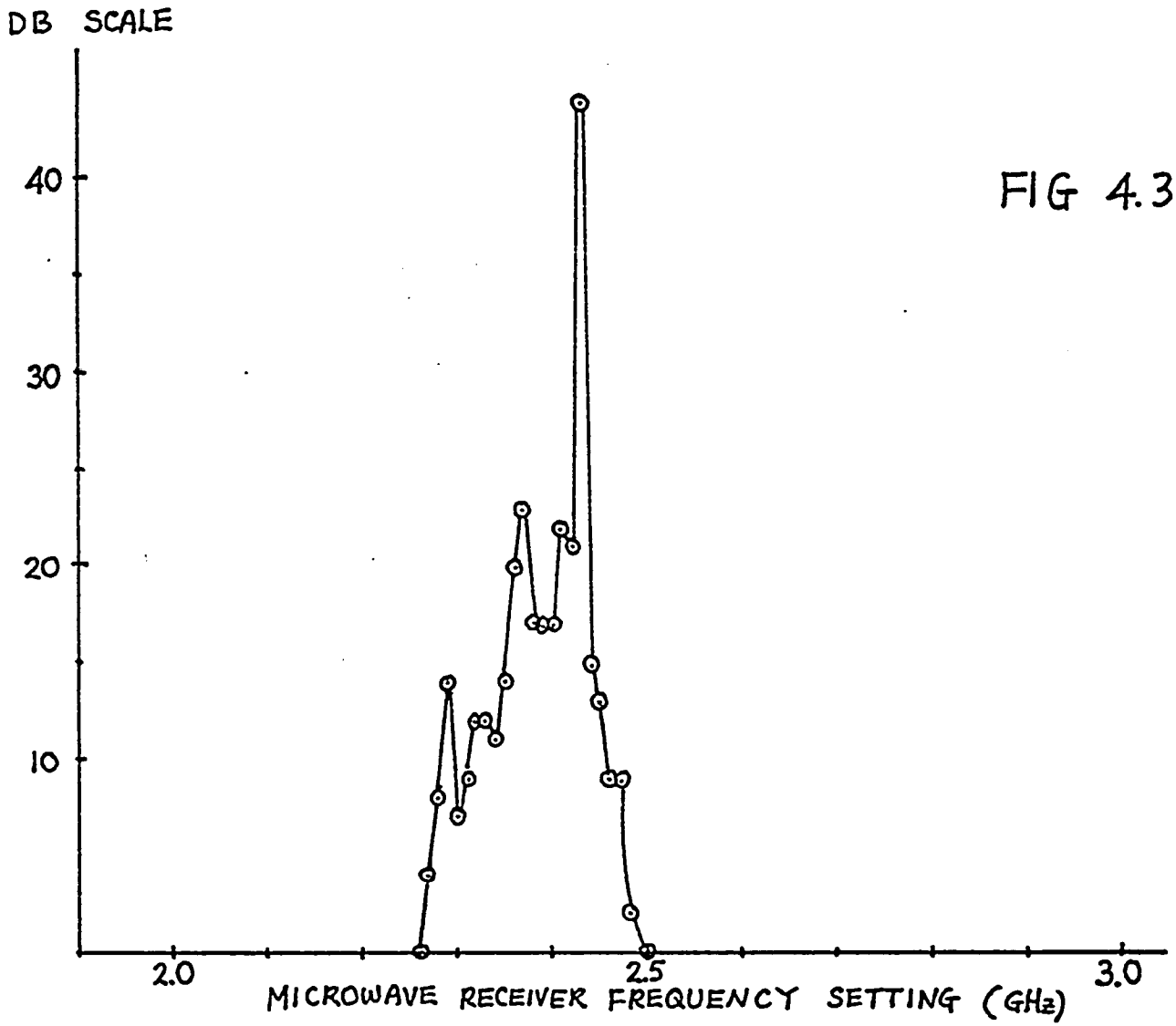
DB SCALE
40
30
20
10
2.0
2.5
3.0
MICROWAVE RECEIVER FREQUENCY SETTING (GHz)

FIG 4.3.4.4

4.3.5 Langmuir Probe

When the center Langmuir probe positioned 1 cm in the chamber is biased at -40 volts, the reflected and the Langmuir probe signal are shown in figure 4.3.5.1. The time scale is 1 ms per division. The same picture is shown in figure 4.3.5.2 with the time scale at 5 μs/div. One can see that the Langmuir Probe signal is out of phase by π with the reflected signal.

When the center Langmuir probe positioned 1 cm in the chamber is biased at +40 volts, the reflected and the Langmuir probe signal are shown in figure 4.3.5.3. The time scale is 1 ms/div. The same picture is shown in figure 4.3.5.4 with the time scale at 5 μs/div. The Langmuir probe signal in figure 4.3.5.4 has been flipped upward so that the peaks are pointing upward. One can see that the Langmuir probe signal is in phase with the reflected signal. The electron current and the ion current are therefore out of phase by π.

FIGURE CAPTIONS

Figure 4.3.5.1 The upper trace is the reflected signal. The lower trace is the Langmuir probe signal when the probe is biased at -40 volts. The time scale is 1 ms/div.

Figure 4.3.5.2 Same as figure 4.3.5.1, the time scale 5 μs/div.

Figure 4.3.5.3 Same as figure 4.3.5.1 but the probe is biased at +40 volts.

Figure 4.3.5.4 Same as figure 4.3.5.3, the time scale is 5 μs/div.

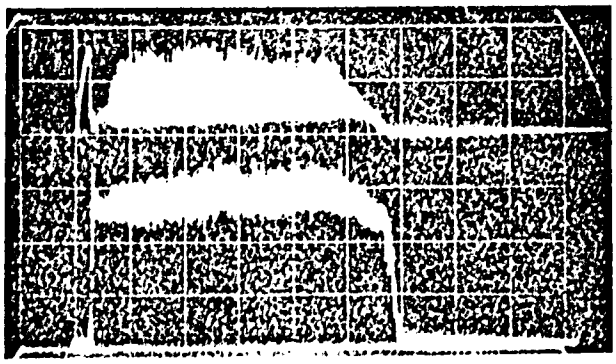

FIG 4.3.5.1

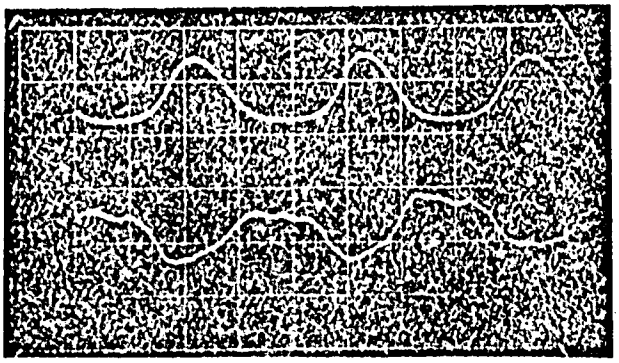

FIG 4.3.5.2

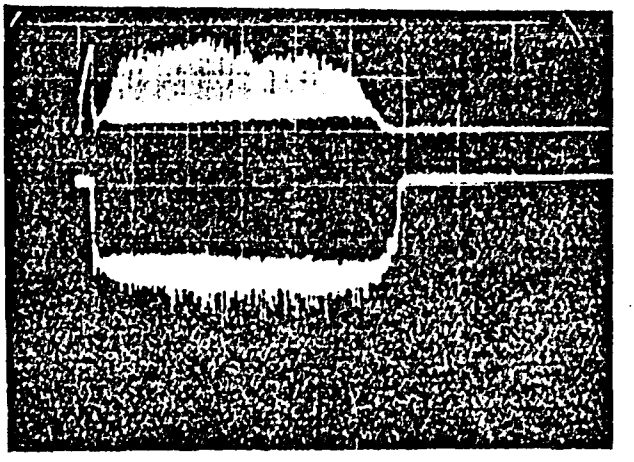

FIG 4.3.5.3

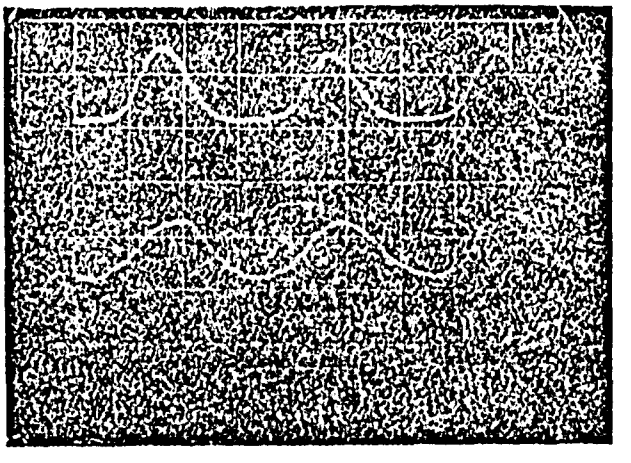

FIG 4.3.5.4

4.3.6 Phase Relationship Between Detected Signals

It is interesting to see the phase relationship between signals. In figure 4.3.6.1, the top trace is the unintegrated diamagnetic coil signal, the middle trace is the optical signal, the lower trace is the reflected signal. In figure 4.3.6.2, the top trace is the optical signal, the middle trace is the transmitted signal, the lower trace is the reflected signal. One can see that the reflected signal is about 4.5 μs ahead of the transmitted signal. In figure 4.3.6.1, the reflected is about 3 μs behind the optical signal. Since the phase shift on the optical signal is 1.5 μs, the optical signal is actually 4.5 μs ahead of the reflected signal. The first zero point before each maximum of the unintegrated diamagnetic coil signal is 0.5 μs before the reflected signal. Since the first zero points coincide with the maxima of the integrated diamagnetic coil signal, the integrated diamagnetic coil signal is 0.5 μs ahead of the reflected signal.

FIGURE CAPTIONS

Figure 4.3.6.1 The top trace is the unintegrated diamagnetic coil signal, the middle trace is the optical signal, the lower trace is the reflected signal. The time scale is 5 μs / div.

Figure 4.3.6.2 The top trace is the optical signal, the middle trace is the transmitted signal, the lower trace is the reflected signal. The time scale is 5 μs / div.

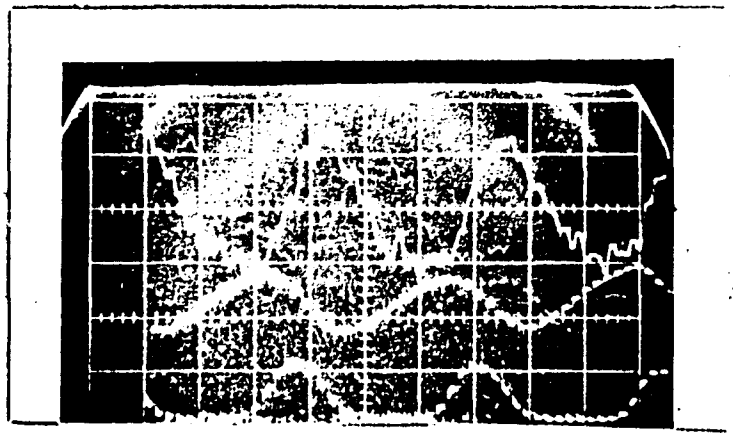

FIG 4.3.6.1

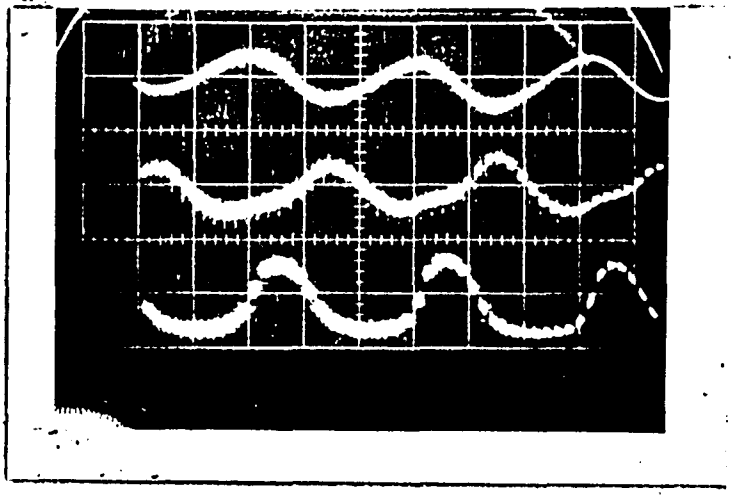

FIG 4.3.6.2

V PHENOMENOLOGICAL THEORY OF THE OSCILLATIONS

Following Mendel and Stern[1], we assume that the incident microwaves are absorbed by a bounded plasma resonance[2]. The temperature and density increase until the microwaves are almost totally reflected and the density and temperature relax. The process then repeats. The frequency of oscillation is determined by[1,2,3]

$$f = \frac{1}{2L}\sqrt{\frac{K_B T_e}{m_i}} \qquad 5.1$$

where L is the length of the plasma. If we put in our experimental values:

$$L = 40 \text{ cm}$$

$$T_e = 31 \text{ ev}$$

f will be 68.1 KHz which is our observed modulation frequency.

In order to explain the phase relationship between the transmitted and the reflected microwave signals, we outline the theory below[4]:

Consider a plasma slab with sharp parallel

boundaries and width L. We assume the incident electromagnetic wave of angular frequency ω traveling in the plasma as shown in figure 5.1 has the form

$$e^{(j\omega t - \gamma z)}$$

where $\gamma = \alpha + j\beta$

α is the absorption coefficient (we assume α is only a function of time)

β is the propagation constant $= \frac{2\pi}{\lambda}\mu$

λ is the waveguide vacuum wavelength

μ is the real part of the refractive index of the plasma, for LHCP

$$\mu \approx \left[1 - \frac{\omega_{pe}^2}{\omega(\omega+\omega_{ce})} \right]^{\frac{1}{2}} \qquad 5.2$$

Assume the reflection coefficient Γ at the boundary to be real:

$$r = \frac{(1-\mu)^2}{(1+\mu)^2} \qquad 5.3$$

Then

$$R = \frac{r\left\{(1-e^{-2\alpha L})^2 + 4e^{-2\alpha L}\sin^2(\beta L)\right\}}{\left[1-re^{-2\alpha L}\right]^2 + 4re^{-2\alpha L}\sin^2(\beta L)} \qquad 5.4$$

$$T = \frac{(1-r)^2 e^{-2\alpha L}}{\left[1-re^{-2\alpha L}\right]^2 + 4re^{-2\alpha L}\sin^2(\beta L)} \qquad 5.5$$

$$A = 1 - R - T \qquad 5.6$$

where R, T are total power reflection and transmission coefficients, A is proportional to the absorbed power. Let us plot out equations 5.4, 5.5 and 5.6, using numbers close to our experimental conditions.

$$\omega_{pe}^2 = \frac{4\pi e n_0}{m_e}\left(1 + \frac{\Delta n}{n_0}\cos(2\pi f t)\right)$$

with $n_0 \sim 10^{10}/cm^3$

$$\omega \sim 2\pi \times 2.43\times 10^9 \sim \omega_{ce}$$

$$\frac{\Delta n}{n_0} \sim 0.05$$

$$\frac{4\pi n_0}{m_e} \sim 0.9$$

Then

$$\mu = \left[1 - 0.9(1 + 0.05 \cos(2\pi f t)) \right]$$

$$\lambda \sim 20 \text{ cm}$$

Assume

$$\frac{L}{\lambda} \sim 1.2$$

Assume absorption is out of phase with n_e by 70°, and set

$$2\alpha L = 0.5 \left[1 + \cos(2\pi f t + 70^\circ) \right]$$

We get the R, T, A, curves as shown in figure 5.2. We see that the reflected and the transmitted signals are not out of phase by π, and all three signals are modulated at the same frequency. Observed signals are shown in figure 5.3. We can see that the calculated signals are remarkably similar to the observed signals.

FIGURE CAPTIONS

Figure 5.1 Plasma slab.

Figure 5.2 Calculated curves of the reflected signal R, the transmitted signal T, and the absorption curve A.

Figure 5.3 Observed signals.

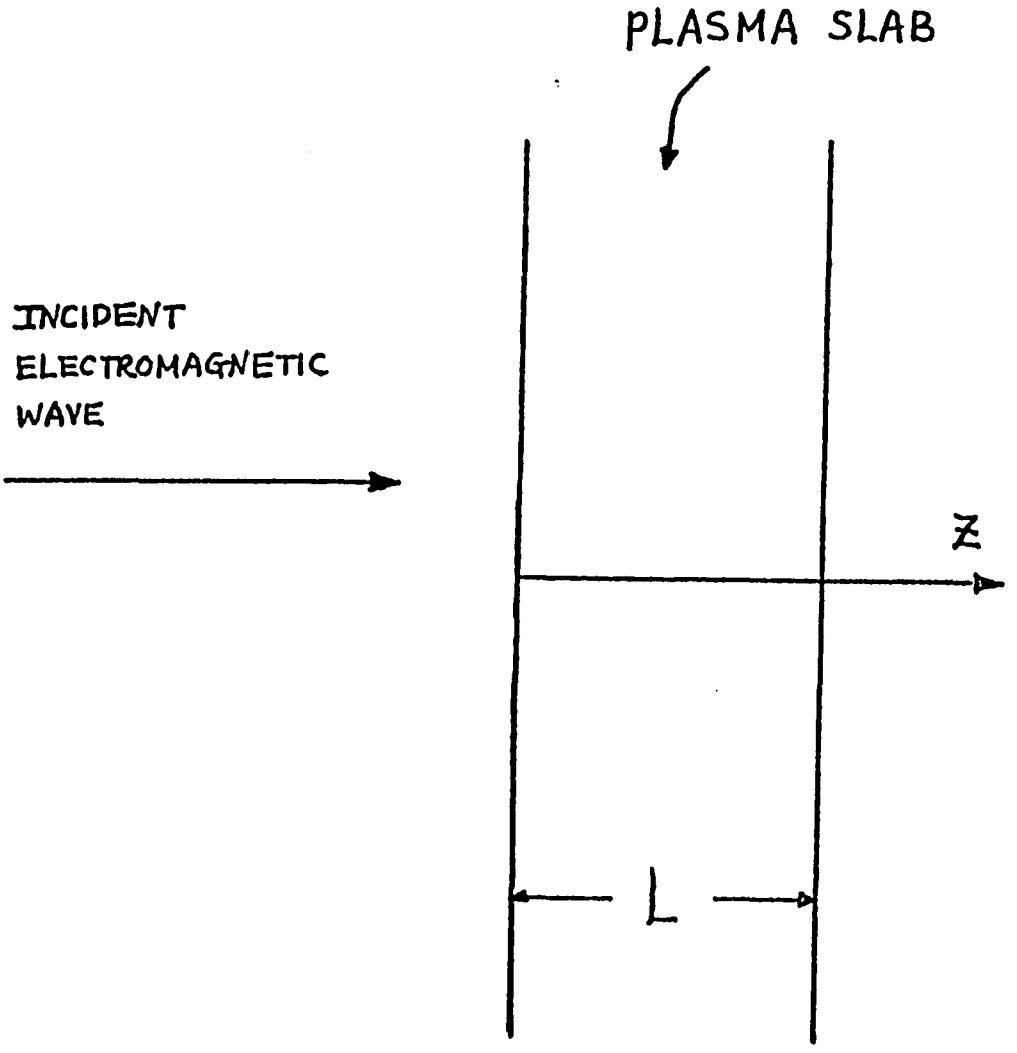

FIG 5.1

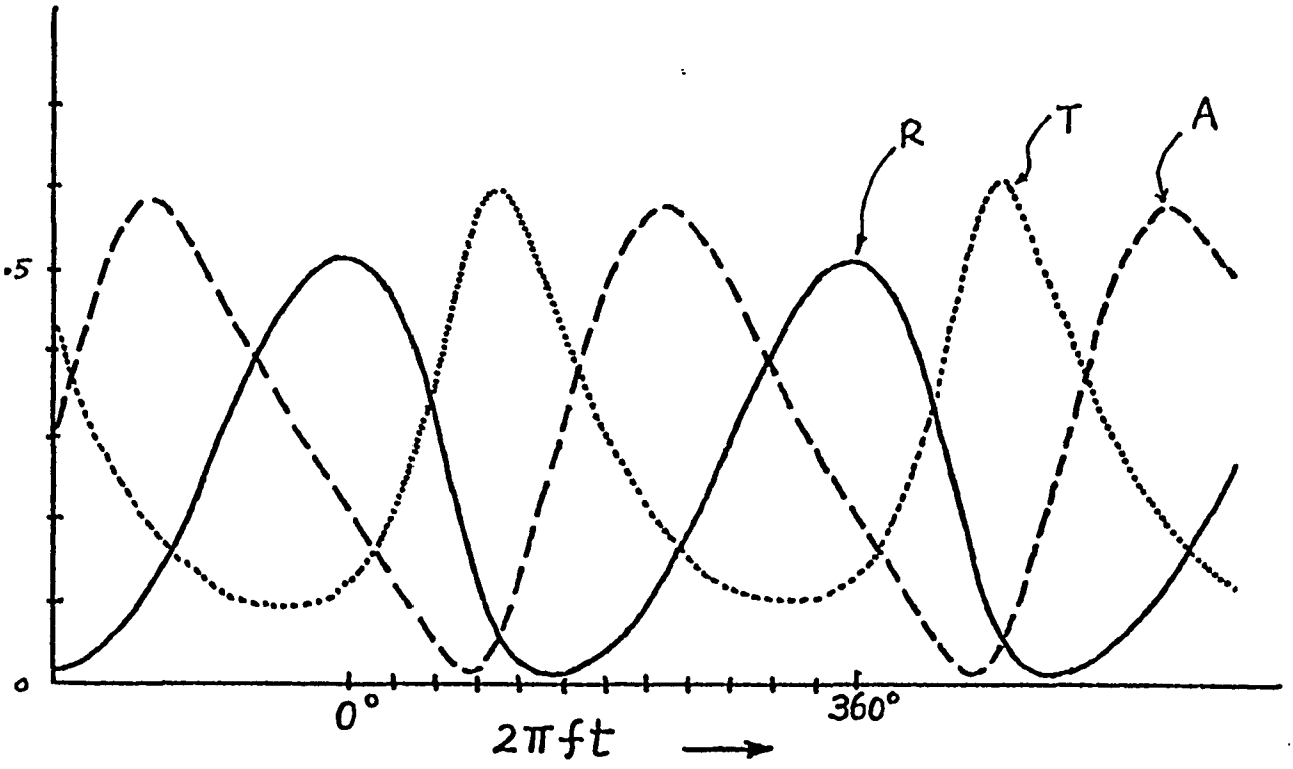
R
T
A
.5
0
0°
360°
2πft

FIG 5.2

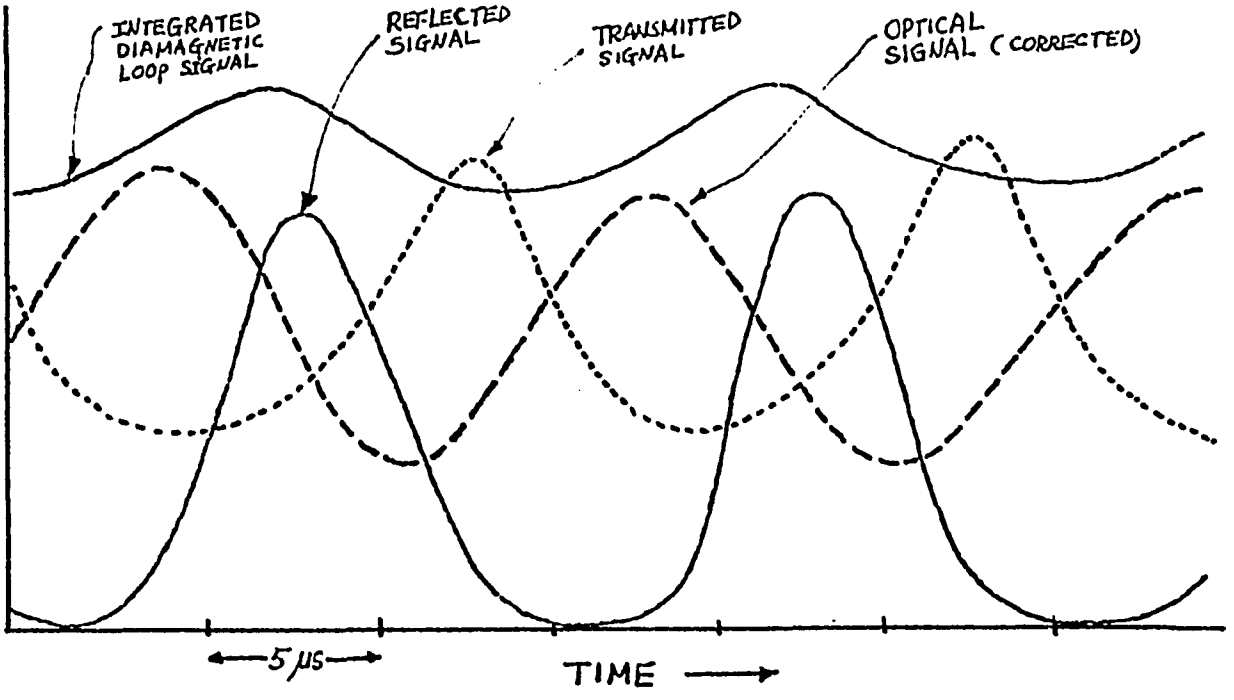
INTEGRATED DIAMAGNETIC LOOP SIGNAL
REFLECTED SIGNAL
TRANSMITTED SIGNAL
OPTICAL SIGNAL (CORRECTED)
5 μs
TIME

FIG 5.3

REFERENCES

1. C. W. Mendel and R. A. Stern, J. Appl. Phys. 41, 734 (1970).

2. A. M. Messiaen and P. E. Vandenplas, Phys Fluids, 12, 2406 (1969).

3. A. I. Anisimov et al, Sov. Phys.- Tech. Phys., 13, 1529 (1969).

4. M. A. Heald and C. B. Wharton, Plasma Diagnostics with Microwaves, John Wiley & Sons Inc., (1965) pp 127-130.

VI DISCUSSION OF RESULTS AND CONCLUSION

Experimentally, it is found that whenever we put probes into the plasma, we affect the modulation to an appreciable extent. Also, since the RF field and the modulations of the field can potentially have a profound effect on the probe characteristics and its interpretation , we have used the Langmuir probes primarily to obtain an estimate of the electron temperature. Diamagnetic coils wound around the inner tube of the plasma chamber, and optical observation are used in order to minimize. the distortion of the plasma. The Langmuir probe used in this experiment was placed so that it was at the outer edge of the plasma. The RF loop probe was placed outside the magnetic field maximum so that the distortion was minimized.

The density from the Langmuir probe is in surprisingly fair agreement with the results from the diamagnetic coils. Both are lower than the results from the microwave interferometer. This is probably due to the multiple reflections of the K band microwave signals in the plasma chamber.

From figure 4.3.4.1, we can see that both the reflected and the transmitted signals are modulated at the same frequency with the reflected signal about 4.5 μs ahead of the transmitted signal (both signals were detected by crystal detectors). In figure 4.3.4.2, the

crystal detector was used to detect the reflected signal and the microwave receiver was used to detect the transmitted signal. One can see that the reflected signal is still about 4.5 μs ahead of the transmitted signal, and both signals were modulated at the same frequency. Figure 4.3.4.3 was taken at the same condition as figure 4.3.4.2, except that the microwave receiver was set at 4.89 GHz. (The funny shape of the microwave receiver signals is due to improper grounding of the microwave receiver circuitry). One can see that for the second harmonic the transmitted signal and the reflected signal are out of phase by π as one might expect for the case of no absorption (see page 132). It seems clear that the plasma absorbs at 2.43 GHz but not at 4.89 GHz.

When we increase the aiding coil current, we reduce the width of the magnetic well and we reduce the length of the plasma. This is consistent with the equation $f = \frac{1}{2L}\sqrt{\frac{KT_e}{m_i}}$ (see page 141). The reason that the modulation frequency is unchange over a limited range of the external DC magnetic field is because the shape of the magnetic well is not changed. If the external magnetic field is changed too far from the electron cyclotron resonance, the modulations will disappear. The same arguments apply to the duration of the modulation as the external DC magnetic field is changed.

In our results, we found that the higher the input power, the higher the modulation frequency and the longer the duration of the modulation. This is reasonable because of the higher T_e . The higher the neutral hydrogen pressure, the shorter the duration of modulation because the plasma cools off sooner due to collision with the neutral hydrogen gas. However, it is not clear why the modulation frequency is increased.

Comparing figure 4.3.3.1 which shows the optical signal from the side port of the plasma chamber, and figure 4.3.3.2 which shows the optical signal from the end flange, on car see that the optical signals are about 3.5 μs ahead of the reflected signal. This fact gives us the answer as to whether the plasma oscillation is a travelling of standing wave. If the oscillation is due to a travelling wave, we would expect that the optical signal from the end flange should be continuous. Since the optical signal from the side of the plasma chamber is in phase with the optical signal from the end flange, the plasma oscillation is a standing wave instead of a travelling wave.

Both the integrated and the unintegrated diamagnetic signal indicated oscillation around 70 KHz. From the unintegrated signal, we find that the oscillations are all in phase at all points. The amplitude of the oscillation approaches a minimum at the magnetic field maxima. This indicates that the perpendicular plasma

pressure varied periodically and in phase throughout the plasma and had nodes at the magnetic field maxima. It is a standing wave in agreement with the optical signals.

Figure 4.3.1.15 shows the output signal of the spectrum analyzer for the reflected signal with the center frequency at 2.43 GHz. Figure 4.3.1.16 shows the output signal of the spectrum analyzer for a modulated (70 KHz) CW microwave signal with center frequency at 2.43 GHz. Figure 4.3.1.15 alone indicates that the reflected signal contains three frequencies; a component at 2.43 GHz and side bands at 2.43 GHz ± 70 KHz. However, if one looks at figure 2.4.1.15, one can equally well conclude that the two bumps are due to the amplitude modulation of the reflected signal. From the reflected and the transmitted signals, we see that the energy is being absorbed periodically by the plasma. It seems likely that we do not have a four waves process but instead we have relaxation type oscillation.

Figure 5.2 suggests the following series of events. The plasma density rises up to the point when most of the microwaves were reflected which corresponds to the maximum reflection of the reflected signal. After the maximum reflection, the plasma density decreases. As a result, the transmission of the microwaves increases. Then the electrons are heated up by the microwaves. The electrons collide with the neutral atoms

and produce an increase in the optical signal emitted. The heated electrons cause an increase in the ionization of the neutral atoms and increase the density of the plasma. Then, the optical activity decrease is followed by an increase in plasma pressure $n T_e$, and we observed the peak of the integrated diamagnetic coil signals. As the plasma density increases, the maximum reflection occurs. The whole cycle repeats.

Finally, we postulate by analogy with Mendel and Stern that the absorption mechanism is a result of bounded plasma resonance and the frequency is determined by the loss rate and the ionization rate.